ADAPTIVE CONTROL OF A PARALLEL ROBOT VIA BACKSTEPPING TECHNIQUE

LI WANG ©

Supervised by: Dr. Xiaoping Liu

Co-supervised by: Dr. Kefu Liu and Dr. M. Uddin

A THESIS SUBMITTED IN PARTIAL FULFILLMENT OF THE

REQUIREMENTS OF MScENG DEGREE IN CONTROL ENGINEERING

FACULTY OF ENGINEERING

LAKEHEAD UNIVERSITY

THUNDER BAY, ONTARIO

P7B 5E1

MAY 22, 2006

Your file Votre référence
ISBN: 978-0-494-21522-7
Our file Notre référence
ISBN: 978-0-494-21522-7

ABSTRACT

Parallel robots have attracted more and more attention in recent years due to their kinematical and mechanical advantages. However the complicated high nonlinear model with unknown parameters and singularities make the control of a parallel robot much more difficult than a serial robot. Nonlinear control has been made great progress since backstepping technique was developed. Backstepping technique is a recursive design procedure and feasible for lower triangular nonlinear systems. Moreover, the adaptive backstepping is able to handle nonlinear systems with unknown parameters, which turns out to be a suitable control design methodology for parallel robots.

The adaptive backstepping technique is applied to set point and tracking control of a planar parallel robot in this thesis. The dynamic model of the robot is characterized by a set of differential algebraic equations (DAEs) and further reduced to a set of ordinary differential equations (ODEs). The inverse kinematics is also under investigation. For set point control, a model-based adaptive controller is designed based on backstepping technique, and an adaptive PD controller is also constructed for comparison. For tracking control, adaptive backstepping controller is designed based on the model with unknown parameters. The adaptive PD controller is also implemented for comparison. The performances of the controllers are tested by experiments. Desired trajectories such as circle, line, and square are tracked in experiments for two cases: with no load and with load at the end effector.

It is shown that adaptive controllers can achieve less steady state errors in set point control, and smaller tracking errors in tracking control than non-adaptive controllers, especially when there is a load attached to the end effector.

Key Words: parallel robot, adaptive backstepping, nonlinear control, differential algebraic equation (DAE) systems

ACKNOWLEDGEMENTS

This thesis results from two year work. In the past two years, I have been accompanied and supported by many people. I am glad to take this opportunity to express my gratitude to all of them.

I would like to express my deepest gratitude to my supervisor Dr. Xiaoping Liu for his mentorship and guidance. I appreciate his encouragement, suggestion and patience during the past two years. I am grateful to my co-supervisor Dr. Kefu Liu for his help in mechanical field, and Dr. M. Uddin and Dr. Krishnamoorthy Natarajan for their help in electrical field. I am thankful to Dr. Wilson Wang for his review of this thesis and valuable suggestions. I would like to thank Mr. Manfred Klein, Mr. Kailash Bhatia, and Mr. Willy Cheung for their help in the experimental parts of the thesis.

I extend my thanks to my fellow graduate students for their suggestions and discussions, which were valuable and positive.

Finally, I would like to thank my family for many reasons, which allow me to complete this work.

Contents

List of Figures

Chapter 1

Introduction

1.1 Background

Generally there are two main types of robot manipulators, which are serial manipulators and parallel manipulators. Typically, links of serial robots are connected in series, thus forming open-chain mechanisms and all their joints are actuated. The human arm is a good example of a serial manipulator. On the other hand, links of parallel robots are connected in a combination of both serial and parallel fashions, thus forming closed-chain mechanisms and not all their joints are actuated. The actuators of parallel robots are placed on the base or close to the base, which results in lighter moving parts. Consequently a parallel robot generally has the following properties, such as high capacity of load for the same number of actuators, high accelerations at the end-effector and high mechanical stiffness to weight ratio. Compared with the serial robots, the inconveniences of parallel robots are complex dynamic model and presence of singularities which lead to loosing control, even to a deterioration of mechanics. Thus the modeling and controller design are appealed for a parallel robot control system.

In general, the model governing a parallel robot is highly nonlinear and a precise knowledge of its parameters is not readily available. Adaptive backstepping is able to handle nonlinear systems with unknown parameters, which appears to be a suitable control design methodology for parallel robots. However, it should be noted that there has been no report on application of the adaptive backstepping technique to control of parallel robots.

There is great progress in nonlinear control since backstepping technique is proposed by

[15]. Backstepping is a recursive procedure that combines the choice of a Lyapunov function with the design of feedback control and it can be applied to a class of nonlinear system called "lower triangular" nonlinear system. Moreover adaptive backstepping can handle such a class of nonlinear system with unknown parameters.

In this thesis, an adaptive backstepping-based control scheme is applied to set point and tracking control for a planar 2-DOF (degree-of-freedom) parallel robot. By assuming that inertia parameters and some geometric dimensions of the robot are not known precisely, an adaptive backstepping controller is designed. For the purpose of comparison, an adaptive proportional and derivative (PD) controller is designed as well. The performance of each controller is tested by experiments.

1.2 Literature Review

In the past decades, many researchers have studied parallel mechanisms [26], [14], [7], [11], [3], [30], and showed that parallel mechanisms have the potential advantages of high stiffness, high speeds, low inertia and large payload capacities. Therefore, more and more researchers have applied such mechanisms in different kinds of practical uses, such as aircraft simulator, robotic machining, mining machines, pointing devices, and micro-positioning devices.

In general, modeling of parallel robots is more challenging than that of serial robots. In [9], the modeling methods for parallel robots are classified into three categories. In the first category, the dynamic model is derived for a special closed-chain or a closed-chain with a particular structure. The dynamics of a 3-DOF spatial parallel manipulator with flexible links is studied in [6]. [12] introduces a novel approach for the computation of the inverse dynamics of a parallel manipulator. For those specific closed-chains, closed-form equations of motion are possible to be derived explicitly in terms of the actuated joint variables. Thus the resulting dynamic equations are similar to motion equations of open-chain structure. In this case, all the control laws for open-chain mechanisms are applicable to closed-chain mechanisms with the difference that the guaranteed (Lyapunov) stability conclusions will at best be local.

Using the method of the second category, the equations of motion are derived for general closed-chain structures. The method is to first virtually cut open the closed-chains at passive joints and then derive the equations of motion of the resulting open-chains, which can be expressed by n' dependent differential equations. If the closed-chain mechanism has n DOF, there will be $n' - n$ algebraic holonomic constraints corresponding to the virtually cut joints, which, together with the n' differential equations, compose the full equations of motion of the n DOF closed-chain expressed as a set of differential algebraic equations. A set of n' differential equations results from eliminating the Lagrange multipliers introduced from the constraints in the full equations, the number of which is larger than degrees of freedom, thus it is difficult to extend the existing control laws of open-chains to closed-chains modeled based on the method of the second category. The obtained equations are mostly suited for simulation and computation but not best suited for a model-based control design, thus only the numerical results and illustrative examples are given in [20], [25], and [22].

In [9] it is concluded that the method of the third category [5], [28] is preferable if a model-based control design is employed, which has been proved in [10] based on tracking control. This method starts with formulating the equations of motion in terms of n' dependent generalized coordinates and then eliminating $n' - n$ holonomic constraints to obtain n independent differential equations with n independent generalized coordinates corresponding to the number of DOF of the parallel robot. Unfortunately, the resulting dynamic equations are not in an explicit form of the independent generalized coordinates or actuated joints. Calculation of these implicit relations in real time imposes a severe constraint on application of many well-established control methods for serial robots to parallel robots. Therefore, some early attempts in control of parallel robots focused on the use of non-model based control methods, such as proportional integral derivative (PID) control [1], [16] and artificial intelligence-based algorithms [2], [8]. However, as pointed out in [9], these methods have no guarantee of stability and performance. Some efforts have been made to extend model-based control algorithms for serial robots to parallel robots. The study reported in [13] proposed a parallel computational algorithm to speed up on-line computation. In [4], the mass and inertia of the links were neglected in the dynamic model in order to implement the computed-torque control. A PD plus simple gravity compensation control law is proposed in [9] for set point control for a planar 2-DOF parallel robot. With the proved skew symmetry property, this controller guarantees a local asymptotical stability. For set point control the simple gravity compensation is a constant term which can be computed off-line to any degree of accuracy. In [18], the control problems are considered in the design stage of a parallel robot to find an appropriate mechanical structure with a simple dynamic model, which results in a simple control algorithm to achieve a satisfactory control performance. In [29], a predictive functional control strategy is implemented for tracking control of a H4 parallel robot. The dynamic model is simplified by neglecting the effect of arm mass, which greatly facilitates the implementation of the controller.

Backstepping refers to a recent powerful approach for a design of stabilizing controllers for nonlinear systems both for tracking and regulation purposes [17] since a Lyapunov function for the closed loop system can be constructed systematically based on backstepping technique. The adaptive version of those designs, with the tuning functions design, offers the possibility to synthetize controllers for a wide class of nonlinear system with known strict-feedback structure and unknown parameters in a recursive way.

In [15] a systematic procedure is developed for the design of new adaptive regulation and tracking schemes for linearly parameterized system in strict feedback form, for which global stabilization can be achieved with any type of smooth nonlinearities. Adaptive backstepping technique has been applied to various fields. In [31] a nonlinear adaptive controller is designed step by step for the field weakening area of a separately excited DC motor with unknown parameters such as the inertia and load torque, and the simulation results show that the proposed controller is robust to the parameter uncertainties. An adaptive backstepping controller is proposed to control the mover position of a linear induction motor drive to periodic reference inputs in [19], and the controller possesses the nice transient control performance and is robust for parameter variations and external force disturbances confirmed by both simulation and experimental results.

Backstepping design technique has been applied to control serial robots and wheeled mobile robots. Integrator backstepping technique is applied to trajectory tracking control for serial robot manipulator in presence of parameters uncertainty and disturbance in [21] and [27] incorporating actuator dynamics. A backstepping approach for the design of discontinuous state feedback controller is used for the design of the controller to stabilize a wheeled mobile robot in [24] and an adaptive controller based on backstepping technique is proposed and applied to a two-wheeled welding mobile robot to track a smooth curved welding path in [23].

1.3 Thesis Overview

The thesis consists of six chapters. A general background on adaptive controller application based on backstepping technique is discussed in the first chapter: Introduction. Chapter 2 gives the dynamic model and inverse kinematics of the planar 2-DOF parallel robot built for experiments. Chapter 3 presents adaptive controller design procedures and simulation results for set point control. Design of adaptive backstepping controller and adaptive PD controller with compensation terms for tracking control is given in Chapter 4. Simulations are performed to illustrate control performances of the adaptive backstepping controller and adaptive PD controllers. Chapter 5 provides the experimental results for set point and tracking control. Both adaptive and non-adaptive controller performances are discussed in both set point and tracking control. In order to test the adaptability, the experiments are performed in both without load and with load attached to the end effector. Chapter 6 concludes the thesis by comparing the experimental results based on different controllers for set point and tracking control and presents some proposals for future work.

Chapter 2

Dynamic Model and Inverse Kinematics

2.1 Dynamic Model

A schematic of a planar 2-DOF parallel robot is shown in Fig. 2-1 where m_i, a_i, and l_i are the mass, length of link i and the distance to the center of mass from the lower joint of link i, respectively, I_i denotes the mass moment of inertia of link i with respect to a frame parallel to the body-attached frame with the origin located at the center of mass. Joints q_1 and q_2 are actuated while joints q_3 and q_4 are passive. In this thesis, the following factors are not taken into account: friction between joints, motor dynamics, gear train backlash, and link elasticity.

The dynamical model of the robot, presented in [26], is described as follows:

$$D'(q')\ddot{q}' + C'(q',\dot{q}')\dot{q}' + g'(q') = u' \tag{2.1}$$

$$\phi(q') = 0 \tag{2.2}$$

where $q' = \begin{bmatrix} q_1 & q_2 & q_3 & q_4 \end{bmatrix}^T$ is the vector of dependent generalized coordinates, $u' = \begin{bmatrix} u_1 & u_2 & 0 & 0 \end{bmatrix}^T$ with u_1 and u_2 torque applied on joints q_1 and q_2, respectively, $D'(q') \in R^{4\times4}$ is the inertia matrix, $C'(q',\dot{q}')\dot{q}' \in R^4$ represents the centrifugal and Coriolis terms, and $g'(q') \in R^4$ is the gravity vector, $\phi(q')$ represents the constraints of two independent alge-

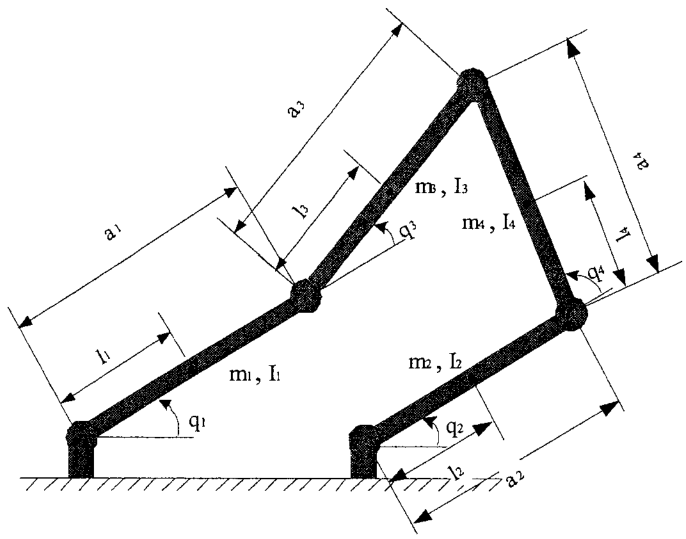

Figure 2-1: Schematic of a 2-DOF parallel robot.

braic equations which are at least twice continuously differentiable. Assume that the parameters m_i, l_i, and I_i are not known precisely. For simplicity, let $\theta_1 = m_1 l_1^2 + m_3 a_1^2 + I_1$, $\theta_2 = m_2 l_2^2 + m_4 a_2^2 + I_2$, $\theta_3 = m_3 l_3^2 + I_3$, $\theta_4 = m_4 l_4^2 + I_4$, $\theta_5 = m_3 a_1 l_3$, $\theta_6 = m_4 a_2 l_4$, $\theta_7 = (m_1 l_1 + m_3 a_1) g$, $\theta_8 = (m_2 l_2 + m_4 a_2) g$, $\theta_9 = m_3 l_3 g$, and $\theta_{10} = m_4 l_4 g$ ($g = 9.81\ m/s^2$) denote the unknown parameters. Then, $D'(q')$, $C'(q', \dot{q}')$, $g'(q')$ and constraints $\phi(q')$ can be expressed as follows:

$$D'(q') = \begin{bmatrix} d_{11} & 0 & d_{13} & 0 \\ 0 & d_{22} & 0 & d_{24} \\ d_{31} & 0 & d_{33} & 0 \\ 0 & d_{42} & 0 & d_{44} \end{bmatrix} \tag{2.3}$$

$$C'(q', \dot{q}') = \begin{bmatrix} c_{11} & 0 & c_{13} & 0 \\ 0 & c_{22} & 0 & c_{24} \\ c_{31} & 0 & 0 & 0 \\ 0 & c_{42} & 0 & 0 \end{bmatrix} \tag{2.4}$$

$$g'(q') = \begin{bmatrix} \theta_7 \cos(q_1) + \theta_9 \cos(q_1 + q_3) \\ \theta_8 \cos(q_1) + \theta_{10} \cos(q_1 + q_3) \\ \theta_9 \cos(q_1 + q_3) \\ \theta_{10} \cos(q_2 + q_4) \end{bmatrix} \tag{2.5}$$

$$\phi(q') = \begin{bmatrix} \phi_1(q') \\ \phi_2(q') \end{bmatrix} = 0 \tag{2.6}$$

where

$$\begin{aligned}
d_{11} &= \theta_1 + \theta_3 + 2\theta_5 \cos(q_3) \\
d_{13} &= \theta_3 + \theta_5 \cos(q_3) \\
d_{22} &= \theta_2 + \theta_4 + 2\theta_6 \cos(q_4) \\
d_{24} &= \theta_4 + \theta_6 \cos(q_3) \\
d_{31} &= d_{13}, d_{33} = \theta_3 \\
d_{42} &= d_{24} \\
d_{44} &= \theta_4 \\
c_{11} &= -\theta_5 \sin(q_3)\dot{q}_3 \\
c_{13} &= -\theta_5 \sin(q_3)(\dot{q}_1 + \dot{q}_3) \\
c_{22} &= -\theta_6 \sin(q_4)\dot{q}_4 \\
c_{24} &= -\theta_6 \sin(q_4)(\dot{q}_2 + \dot{q}_4) \\
c_{31} &= \theta_5 \sin(q_3)\dot{q}_1 \\
c_{42} &= \theta_6 \sin(q_4)\dot{q}_2 \\
\phi_1(q') &= a_1 \cos(q_1) + a_3 \cos(q_1 + q_3) - c - a_2 \cos(q_2) - a_4 \cos(q_2 + q_4) \\
\phi_2(q') &= a_1 \sin(q_1) + a_3 \sin(q_1 + q_3) - a_2 \sin(q_2) - a_4 \sin(q_2 + q_4)
\end{aligned}$$

It can be found that $c_{kj} = \sum_{i=1}^{4} \frac{1}{2}\left(\frac{\partial d_{kj}}{\partial q_i} + \frac{\partial d_{ki}}{\partial q_j} - \frac{\partial d_{ij}}{\partial q_k}\right)\dot{q}_i$, where k, j are from 1 to 4, thus $\dot{D}'(q') - 2C'(q', \dot{q}')$ is skew symmetric.

Equations (2.1) and (2.2) are a set of differential algebraic equations (DAEs) in the dependent generalized coordinates q'. The independent generalized coordinates q or active joints are related to q' by:

$$q = \begin{bmatrix} q_1 \\ q_2 \end{bmatrix} = \begin{bmatrix} 1 & 0 & 0 & 0 \\ 0 & 1 & 0 & 0 \end{bmatrix} q' \tag{2.7}$$

In order to obtain a formulation that is suitable for model-based control, a reduced model in the independent generalized coordinates is derived following the procedure given in [9] and is given below:

$$\begin{aligned} D(q')\,\ddot{q} + C(q', \dot{q}')\dot{q} + g(q') &= u && (2.8) \\ \dot{q}' &= \rho(q')\dot{q} && (2.9) \\ q' &= \sigma(q) && (2.10) \end{aligned}$$

where:

$$D(q') = \begin{bmatrix} D_{11} & D_{12} \\ D_{21} & D_{22} \end{bmatrix} = \rho(q')^T D'(q')\rho(q') \tag{2.11}$$

$$C(q', \dot{q}') = \begin{bmatrix} C_{11} & C_{12} \\ C_{21} & C_{22} \end{bmatrix} = \rho(q')^T C'(q', \dot{q}')\rho(q') + \rho(q')^T D'(q')\dot{\rho}(q') \tag{2.12}$$

$$g(q') = \begin{bmatrix} g_1 \\ g_2 \end{bmatrix} = \rho(q')^T g'(q') \tag{2.13}$$

$$\rho(q') = \psi_{q'}^{-1}(q') \begin{bmatrix} 0 & 0 \\ 0 & 0 \\ 1 & 0 \\ 0 & 1 \end{bmatrix} = \begin{bmatrix} 1 & 0 \\ 0 & 1 \\ \rho_{31} & \rho_{32} \\ \rho_{41} & \rho_{42} \end{bmatrix} \tag{2.14}$$

$$\psi_{q'}(q') = \begin{bmatrix} \psi_{q'11} & \psi_{q'12} & \psi_{q'13} & \psi_{q'14} \\ \psi_{q'21} & \psi_{q'22} & \psi_{q'23} & \psi_{q'24} \\ 1 & 0 & 0 & 0 \\ 0 & 1 & 0 & 0 \end{bmatrix} \tag{2.15}$$

$$\dot{\rho}(q') = \begin{bmatrix} 0 & 0 \\ 0 & 0 \\ \dot{\rho}_{31} & \dot{\rho}_{32} \\ \dot{\rho}_{41} & \dot{\rho}_{42} \end{bmatrix} = -\psi_{q'}^{-1}(q')\dot{\psi}_{q'}(q',\dot{q}')\rho(q') \tag{2.16}$$

with

$$\begin{aligned}
\psi_{q'11} &= -a_1\sin(q_1) - a_3\sin(q_1+q_3) \\
\psi_{q'12} &= a_2\sin(q_2) + a_4\sin(q_2+q_4) \\
\psi_{q'13} &= -a_3\sin(q_1+q_3) \\
\psi_{q'14} &= a_4\sin(q_2+q_4) \\
\psi_{q'21} &= a_1\cos(q_1) + a_3\cos(q_1+q_3) \\
\psi_{q'22} &= -a_2\cos(q_2) - a_4\cos(q_2+q_4) \\
\psi_{q'23} &= a_3\cos(q_1+q_3) \\
\psi_{q'24} &= -a_4\cos(q_2+q_4)
\end{aligned}$$

It should be noted that $\dot{D}(q') - 2C(q',\dot{q}')$ is also skew symmetric [9].

The elements D_{jk}, C_{jk} and g_j with j, $k = 1,2$ in $D(q')$, $C(q',\dot{q}')$ and $g(q')$ can be expressed as $D_{ojk}\Theta$, $C_{ojk}\Theta$ and $g_{oj}\Theta$ with

$$\begin{aligned}
D_{ojk} &= \begin{bmatrix} D_{ojk1} & D_{ojk2} & \cdots & D_{ojk10} \end{bmatrix} \\
C_{ojk} &= \begin{bmatrix} C_{ojk1} & C_{ojk2} & \cdots & C_{ojk10} \end{bmatrix} \\
g_{oj} &= \begin{bmatrix} g_{oj1} & g_{oj2} & \cdots & g_{oj10} \end{bmatrix} \\
\Theta &= \begin{bmatrix} \theta_1 & \theta_2 & \cdots & \theta_{10} \end{bmatrix}
\end{aligned} \tag{2.17}$$

where

$$\begin{aligned}
D_{o111} &= 1 \\
D_{o113} &= (1+\rho_{31})^2
\end{aligned}$$

$$
\begin{aligned}
D_{o114} &= \rho_{41}^2 \\
D_{o115} &= 2(1+\rho_{31})\cos(q_3) \\
D_{o123} &= D_{o213} = (1+\rho_{31})\rho_{32} \\
D_{o124} &= D_{o214} = (1+\rho_{42})\rho_{41} \\
D_{o125} &= D_{o215} = \rho_{32}\cos(q_3) \\
D_{o126} &= D_{o216} = \rho_{41}\cos(q_4) \\
D_{o222} &= 1 \\
D_{o223} &= \rho_{32}^2 \\
D_{o224} &= (1+\rho_{42})^2 \\
D_{o226} &= 2(1+\rho_{42})\cos(q_4) \\
C_{o113} &= (1+\rho_{31})\dot\rho_{31} \\
C_{o114} &= \rho_{41}\dot\rho_{41} \\
C_{o115} &= \dot\rho_{31}\cos(q_3) - (1+\rho_{31})\dot q_3\sin(q_3) \\
C_{o123} &= (1+\rho_{31})\dot\rho_{32} \\
C_{o124} &= \rho_{41}\dot\rho_{42} \\
C_{o125} &= \dot\rho_{32}\cos(q_3) - (\dot q_1+\dot q_3)\rho_{32}\sin(q_3) \\
C_{o126} &= \rho_{41}\dot q_2\sin(q_4) \\
C_{o213} &= \rho_{32}\dot\rho_{31} \\
C_{o214} &= (1+\rho_{42})\dot\rho_{41} \\
C_{o215} &= \rho_{32}\dot q_1\sin(q_3) \\
C_{o216} &= \dot\rho_{41}\cos(q_4) - (\dot q_2+\dot q_4)\rho_{41}\sin(q_4) \\
C_{o223} &= \rho_{32}\dot\rho_{32} \\
C_{o224} &= (1+\rho_{42})\dot\rho_{42} \\
C_{o226} &= \dot\rho_{42}\cos(q_4) - (1+\rho_{42})\dot q_4\sin(q_4) \\
g_{o17} &= \cos(q_1) \\
g_{o19} &= (1+\rho_{31})\cos(q_1+q_3)
\end{aligned}
$$

$$
\begin{aligned}
g_{o110} &= \rho_{41}\cos(q_2+q_4) \\
g_{o28} &= \cos(q_2) \\
g_{o29} &= \rho_{32}\cos(q_1+q_3) \\
g_{o210} &= (1+\rho_{42})\cos(q_2+q_4)
\end{aligned}
$$

and all the other elements are zero.

The dependent coordinates q_3 and q_4 can be determined from the geometric relationship which is not linear in terms of q_1 and q_2. Thus $\sigma(q)$ in Eq. (2.10) is given by

$$
q' = \sigma(q) = \begin{bmatrix} \sigma_1 & \sigma_2 & \sigma_3 & \sigma_4 \end{bmatrix}^T
$$

where

$$
\begin{aligned}
\sigma_1 &= q_1 \\
\sigma_2 &= q_2 \\
\sigma_3 &= \tan^{-1}((\mu + a_4\sin(q_2+q_4))/(\lambda + a_4\cos(q_2+q_4)) - q_1 \\
\sigma_4 &= \pm\tan^{-1}(\sqrt{\bar{A}^2+\bar{B}^2-\bar{C}^2}/\bar{C}) + \tan^{-1}(\bar{B}/\bar{A}) - q_2
\end{aligned}
$$

with

$$
\begin{aligned}
\bar{A} &= 2a_4\lambda \\
\bar{B} &= 2a_4\mu \\
\bar{C} &= a_3^2 - a_4^2 - \lambda^2 - \mu^2 \\
\lambda &= a_2\cos(q_2) - a_1\cos(q_1) + c \\
\mu &= a_2\sin(q_2) - a_1\sin(q_1)
\end{aligned}
$$

It should be noted that the reduced model is an implicit model since the parameterization $q' = \sigma(q)$ is implicit, and it is only valid locally due to the presence of singularity.

The parameter values for the parallel robot built for the experiments are shown in Table

2-1.The distance between the two motor shafts is $c = 0.4240$ m.

Table 2-1. Link Parameters

Link i	m_i (kg)	a_i (m)	l_i (m)	I_i (kg·m^2)
1	0.1950	0.4600	0.3367	4.567×10^{-3}
2	0.1950	0.4600	0.3367	4.567×10^{-3}
3	0.2538	0.4600	0.2400	8.626×10^{-3}
4	0.2538	0.4600	0.2400	8.626×10^{-3}

The nominal values of the unknown parameters, Θ_n, can be calculated based on Table 2-1 as follows:

$$\Theta_n = \begin{bmatrix} 0.0804 & 0.0804 & 0.0232 & 0.0232 & 0.0280 & 0.0280 & 1.7894 & 1.7894 & 0.5975 & 0.5975 \end{bmatrix} \tag{2.18}$$

2.2 Inverse Kinematics

The inverse kinematics is needed to ensure that the end effector can track different trajectories in non-singular region. Let (x, y) represent coordinates of the end effector defined in Fig. 2-2 where the range of q_i is defined from $-\pi$ to π. Then, the link angles q_1, q_2, q_3, q_4 can be determined by using the inverse kinematics. From Fig. 2-2, the following equations can be obtained:

$$x = a_1 \cos(q_1) + a_3 \cos(q_1 + q_3) - \frac{c}{2} \tag{2.19}$$

$$y = a_1 \sin(q_1) + a_3 \sin(q_1 + q_3) \tag{2.20}$$

$$x = a_2 \cos(q_2) + a_4 \cos(q_2 + q_4) + \frac{c}{2} \tag{2.21}$$

$$y = a_2 \sin(q_2) + a_4 \sin(q_2 + q_4) \tag{2.22}$$

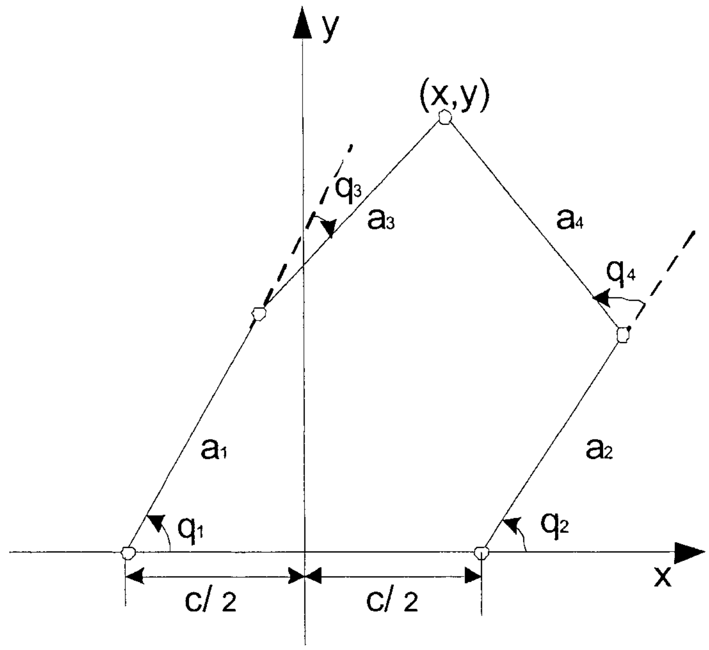

Figure 2-2: The coordinates defined for the inverse kinematics investigation.

Then the region of the possible positions of the end effector is shown in Fig. 2-3 and the singular points are also shown in this figure, which satisfy $det\left[\psi_{q'}(q')\right] = \sin(q_1 + q_3 - q_2 - q_4) = 0$. Those trajectories in the reachable region without crossing or approaching the singular points are possible to be tracked, which means that $q_1 + q_3 - q_2 - q_4 \neq n\pi$ with an integer n. The reachable region is shown in the shaded area A in Fig. 2-3.

With the position of the end effector known, the link angles q_i can be determined by using inverse kinematics. As a matter of fact, summing the squares of Eq. (2.19) and Eq. (2.20) yields

$$\left(x + \frac{c}{2}\right)^2 + y^2 = a_1^2 + a_3^2 + 2a_1a_3\cos(q_3) \tag{2.23}$$

Solving Eq. (2.23) for q_3 gives

$$q_3 = \pm\cos^{-1}\left(\frac{\left(x + \frac{c}{2}\right)^2 + y^2 - a_1^2 - a_3^2}{2a_1a_3}\right) \tag{2.24}$$

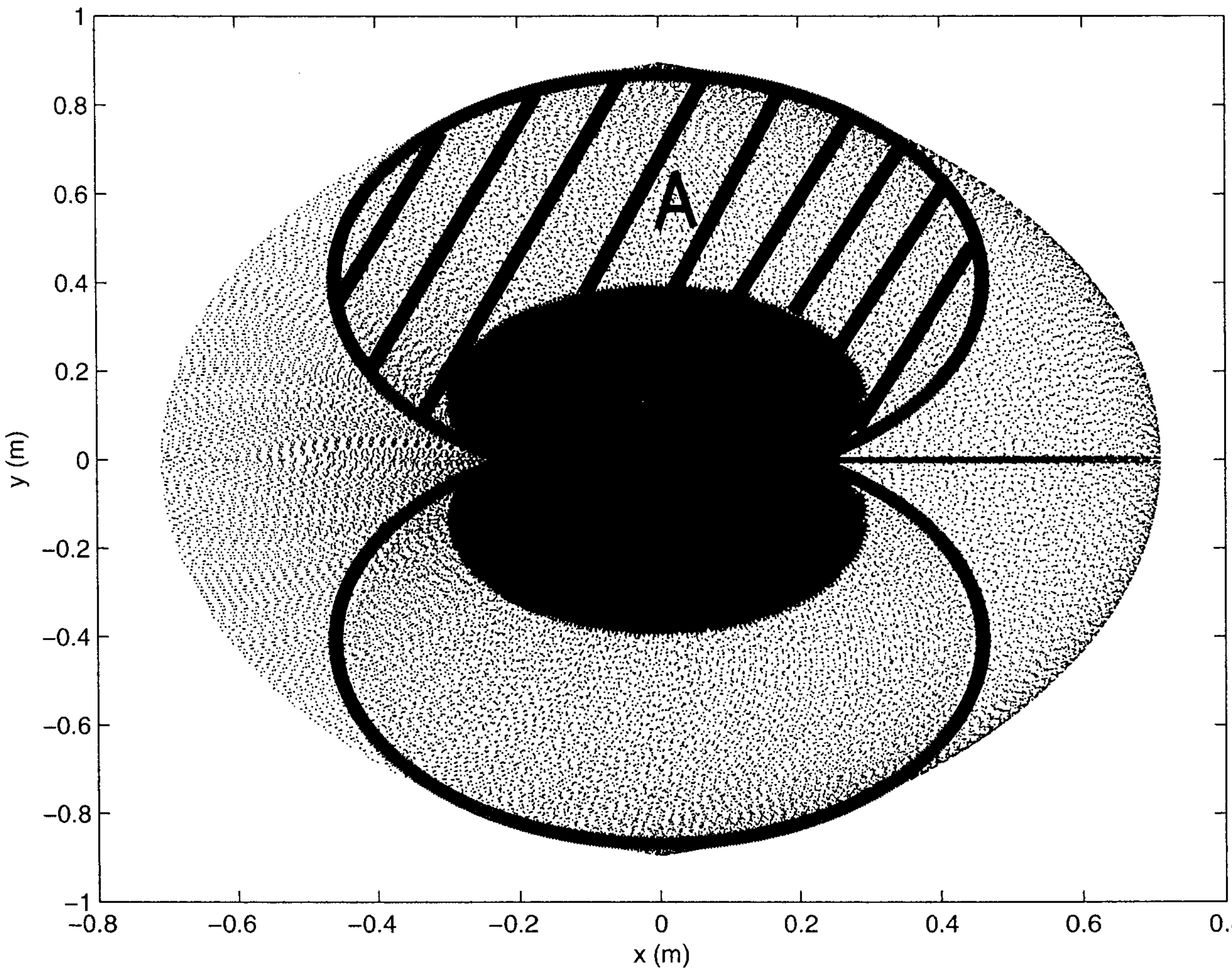

Figure 2-3: The reachable region of the end effector and the singular points. Dotted area — reachable region, solid area — singular region, shaded area A — the region of interest.

With the similar procedure, from Eq. (2.21) and Eq. (2.22), q_4 can be obtained as

$$q_4 = \pm \cos^{-1}\left(\frac{\left(x - \frac{c}{2}\right)^2 + y^2 - a_2^2 - a_4^2}{2a_2a_4}\right) \tag{2.25}$$

Since q_1 and q_2 are in $[0, \pi]$, $\sin(q_1)$ and $\sin(q_2)$ should be positive and determined by

$$\begin{aligned} \sin(q_1) &= \sqrt{1 - \cos^2(q_1)} && (2.26) \\ \sin(q_2) &= \sqrt{1 - \cos^2(q_2)} && (2.27) \end{aligned}$$

Substitute Eq. (2.26), Eq. (2.27) into Eq. (2.19), Eq. (2.21) separately and take square of both sides of the equations to get

$$\begin{aligned} \bar{A}_{13}\cos^2(q_1) + \bar{B}_{13}\cos(q_1) + \bar{C}_{13} &= 0 && (2.28) \\ \bar{A}_{24}\cos^2(q_2) + \bar{B}_{24}\cos(q_2) + \bar{C}_{24} &= 0 && (2.29) \end{aligned}$$

where

$$\begin{aligned} \bar{A}_{13} &= a_1^2 + a_3^2 + 2a_1a_3\cos(q_3) \\ \bar{B}_{13} &= -2\left(x + \frac{c}{2}\right)(a_1 + a_3\cos(q_3)) \\ \bar{C}_{13} &= \left(x + \frac{c}{2}\right)^2 - a_3^2\sin^2(q_3) \\ \bar{A}_{24} &= a_2^2 + a_4^2 + 2a_2a_4\cos(q_4) \\ \bar{B}_{24} &= -2\left(x - \frac{c}{2}\right)(a_2 + a_4\cos(q_4)) \\ \bar{C}_{24} &= \left(x - \frac{c}{2}\right)^2 - a_4^2\sin^2(q_4) \end{aligned}$$

Finally solving Eq. (2.28) and (2.29) for q_1 and q_2 produces

$$\begin{aligned} q_1 &= \cos^{-1}\left(\frac{-\bar{B}_{13} \pm \sqrt{\bar{B}_{13}^2 - 4\bar{A}_{13}\bar{C}_{13}}}{2\bar{A}_{13}}\right) && (2.30) \\ q_2 &= \cos^{-1}\left(\frac{-\bar{B}_{24} \pm \sqrt{\bar{B}_{24}^2 - 4\bar{A}_{24}\bar{C}_{24}}}{2\bar{A}_{24}}\right) && (2.31) \end{aligned}$$

Chapter 3

Adaptive Set Point Control

3.1 Controller Design

3.1.1 Adaptive Backstepping Controller Design

In order to formulate Eq. (2.8) into a form suitable for set point control using the adaptive backstepping technique, assign $x_1 = q_1 - q_1^d$, $x_2 = q_2 - q_2^d$, $x_3 = \dot{q}_1$, $x_4 = \dot{q}_2$ with q_1^d and q_2^d being the desired angles for q_1 and q_2, respectively. Let $\hat{\Theta}$ be the estimation of Θ. A lower triangular form is obtained as:

$$\dot{x}_1 = x_3 \tag{3.1}$$

$$\dot{x}_2 = x_4 \tag{3.2}$$

$$D(q') \begin{bmatrix} \dot{x}_3 \\ \dot{x}_4 \end{bmatrix} = u - C\dot{q} - g(q') \tag{3.3}$$

Following the backstepping design procedure, first, choose the Lyapunov function candidate:

$$V_1 = \frac{1}{2}x_1^2 + \frac{1}{2}x_2^2 \tag{3.4}$$

By introducing virtual controllers: $\alpha_1 = -c_1 x_1$, $\alpha_2 = -c_2 x_2$, where c_1 and c_2 are positive numbers, $\dot{V}_1$ can be rewritten into:

$$\dot{V}_1 = -c_1 x_1^2 - c_2 x_2^2 + x_1(x_3 - \alpha_1) + x_2(x_4 - \alpha_2)$$

Now, choose the Lyapunov function candidate:

$$V_2 = V_1 + \frac{1}{2}\begin{bmatrix} x_3 - \alpha_1 \\ x_4 - \alpha_2 \end{bmatrix}^T D \begin{bmatrix} x_3 - \alpha_1 \\ x_4 - \alpha_2 \end{bmatrix} + \frac{1}{2}\left(\Theta - \hat{\Theta}\right)^T \Gamma \left(\Theta - \hat{\Theta}\right) \tag{3.5}$$

where Γ =diag$\begin{bmatrix} \gamma_1 & \gamma_2 & \cdots & \gamma_{10} \end{bmatrix}$ is a positive definite matrix. Note that D is positive definite. Differentiating V_2 with respect to time yields:

$$\begin{aligned} \dot{V}_2 &= -c_1 x_1^2 - c_2 x_2^2 + x_1(x_3 - \alpha_1) + x_2(x_4 - \alpha_2) \\ &+ \begin{bmatrix} x_3 - \alpha_1 \\ x_4 - \alpha_2 \end{bmatrix}^T D \begin{bmatrix} \dot{x}_3 - \dot{\alpha}_1 \\ \dot{x}_4 - \dot{\alpha}_2 \end{bmatrix} + \frac{1}{2}\begin{bmatrix} x_3 - \alpha_1 \\ x_4 - \alpha_2 \end{bmatrix}^T \dot{D} \begin{bmatrix} x_3 - \alpha_1 \\ x_4 - \alpha_2 \end{bmatrix} \\ &- \dot{\hat{\Theta}}^T \Gamma \left(\Theta - \hat{\Theta}\right) \end{aligned} \tag{3.6}$$

As pointed out in [9], the matrix $\dot{D} - 2C$ is skew symmetric. As a result, we can have:

$$\frac{1}{2}\begin{bmatrix} x_3 - \alpha_1 \\ x_4 - \alpha_2 \end{bmatrix}^T \left(\dot{D}(q') - 2C(q', \dot{q}')\right) \begin{bmatrix} x_3 - \alpha_1 \\ x_4 - \alpha_2 \end{bmatrix} = 0 \tag{3.7}$$

Substituting (3.3), (2.17) and (3.7) into (3.6) yields:

$$\dot{V}_2 = -c_1 x_1^2 - c_2 x_2^2 + \begin{bmatrix} x_3 - \alpha_1 \\ x_4 - \alpha_2 \end{bmatrix}^T \left(u + \begin{bmatrix} x_1 \\ x_2 \end{bmatrix} + \Lambda\right) - \dot{\hat{\Theta}}^T \Gamma \left(\Theta - \hat{\Theta}\right) \tag{3.8}$$

where $\Lambda = \Lambda_o \Theta$ with

$$\Lambda_o = -\begin{bmatrix} \dot{\alpha}_1 D_{o11} + \dot{\alpha}_2 D_{o12} + \alpha_1 C_{o11} + \alpha_2 C_{o12} + g_{o1} \\ \dot{\alpha}_1 D_{o21} + \dot{\alpha}_2 D_{o22} + \alpha_1 C_{o21} + \alpha_2 C_{o22} + g_{o2} \end{bmatrix} \tag{3.9}$$

Apparently, if the controller is chosen to be:

$$u = \begin{bmatrix} u_1 \\ u_2 \end{bmatrix} = -\begin{bmatrix} c_3\left(x_3 - \alpha_1\right) + x_1 \\ c_4\left(x_4 - \alpha_2\right) + x_2 \end{bmatrix} - \Lambda_o \cdot \hat{\Theta} \tag{3.10}$$

and the unknown parameters' updating law is chosen to be:

$$\dot{\hat{\Theta}} = \Gamma^{-1}\Lambda_o^T \begin{bmatrix} x_3 - \alpha_1 \\ x_4 - \alpha_2 \end{bmatrix} \tag{3.11}$$

where c_3 and c_4 are positive numbers, the derivative of V_2 is negative semi-definite, that is,

$$\dot{V}_2 = -c_1 x_1^2 - c_2 x_2^2 - c_3(x_3 - \alpha_1)^2 - c_4(x_4 - \alpha_2)^2 \tag{3.12}$$

which means that the corresponding closed-loop system is stable.

The corresponding non-adaptive controller based on backstepping technique, namely BS, can be obtained by letting $\hat{\Theta} = \Theta$, thus the control effort u satisfy

$$u = \begin{bmatrix} u_1 \\ u_2 \end{bmatrix} = -\begin{bmatrix} c_3\left(x_3 - \alpha_1\right) + x_1 \\ c_4\left(x_4 - \alpha_2\right) + x_2 \end{bmatrix} - \Lambda$$

3.1.2 Adaptive PD Controller Design

It is worthwhile comparing the controller of Eq. (3.10) with an adaptive PD controller. Choose the Lyapunov function candidate:

$$V = \frac{1}{2}\left(q - q^d\right)^T K_p \left(q - q^d\right) + \frac{1}{2}\dot{q}^T D \dot{q} + \frac{1}{2}\left(\Theta_{pd} - \hat{\Theta}_{pd}\right)^T \Gamma_{pd}\left(\Theta_{pd} - \hat{\Theta}_{pd}\right) \tag{3.13}$$

with positive definite matrices $K_p = \text{diag}\begin{bmatrix} k_{p1} & k_{p2} \end{bmatrix}$ and $\Gamma_{pd} = \text{diag}\begin{bmatrix} \gamma_{pd1} & \gamma_{pd2} & \cdots & \gamma_{pd8} \end{bmatrix}$, and $\Theta_{pd} = \begin{bmatrix} \theta_3 & \theta_4 & \cdots & \theta_{10} \end{bmatrix}$. Differentiating V with respect to time yields:

$$\dot{V} = \left(q - q^d\right)^T K_p \dot{q} + \frac{1}{2}\dot{q}^T \dot{D} \dot{q} + \dot{q}^T D \ddot{q} - \dot{\hat{\Theta}}_{pd}^T \Gamma_{pd}\left(\Theta_{pd} - \hat{\Theta}_{pd}\right) \tag{3.14}$$

According to [9] $\dot{D} - 2C$ is skew symmetric, and $\dot{D}$ is symmetric. So we can get:

$$\dot{D} = C + C^T \tag{3.15}$$

Substitute (3.3), (2.17) and (3.15) into (3.14) to get:

$$\dot{V} = \left(q - q^d\right)^T K_p \dot{q} + \dot{q}^T \left[u + \Lambda_{pd}\right] - \dot{\hat{\Theta}}_{pd}^T \Gamma_{pd} \left(\Theta_{pd} - \hat{\Theta}_{pd}\right) \tag{3.16}$$

where $\Lambda_{pd} = \Lambda_{pdo}\Theta_{pd}$ with $\Lambda_{pdo} = \frac{1}{2}\begin{bmatrix} \dot{q}_2(C_{o21} - C_{o12}) - g_{o1} \\ \dot{q}_1(C_{o12} - C_{o21}) - g_{o2} \end{bmatrix}$.

Apparently, if the controller is chosen to be:

$$u = \begin{bmatrix} u_1 \\ u_2 \end{bmatrix} = -K_v \cdot \dot{q} - K_p\left(q - q_d\right) - \Lambda_{pdo} \cdot \hat{\Theta}_{pd} \tag{3.17}$$

and the unknown parameters' updating law is chosen to be:

$$\dot{\hat{\Theta}}_{pd} = \Gamma_{pd}^{-1} \Lambda_{pdo}^T \dot{q} \tag{3.18}$$

where $K_v = diag\begin{bmatrix} k_{v1} & k_{v2} \end{bmatrix}$ is a positive definite matrix, the derivative of V is negative semi-definite, i.e.,

$$\dot{V} = -\dot{q}^T K_v \dot{q} \tag{3.19}$$

which means that the corresponding closed-loop system is stable.

The corresponding non-adaptive PD controller with compensation terms, namely PD, can also be gained by letting $\hat{\Theta}_{pd} = \Theta_{pd}$, thus the control effort u satisfy

$$u = \begin{bmatrix} u_1 \\ u_2 \end{bmatrix} = -K_v \cdot \dot{q} - K_p\left(q - q_d\right) - \Lambda_{pd}$$

It is worthwhile to note that the dimension of Θ_{pd} is two less than that of Θ, so the adaptive PD controller needs two less unknown parameter estimators than the adaptive backstepping controller. As a result, the adaptive PD controller is less complex and needs less computation

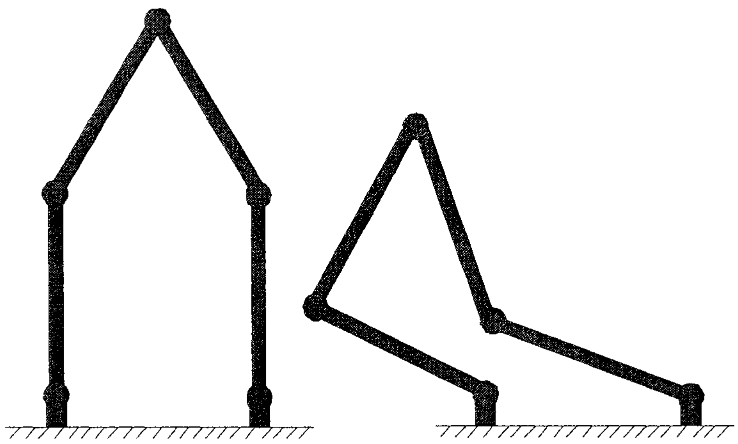

Figure 3-1: Configurations 1 and 2

time than the adaptive backstepping controller.

3.2 Simulation Results

Fig. 3-1 shows two configurations of the robot. It is not difficult to check when the robot moves from configuration one to configuration two and back to configuration, the robot does not enter singularity region. Simulation on controlling the robot from configuration one to configuration two and back to configuration one is carried out.

The initial values of the unknown parameters Θ for set point control based on adaptive backstepping are set to

$$\Theta(0) = \left[\begin{array}{cccccccccc} 0.1 & 0.1 & 0.1 & 0.1 & 0.1 & 0.1 & 1 & 1 & 1 & 1 \end{array}\right]$$

instead of its nominal value Θ_n while $\Theta_{pd}(0)$ is given by

$$\Theta_{pd}(0) = \left[\begin{array}{cccccccc} 0.1 & 0.1 & 0.1 & 0.1 & 1 & 1 & 1 & 1 \end{array}\right]$$

instead of its nominal value

$$\Theta_{pdn} = \begin{bmatrix} 0.0232 & 0.0232 & 0.0280 & 0.0280 & 1.7894 & 1.7894 & 0.5975 & 0.5975 \end{bmatrix}$$

Fig. 3-2 to Fig. 3-4 show the simulation results for the adaptive backstepping controller with $\gamma_i = 30$, $i = 1$ to 7, $\gamma_8 = 60$, $\gamma_9 = 150$, and $\gamma_{10} = 150$. The gains c_1, c_2, c_3, c_4 are adjusted by trial and error in order to obtain better control performances.

Case 1: Fig. 3-2 shows the results with gains of c_1, $c_2 = 3$ and c_3, $c_4 = 10$.

Case 2: Fig. 3-3 shows the results with gains of c_1, $c_2 = 30$ and c_3, $c_4 = 1$.

Case 3: Fig. 3-4 shows the results with gains of c_1, $c_2 = 2.1$ and c_3, $c_4 = 7.2$.

The adaptive PD controller is simulated with $\gamma_{pdi} = 10$, $i = 1$ to 8. The gains k_{pi}, k_{vi}, $i = 1, 2$ are selected according to a standard second order system characteristics, that is, $k_{pi} = \omega_n^2$ and $k_{vi} = 2\zeta\omega_n$ where ζ is the damping ratio and ω_n is the natural frequency.

Case 1: Fig. 3-5 shows the results with gains of $k_{pi} = 31$ $k_{vi} = 10, i = 1, 2$.

Case 2: Fig. 3-6 shows the results with gains of $k_{pi} = 31$ $k_{vi} = 1, i = 1, 2$.

Case 3: Fig. 3-7 shows the results with gains of $k_{pi} = 16$ $k_{vi} = 7.2, i = 1, 2$.

It is not difficult to see that for both adaptive controllers Case 2 is much more underdamping than Case 1, which results in obvious oscillations during the transient process even though the response is much quicker than other two cases. For each case the steady state errors are listed in Table 3-1 corresponding to the movements from Configuration 1 to 2 (downward), and Configuration 2 to 1 (upward), respectively, in which ABS stands for adaptive backstepping controller, and APD represents adaptive PD controller. It can be seen that there exist larger steady state errors in Case 3 for both controllers due to smaller proportional gains. In summary, the controller gains provided in Case 1 produce the best control performances.

Table 3-1 Steady State Error For Downward (D) and Upward (U) Movement

		q_1		q_2	
Movement	Case Number	ABS	APD	ABS	APD
D	1	-1.400	**-1.509**	-1.128	**-1.290**
D	2	**-1.002**	**-1.509**	**-1.004**	**-1.290**
D	3	-2.697	-2.528	-2.169	-2.528
U	1	**0.386**	**0.389**	**-0.386**	**-0.388**
U	2	0.393	**0.389**	-0.394	**-0.388**
U	3	0.746	0.758	-0.746	-0.757

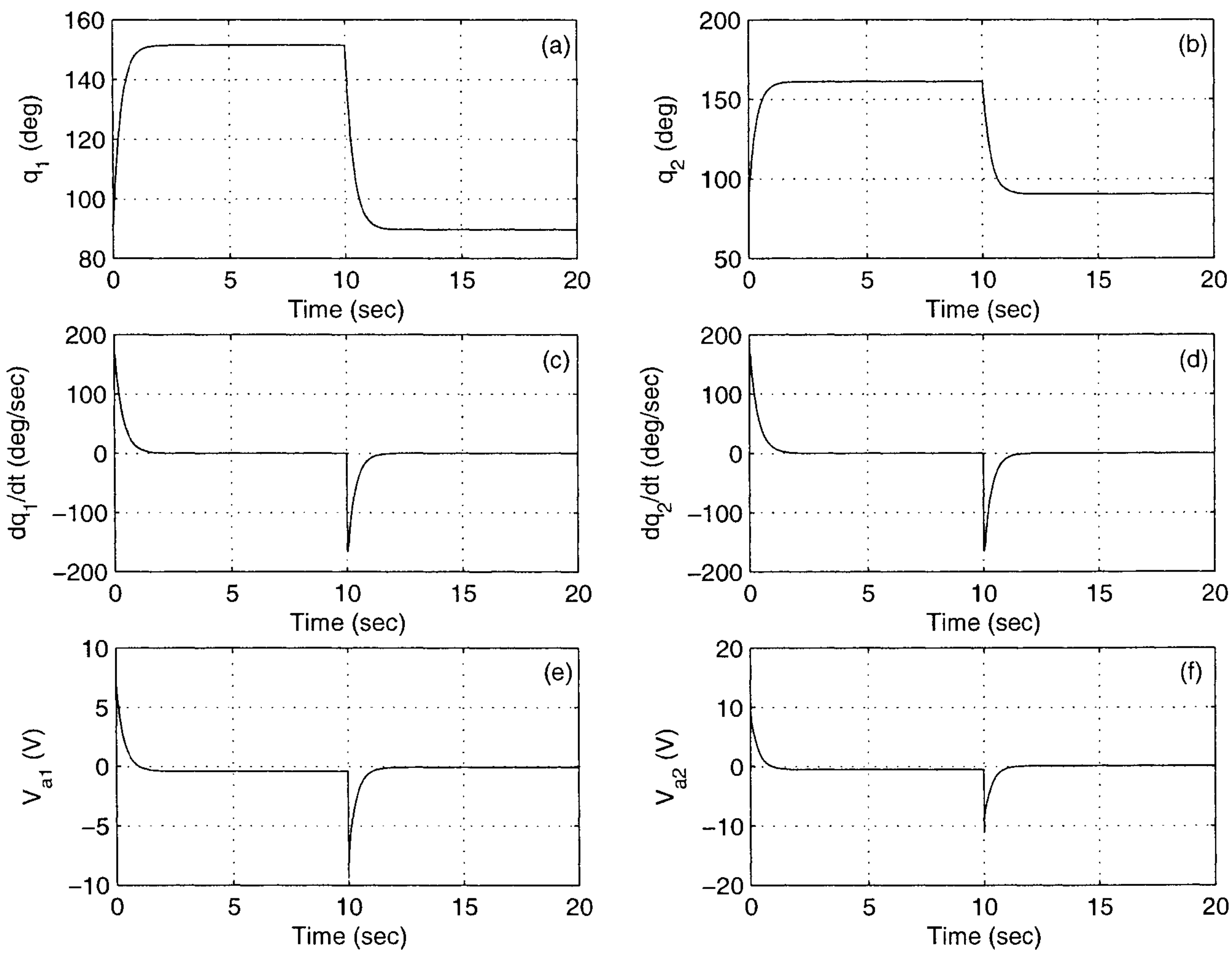

Figure 3-2: The simulation results for set point control based on the ABS in Case 1. (a) q_1, (b) q_2, (c) dq_1/dt, (d) dq_2/dt, (e) Va_1, and (f) Va_2

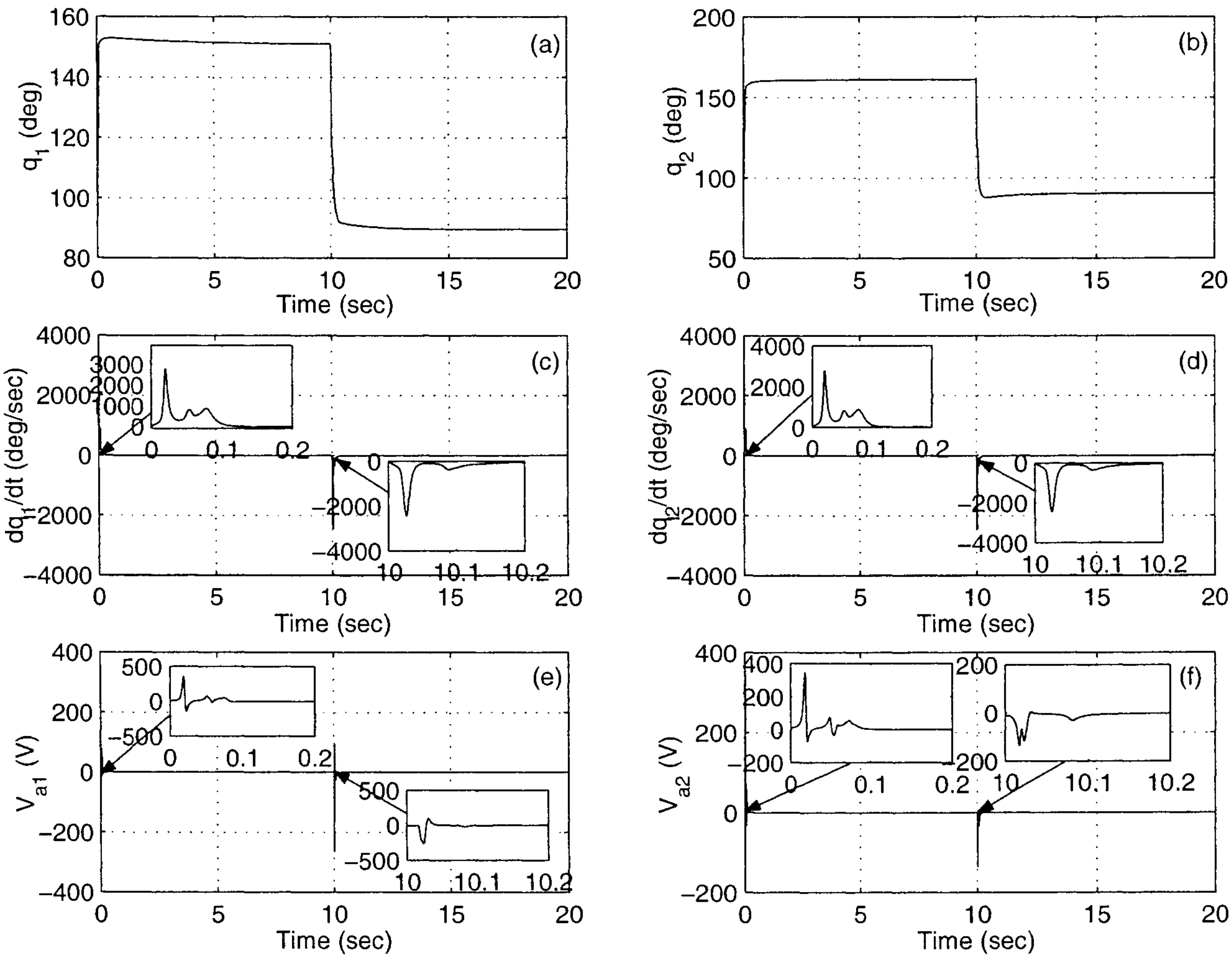

Figure 3-3: The simulation results for set point control based on the ABS in Case 2. (a) q_1, (b) q_2, (c) dq_1/dt, (d) dq_2/dt, (e) Va_1, and (f) Va_2

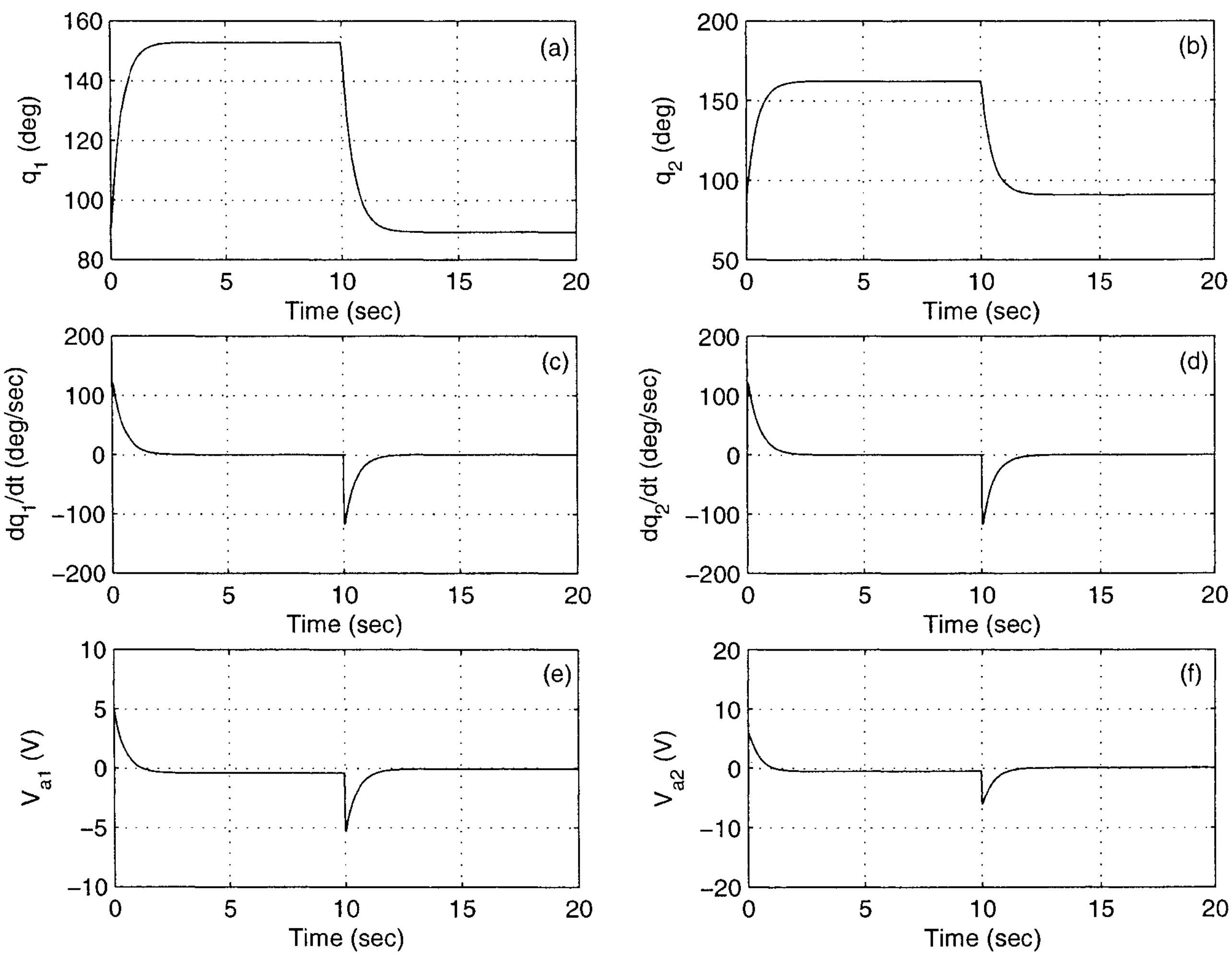

Figure 3-4: The simulation results for set point control based on the ABS in Case 3. (a) q_1, (b) q_2, (c) dq_1/dt, (d) dq_2/dt, (e) Va_1, and (f) Va_2

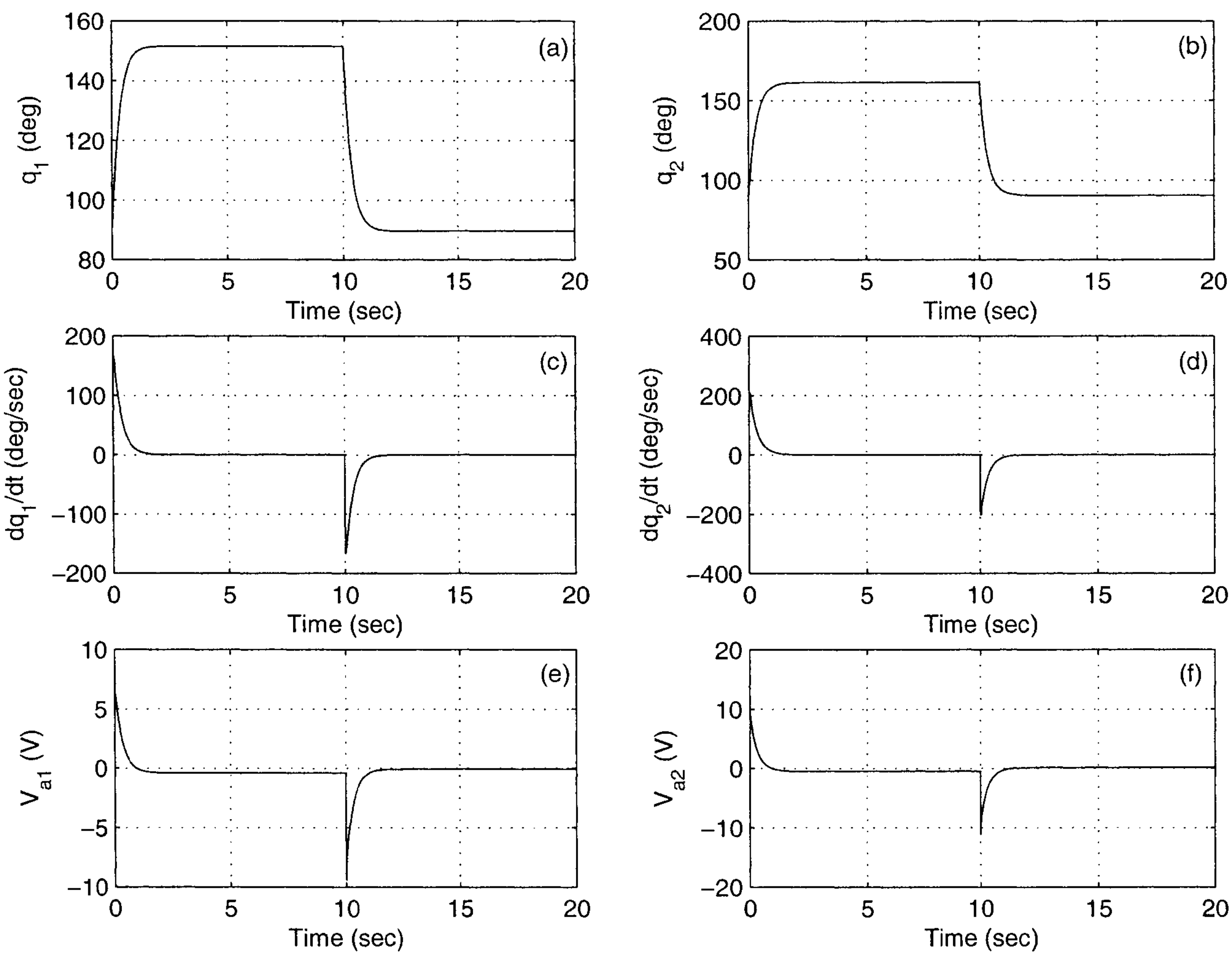

Figure 3-5: The simulation results for set point control based on the APD in Case 1. (a) q_1, (b) q_2, (c) dq_1/dt, (d) dq_2/dt, (e) Va_1, and (f) Va_2

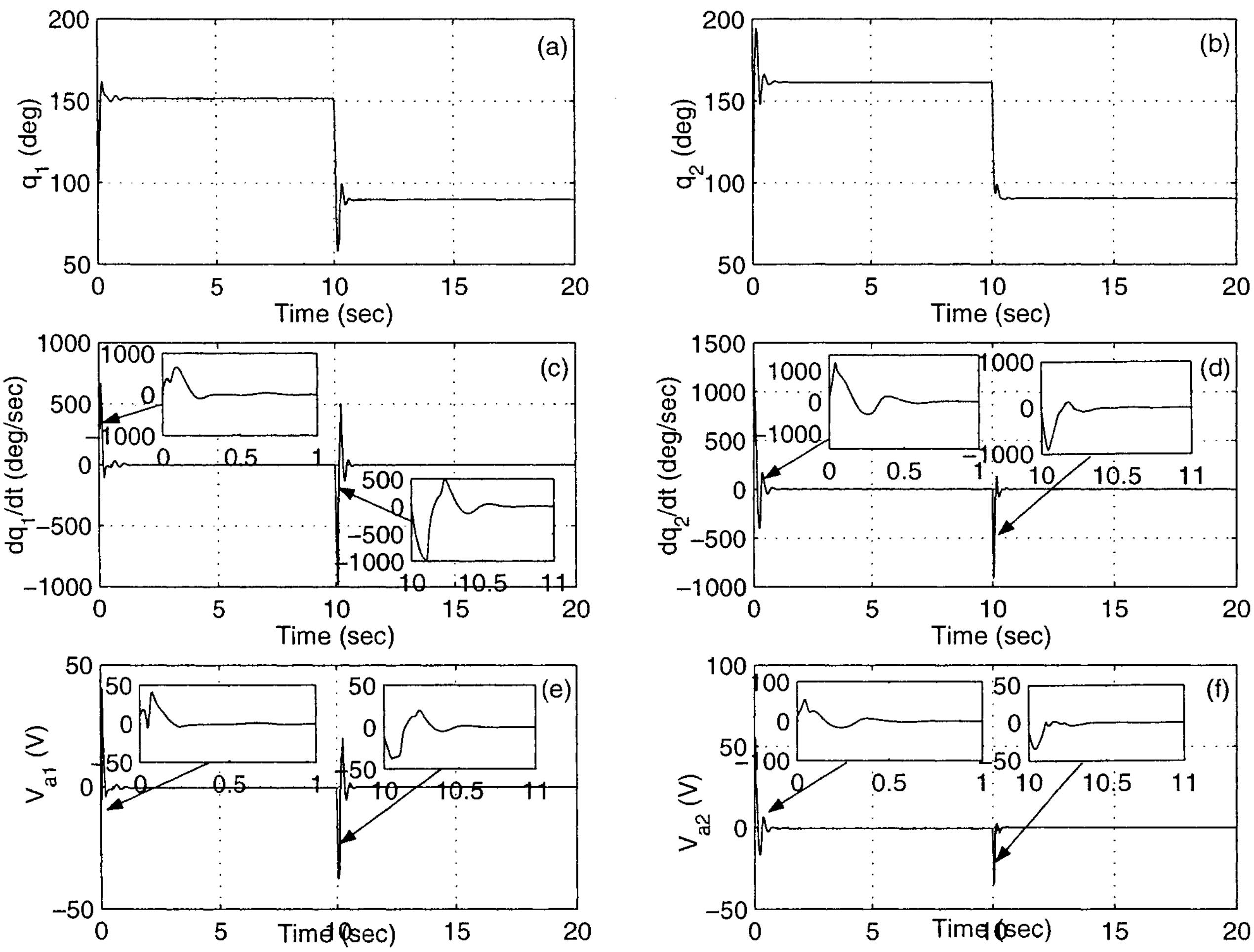

Figure 3-6: The simulation results for set point control based on the APD in Case 2. (a) q_1, (b) q_2, (c) dq_1/dt, (d) dq_2/dt, (e) Va_1, and (f) Va_2

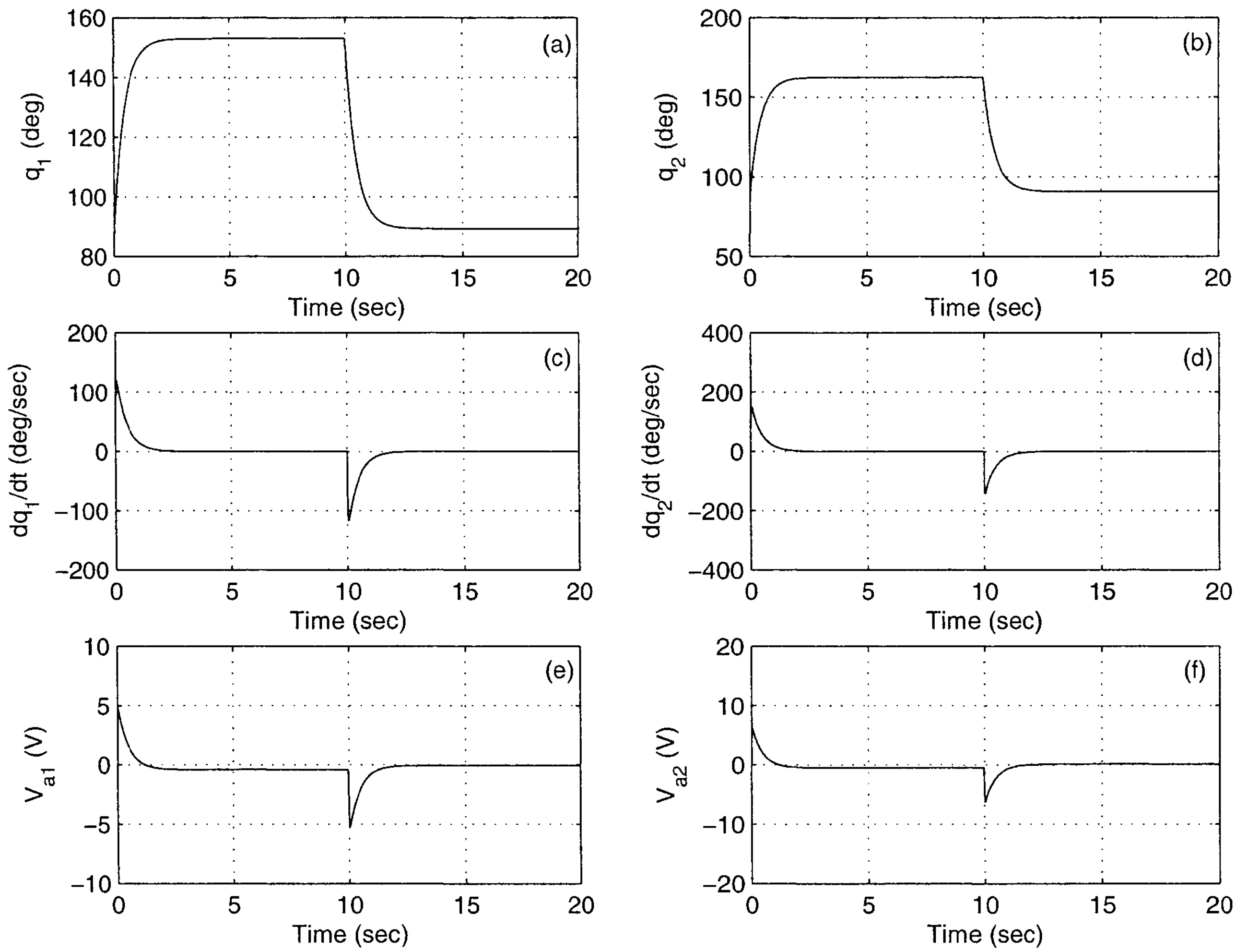

Figure 3-7: The simulation results for set point control based on the APD in Case 3. (a) q_1, (b) q_2, (c) dq_1/dt, (d) dq_2/dt, (e) Va_1, and (f) Va_2

Chapter 4

Adaptive Tracking Control

4.1 Controller Design

In this section, two adaptive controllers are designed: adaptive backstepping controller and adaptive PD controller, to achieve the tracking control. Each controller consists of a control law and an update law for the parameter estimation.

4.1.1 Adaptive Backstepping Controller Design

In order to change Eq. (2.8) into a form suitable for tracking control using the non-adaptive backstepping technique, set $x_1 = q_1 - q_1^d$, $x_2 = q_2 - q_2^d$, $x_3 = \dot{q}_1 - \dot{q}_1^d$, $x_4 = \dot{q}_2 - \dot{q}_2^d$ with q_1^d, q_2^d being the desired angles of q_1, q_2, $\dot{q}_1^d$, $\dot{q}_2^d$ being the desired angular velocities of q_1, q_2, $\ddot{q}_1^d$, $\ddot{q}_2^d$ being the desired angular accelerations of q_1, q_2, respectively. A lower triangular form is obtained as:

$$\dot{x}_1 = x_3 \tag{4.1}$$

$$\dot{x}_2 = x_4 \tag{4.2}$$

$$\begin{bmatrix} \dot{x}_3 \\ \dot{x}_4 \end{bmatrix} = D^{-1}(q')\left(u - C(q',\dot{q}')\,\dot{q} - g(q')\right) - \begin{bmatrix} \ddot{q}_1^d \\ \ddot{q}_2^d \end{bmatrix} \tag{4.3}$$

Based on the lower triangular form shown by Eqs. (4.1), (4.2), and (4.3), and following the backstepping design procedure, first, choose the Lyapunov function candidate:

$$\bar{V}_1 = \frac{1}{2}x_1^2 + \frac{1}{2}x_2^2 \tag{4.4}$$

By introducing virtual controllers: $\alpha_1 = -c_1 x_1$, $\alpha_2 = -c_2 x_2$, where c_1 and c_2 are positive numbers, $\dot{\bar{V}}_1$ can be rewritten into:

$$\dot{\bar{V}}_1 = -c_1 x_1^2 - c_2 x_2^2 + x_1 (x_3 - \alpha_1) + x_2 (x_4 - \alpha_2) \tag{4.5}$$

Let $\hat{\Theta}$ be the estimation of Θ, and choose the second Lyapunov function candidate:

$$\bar{V}_2 = \bar{V}_1 + \frac{1}{2}\begin{bmatrix} x_3 - \alpha_1 \\ x_4 - \alpha_2 \end{bmatrix}^T D(q') \begin{bmatrix} x_3 - \alpha_1 \\ x_4 - \alpha_2 \end{bmatrix} + \frac{1}{2}\left(\Theta - \hat{\Theta}\right)^T \Gamma \left(\Theta - \hat{\Theta}\right) \tag{4.6}$$

where $\Gamma = \text{diag}\begin{bmatrix} \gamma_1 & \gamma_2 & \cdots & \gamma_{10} \end{bmatrix}$ is a positive definite matrix with design parameters γ_i, $i = 1, ..., 10$. Note that $D(q')$ is positive definite. Differentiating $\bar{V}_2$ with respect to time yields:

$$\begin{aligned} \dot{\bar{V}}_2 &= -c_1 x_1^2 - c_2 x_2^2 + x_1 (x_3 - \alpha_1) + x_2 (x_4 - \alpha_2) \\ &+ \begin{bmatrix} x_3 - \alpha_1 \\ x_4 - \alpha_2 \end{bmatrix}^T D(q') \begin{bmatrix} \dot{x}_3 - \dot{\alpha}_1 \\ \dot{x}_4 - \dot{\alpha}_2 \end{bmatrix} + \frac{1}{2}\begin{bmatrix} x_3 - \alpha_1 \\ x_4 - \alpha_2 \end{bmatrix}^T \dot{D}(q', \dot{q}') \begin{bmatrix} x_3 - \alpha_1 \\ x_4 - \alpha_2 \end{bmatrix} \\ &- \dot{\hat{\Theta}}^T \Gamma \left(\Theta - \hat{\Theta}\right) \end{aligned} \tag{4.7}$$

According to [9] the matrix $\dot{D} - 2C$ is skew symmetric, we have:

$$\frac{1}{2}\begin{bmatrix} x_3 - \alpha_1 \\ x_4 - \alpha_2 \end{bmatrix}^T \left(\dot{D}(q', \dot{q}') - 2C(q', \dot{q}')\right) \begin{bmatrix} x_3 - \alpha_1 \\ x_4 - \alpha_2 \end{bmatrix} = 0 \tag{4.8}$$

Substituting (2.17), (4.3) and (4.8) into (4.7) yields:

$$\dot{\bar{V}}_2 = -c_1 x_1^2 - c_2 x_2^2 + \begin{bmatrix} x_3 - \alpha_1 \\ x_4 - \alpha_2 \end{bmatrix}^T \left(u + \begin{bmatrix} x_1 \\ x_2 \end{bmatrix} + \Lambda\right) - \dot{\hat{\Theta}}^T \Gamma \left(\Theta - \hat{\Theta}\right) \tag{4.9}$$

where $\Lambda = \Lambda_o \Theta$ with

$$\Lambda_o = -\left[\begin{array}{c} \left(\dot{\alpha}_1 + \ddot{q}_1^d\right) D_{o11} + \left(\dot{\alpha}_2 + \ddot{q}_2^d\right) D_{o12} + \left(\alpha_1 + \dot{q}_1^d\right) C_{o11} + \left(\alpha_2 + \dot{q}_2^d\right) C_{o12} + g_{o1} \\ \left(\dot{\alpha}_1 + \ddot{q}_1^d\right) D_{o21} + \left(\dot{\alpha}_2 + \ddot{q}_2^d\right) D_{o22} + \left(\alpha_1 + \dot{q}_1^d\right) C_{o21} + \left(\alpha_2 + \dot{q}_2^d\right) C_{o22} + g_{o2} \end{array} \right] \quad (4.10)$$

Apparently, if the controller is chosen to be:

$$u = \left[\begin{array}{c} u_1 \\ u_2 \end{array} \right] = - \left[\begin{array}{c} c_3 \left(x_3 - \alpha_1\right) + x_1 \\ c_4 \left(x_4 - \alpha_2\right) + x_2 \end{array} \right] - \Lambda_o \cdot \hat{\Theta} \quad (4.11)$$

and the unknown parameters' updating law is chosen to be:

$$\dot{\hat{\Theta}} = \Gamma^{-1} \Lambda_o^T \left[\begin{array}{c} x_3 - \alpha_1 \\ x_4 - \alpha_2 \end{array} \right] \quad (4.12)$$

where c_3 and c_4 are positive numbers, the derivative of $\bar{V}_2$ is negative semi-definite, that is,

$$\dot{\bar{V}}_2 = -c_1 x_1^2 - c_2 x_2^2 - c_3 \left(x_3 - \alpha_1\right)^2 - c_4 \left(x_4 - \alpha_2\right)^2 \quad (4.13)$$

which means that the corresponding closed-loop system is stable.

The corresponding non-adaptive controller based on backstepping technique can be obtained by letting $\hat{\Theta} = \Theta$, thus the control effort u satisfy

$$u = \left[\begin{array}{c} u_1 \\ u_2 \end{array} \right] = - \left[\begin{array}{c} c_3 \left(x_3 - \alpha_1\right) + x_1 \\ c_4 \left(x_4 - \alpha_2\right) + x_2 \end{array} \right] - \Lambda$$

4.1.2 Adaptive PD Controller Design

It is worthwhile comparing the controller of (4.11) with an adaptive PD controller. Choose the Lyapunov function candidate:

$$\bar{V} = \frac{1}{2} \left(q - q^d\right)^T K_p \left(q - q^d\right) + \frac{1}{2} \left(\dot{q} - \dot{q}_d\right)^T D\left(q'\right) \left(\dot{q} - \dot{q}_d\right) + \frac{1}{2} \left(\Theta - \hat{\Theta}\right)^T \Gamma_{pd} \left(\Theta - \hat{\Theta}\right) \quad (4.14)$$

with positive definite matrices $K_p = \text{diag}\begin{bmatrix} k_{p1} & k_{p2} \end{bmatrix}$ and $\Gamma_{pd} = \text{diag}\begin{bmatrix} \gamma_{pd1} & \cdots & \gamma_{pd10} \end{bmatrix}$. Differentiating $\bar{V}$ with respect to time yields:

$$\begin{aligned} \dot{\bar{V}} &= \left(q - q^d\right)^T K_p \left(\dot{q} - \dot{q}_d\right) + \frac{1}{2}\left(\dot{q} - \dot{q}_d\right)^T \dot{D}\left(q', \dot{q}'\right)\left(\dot{q} - \dot{q}_d\right) + \left(\dot{q} - \dot{q}_d\right)^T D\left(q'\right)\left(\ddot{q} - \ddot{q}_d\right) \\ &\quad - \dot{\hat{\Theta}}^T \Gamma_{pd}\left(\Theta - \hat{\Theta}\right) \end{aligned} \tag{4.15}$$

According to [9] $\dot{D} - 2C$ is skew symmetric. Thus we can get:

$$\frac{1}{2}\left(\dot{q} - \dot{q}_d\right)^T \left(\dot{D}\left(q', \dot{q}'\right) - 2C\left(q', \dot{q}'\right)\right)\left(\dot{q} - \dot{q}_d\right) = 0 \tag{4.16}$$

Substitute (2.17), (4.3) and (4.16) into (4.15) to get:

$$\dot{\bar{V}} = \left(q - q^d\right)^T K_p \left(\dot{q} - \dot{q}_d\right) + \left(\dot{q} - \dot{q}_d\right)^T \left(u + \Lambda_{pd}\right) - \dot{\hat{\Theta}}^T \Gamma_{pd}\left(\Theta - \hat{\Theta}\right) \tag{4.17}$$

where $\Lambda_{pd} = \Lambda_{pdo}\Theta$, with $\Lambda_{pdo} = -\begin{bmatrix} \ddot{q}_1^d D_{o11} + \ddot{q}_2^d D_{o12} + \dot{q}_1^d C_{o11} + \dot{q}_2^d C_{o12} + g_{o1} \\ \ddot{q}_1^d D_{o21} + \ddot{q}_2^d D_{o22} + \dot{q}_1^d C_{o21} + \dot{q}_2^d C_{o22} + g_{o2} \end{bmatrix}$.

Apparently, if the controller is chosen to be:

$$u = \begin{bmatrix} u_1 \\ u_2 \end{bmatrix} = -K_v \cdot \left(\dot{q} - \dot{q}_d\right) - K_p\left(q - q_d\right) - \Lambda_{pdo} \cdot \hat{\Theta} \tag{4.18}$$

and the unknown parameters' updating law is chosen to be:

$$\dot{\hat{\Theta}} = \Gamma_{pd}^{-1} \Lambda_{pdo}^T \left(\dot{q} - \dot{q}_d\right) \tag{4.19}$$

where $K_v = diag\begin{bmatrix} k_{v1} & k_{v2} \end{bmatrix}$ is a positive definite matrix, the derivative of $\bar{V}$ is negative semi-definite, i.e.,

$$\dot{\bar{V}} = -\left(\dot{q} - \dot{q}_d\right)^T K_v \left(\dot{q} - \dot{q}_d\right) \tag{4.20}$$

which means that the corresponding closed-loop system is stable.

The corresponding non-adaptive PD controller, can also be gained by letting $\hat{\Theta} = \Theta$, thus the control effort u satisfy

$$u = \begin{bmatrix} u_1 \\ u_2 \end{bmatrix} = -K_v \cdot (\dot{q} - \dot{q}_d) - K_p (q - q_d) - \Lambda_{pd}$$

4.2 Simulation Results

The two controllers ABS and APD were compared for tracking control by simulations. The desired trajectories to be tracked are circle, line, and square. The initial values of the unknown parameters Θ are set to $\Theta(0)$

$$\Theta(0) = \begin{bmatrix} 0.1 & 0.1 & 0.1 & 0.1 & 0.1 & 0.1 & 1 & 1 & 1 & 1 \end{bmatrix}$$

which are determined by introducing some deviations around the nominal values Θ_n in (2.18). Those non-adaptive controllers, BS and PD, perform similarly to ABS and APD, which are not shown in the thesis any more.

4.2.1 Circle Tracking

For the circular trajectory, the tracking speed is specified by the angular velocity $2\pi f$ with which the end effector is rotating about the center of the circle, where f is the tracking frequency of the end effector. The desired circle is centered at $(0, 0.85 - r)$ based on the coordinates defined in Fig. 2-2, where r is the radius of the circle. It can be checked that this circle does not contain any singular points and the area encompassed by the circle is at least 5 centimeters away from the singular region.

Fig. 4-1 to Fig. 4-6 show the results of tracking a circle with $r = 0.2\ m$ and $f = 0.2\ Hz$ based on the ABS controller with different gains c_i, $i = 1$ to 4.

Case 1: Fig. 4-1 and Fig. 4-4 show the results with gains of c_1, $c_2 = 20$ and c_3, $c_4 = 80$.

Case 2: Fig. 4-2 and Fig. 4-5 show the results with gains of c_1, $c_2 = 50$ and c_3, $c_4 = 32$.

Case 3: Fig. 4-3 and Fig. 4-6 show the results with gains of c_1, $c_2 = 10$ and c_3, $c_4 = 40$.

Similar to set point control, the gains for the adaptive PD controller are also selected based on the standard second order system characteristics, that is, $k_{pi} = \omega_n^2$ and $k_{vi} = 2\zeta\omega_n$.

Case 1: Fig. 4-7 and Fig. 4-10 show the results with gains of $k_{pi} = 1600$, $k_{vi} = 80, i = 1, 2$.

Case 2: Fig. 4-8 and Fig. 4-11 show the results with gains of $k_{pi} = 1600$, $k_{vi} = 32, i = 1, 2$.

Case 3: Fig. 4-9 and Fig. 4-12 show the results with gains of $k_{pi} = 400$, $k_{vi} = 40, i = 1, 2$.

By comparing Fig. 4-1, Fig. 4-2, and Fig. 4-3, it can be seen that the errors at the bottom of the circles in Case 2 are smaller than the other two cases, but the errors at the top of the circle are larger than Case 1 when the ABS controller is applied. Moreover, it follows from Fig. 4-7, Fig. 4-8, and Fig. 4-9 that for the adaptive PD controller, there are no noticeable differences between Case 1 and Case 2, but the errors in Case 3 is bigger than other cases.

The average 2-norm values of the tracking errors based on different controllers are listed in Table 4-1. It is seen that there exist larger errors in Case 3 for both controllers due to smaller gains. The best scenario is given by Case 1.

Table 4-1 Average 2-Norm of Tracking Error Based On ABS and APD

	q_1 (degree)		q_2 (degree)	
	ABS	APD	ABS	APD
Case 1	$\mathbf{0.864}\times10^{-3}$	$\mathbf{0.623}\times10^{-3}$	$\mathbf{1.304}\times10^{-3}$	$\mathbf{0.618}\times10^{-3}$
Case 2	1.608×10^{-3}	1.072×10^{-3}	2.352×10^{-3}	1.066×10^{-3}
Case 3	2.991×10^{-3}	3.149×10^{-3}	5.104×10^{-3}	3.101×10^{-3}

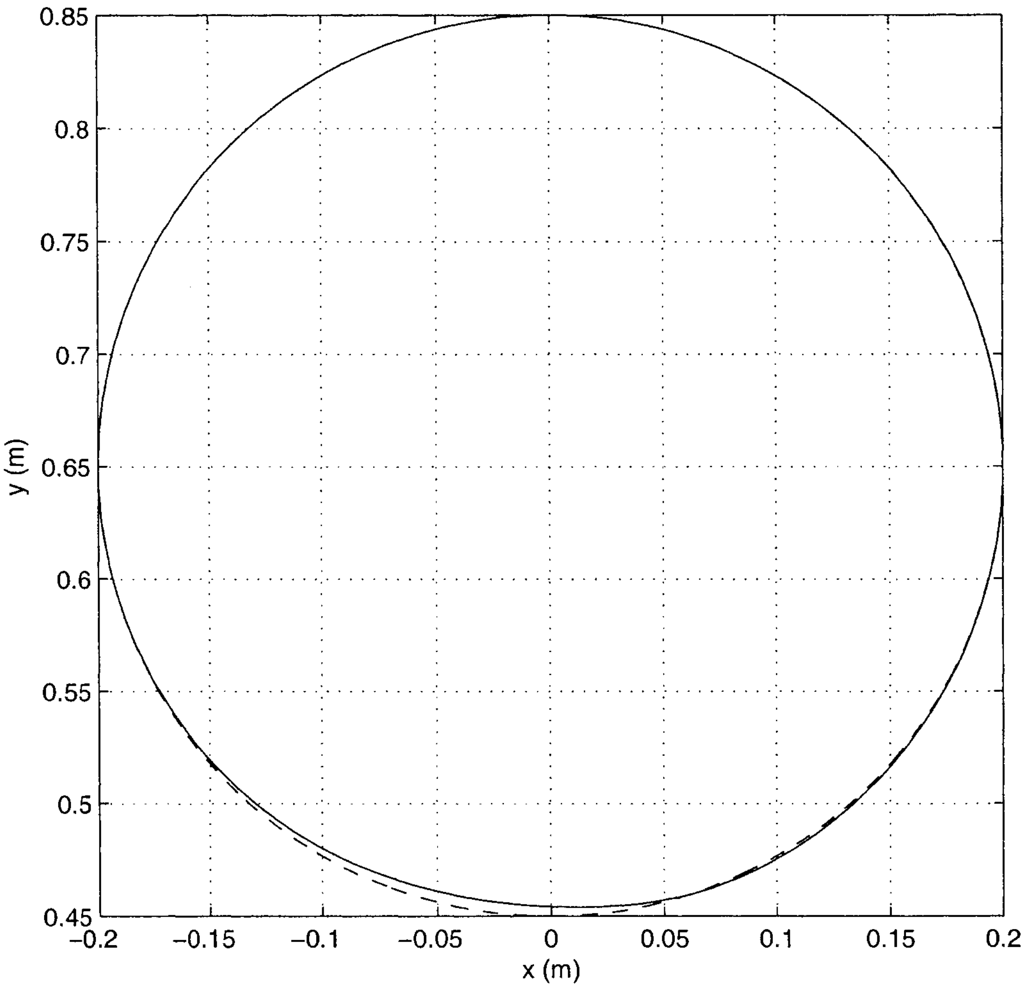

Figure 4-1: The end effector trajectory of tracking a circular trajectory in Case 1 based on the ABS in simulation. Dashed line — the desired, solid line — the actual.

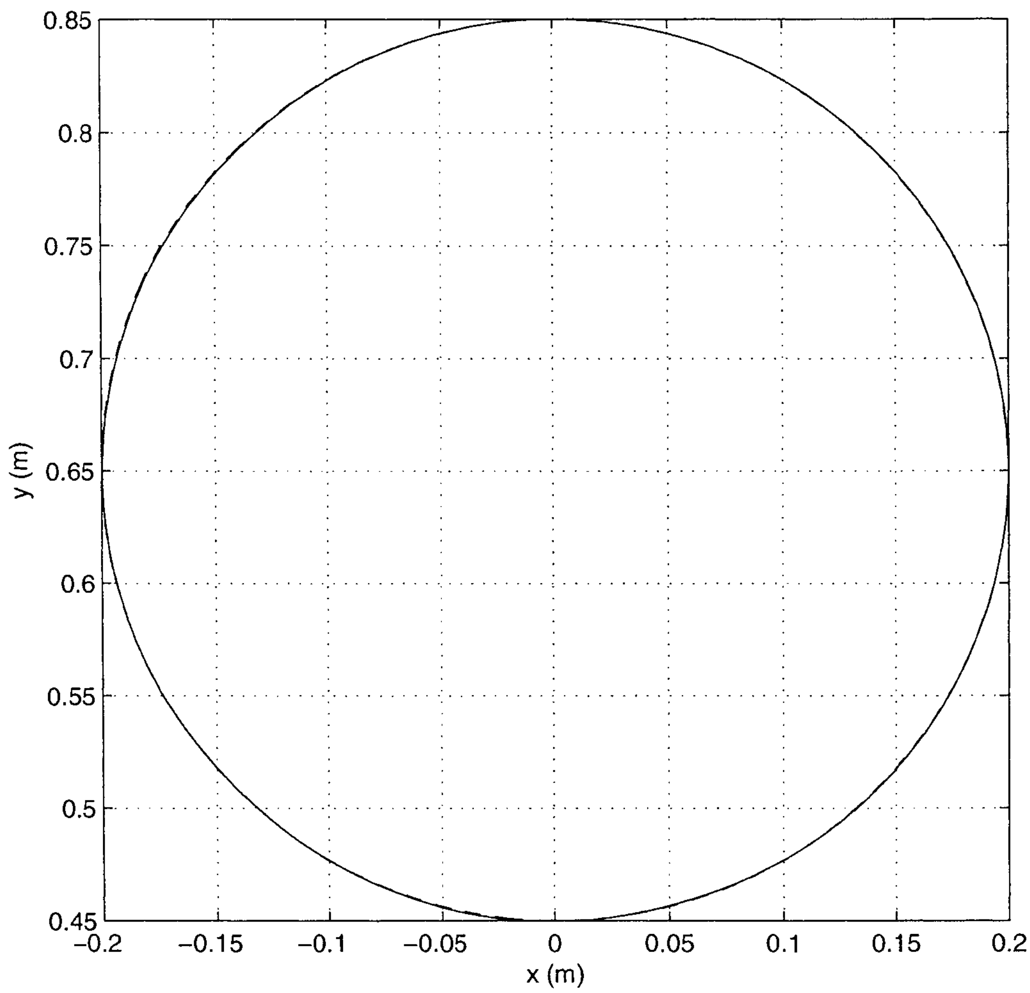

Figure 4-2: The end effector trajectory of tracking a circular trajectory in Case 2 based on the ABS in simulation. Dashed line — the desired, solid line — the actual.

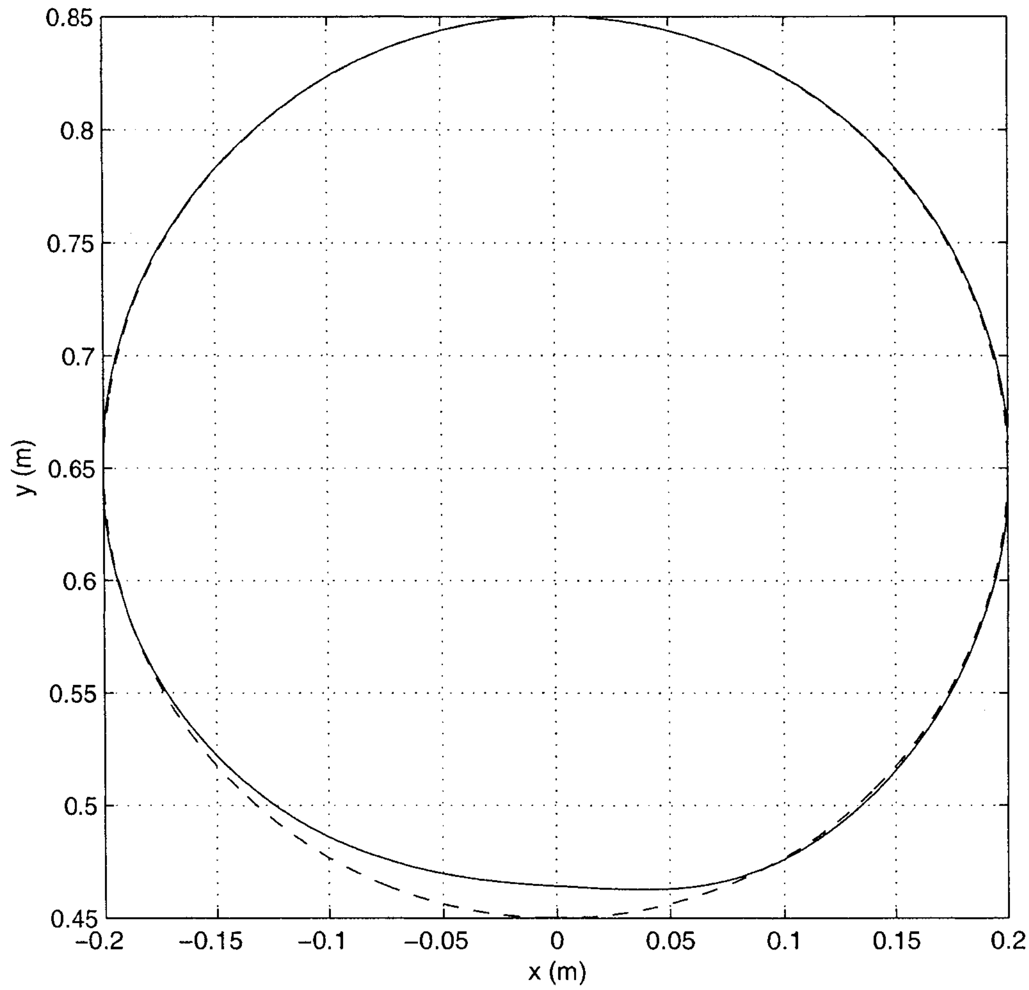

Figure 4-3: The end effector trajectory of tracking a circular trajectory in Case 3 based on the ABS in simulation. Dashed line — the desired, solid line — the actual.

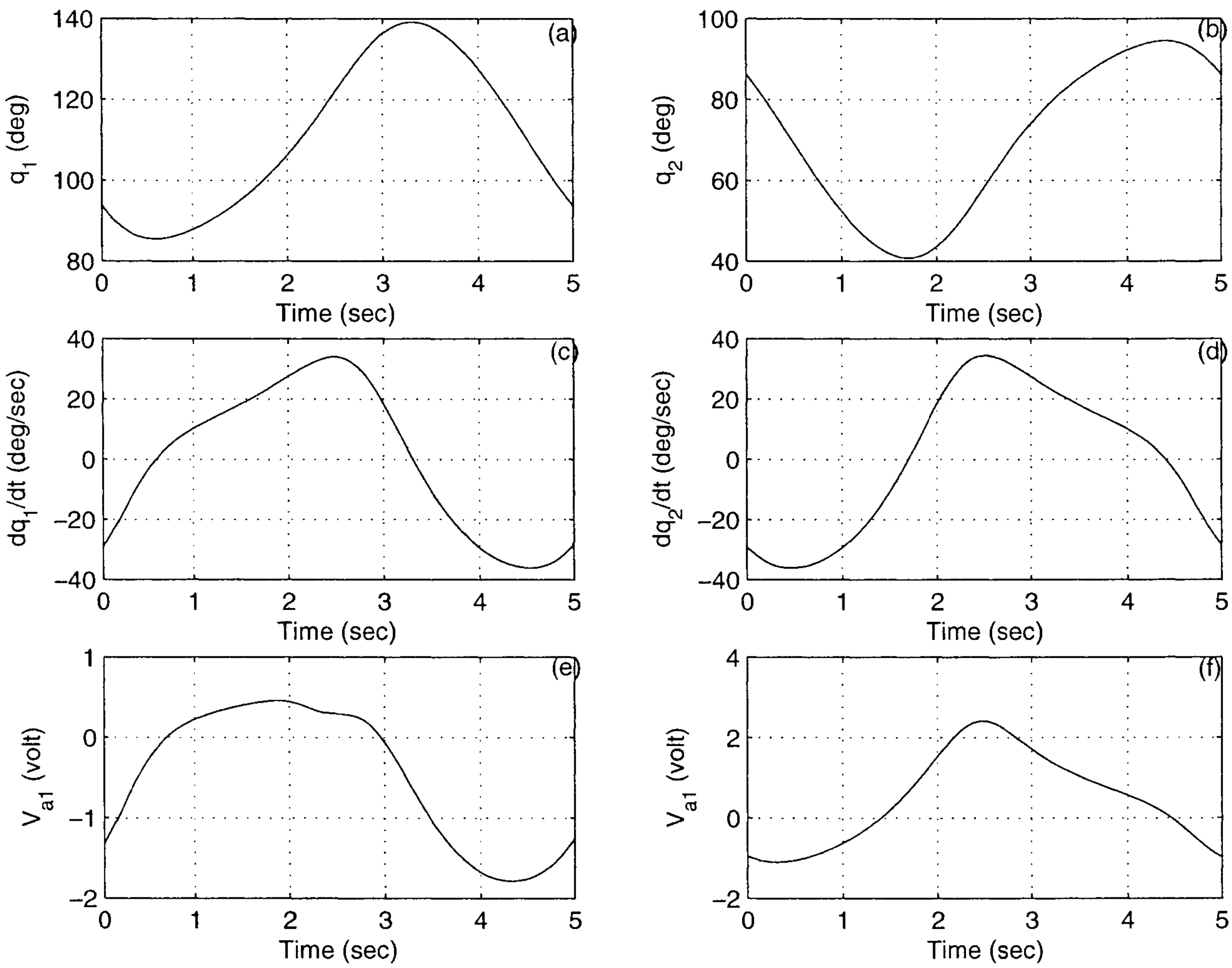

Figure 4-4: The simulation results for tracking a circle in Case 1 based on the ABS. (a) q_1, (b) q_2, (c) dq_1/dt, (d) dq_2/dt, (e) Va_1, and (f) Va_2.

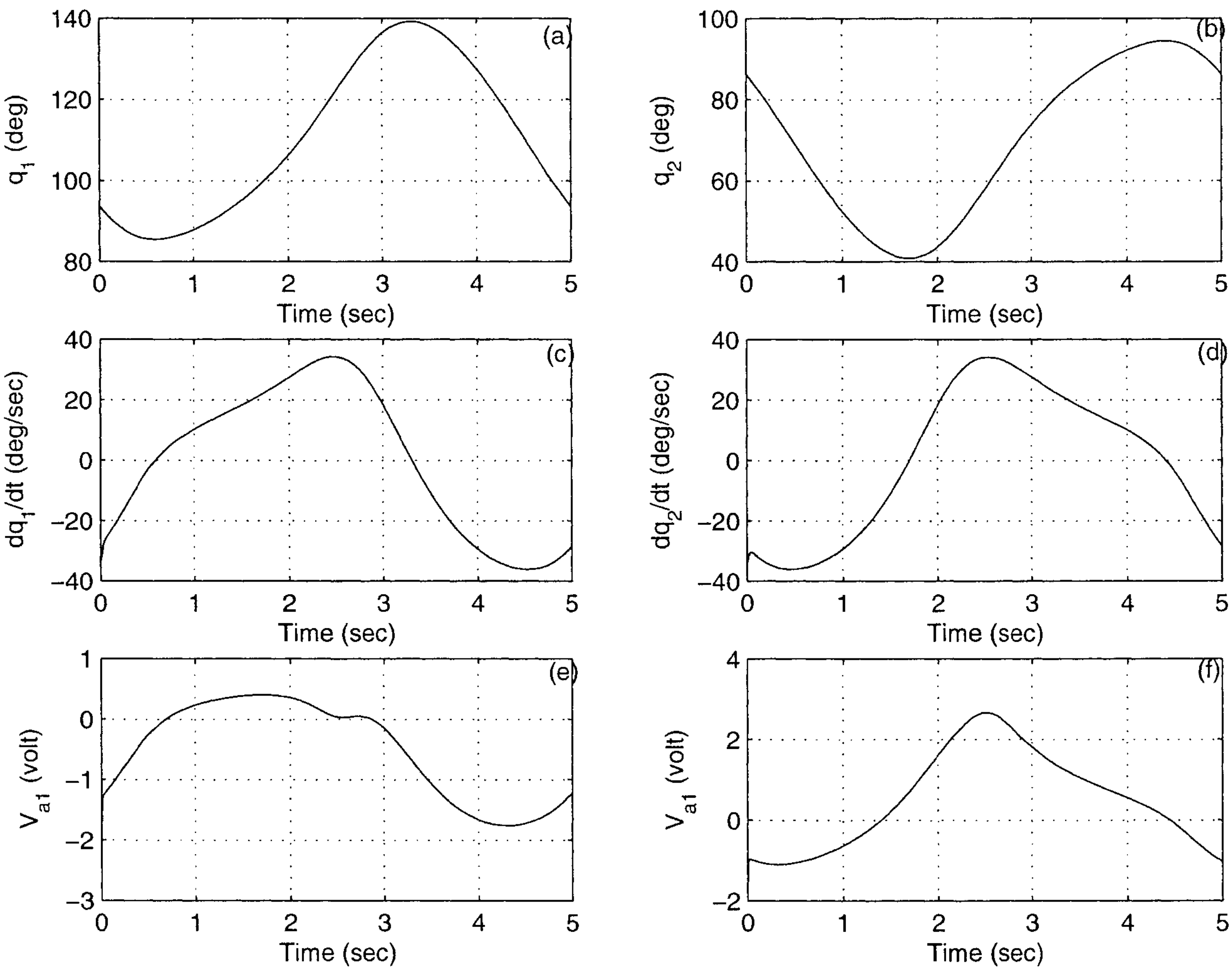

Figure 4-5: The simulation results for tracking a circle in Case 2 based on the ABS. (a) q_1, (b) q_2, (c) dq_1/dt, (d) dq_2/dt, (e) Va_1, and (f) Va_2.

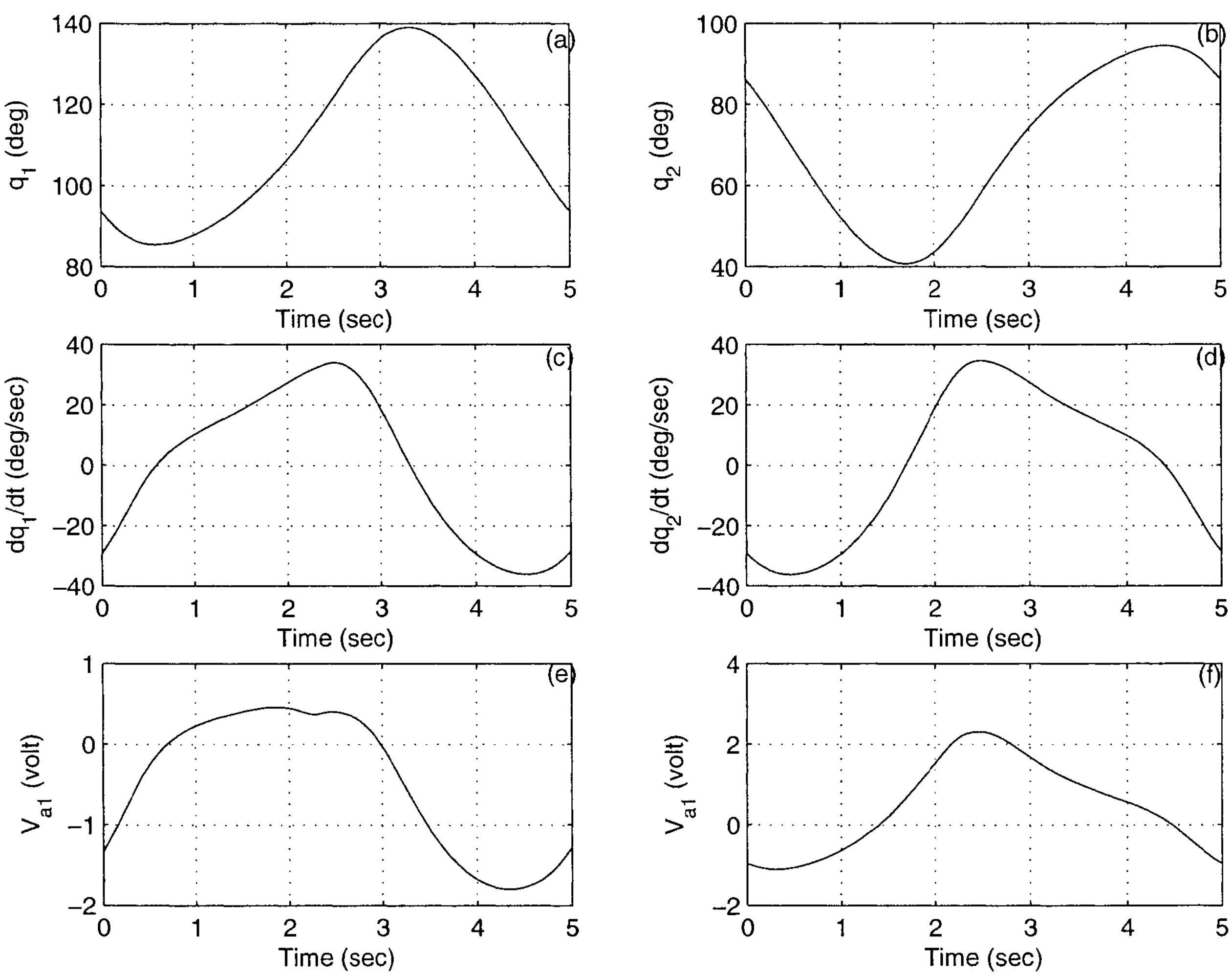

Figure 4-6: The simulation results for tracking a circle in Case 3 based on the ABS. (a) q_1, (b) q_2, (c) dq_1/dt, (d) dq_2/dt, (e) Va_1, and (f) Va_2.

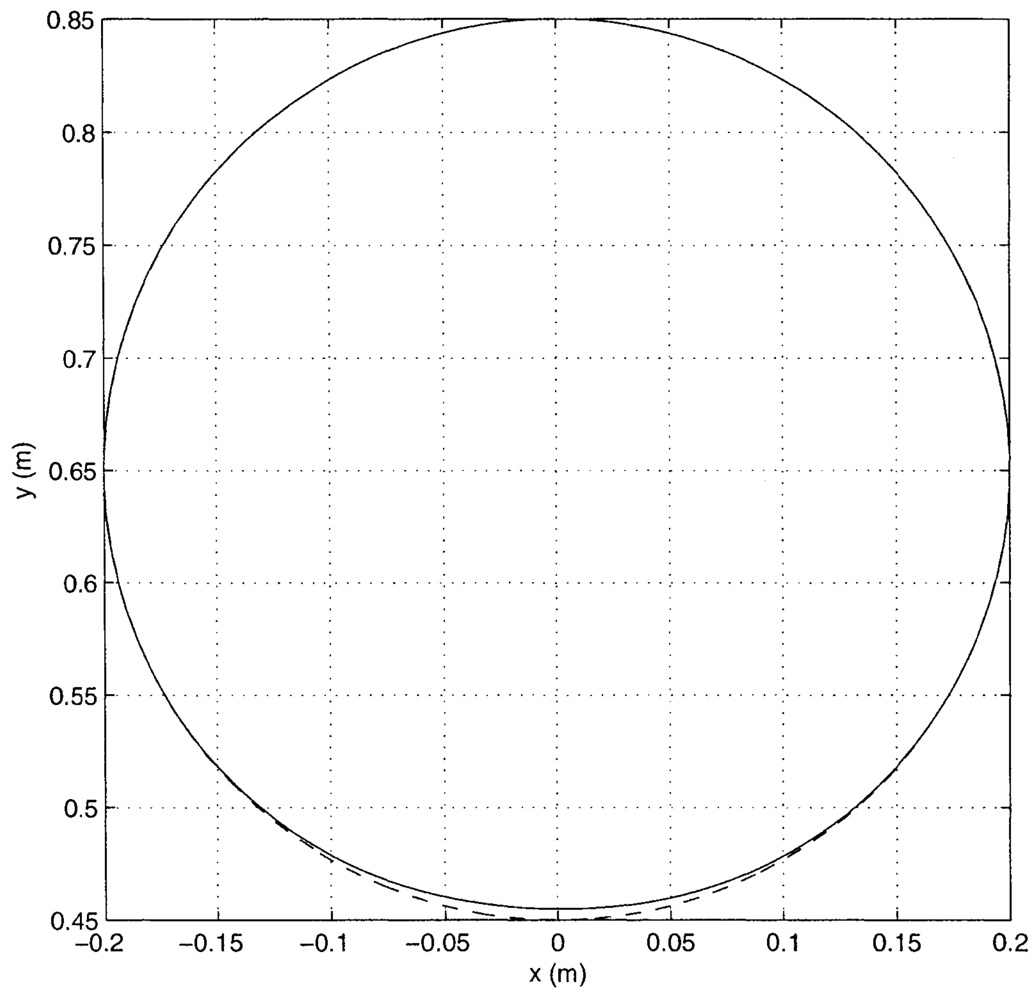

Figure 4-7: The end effector trajectory of tracking a circular trajectory in Case 1 based on the APD in simulation. Dashed line — the desired, solid line — the actual.

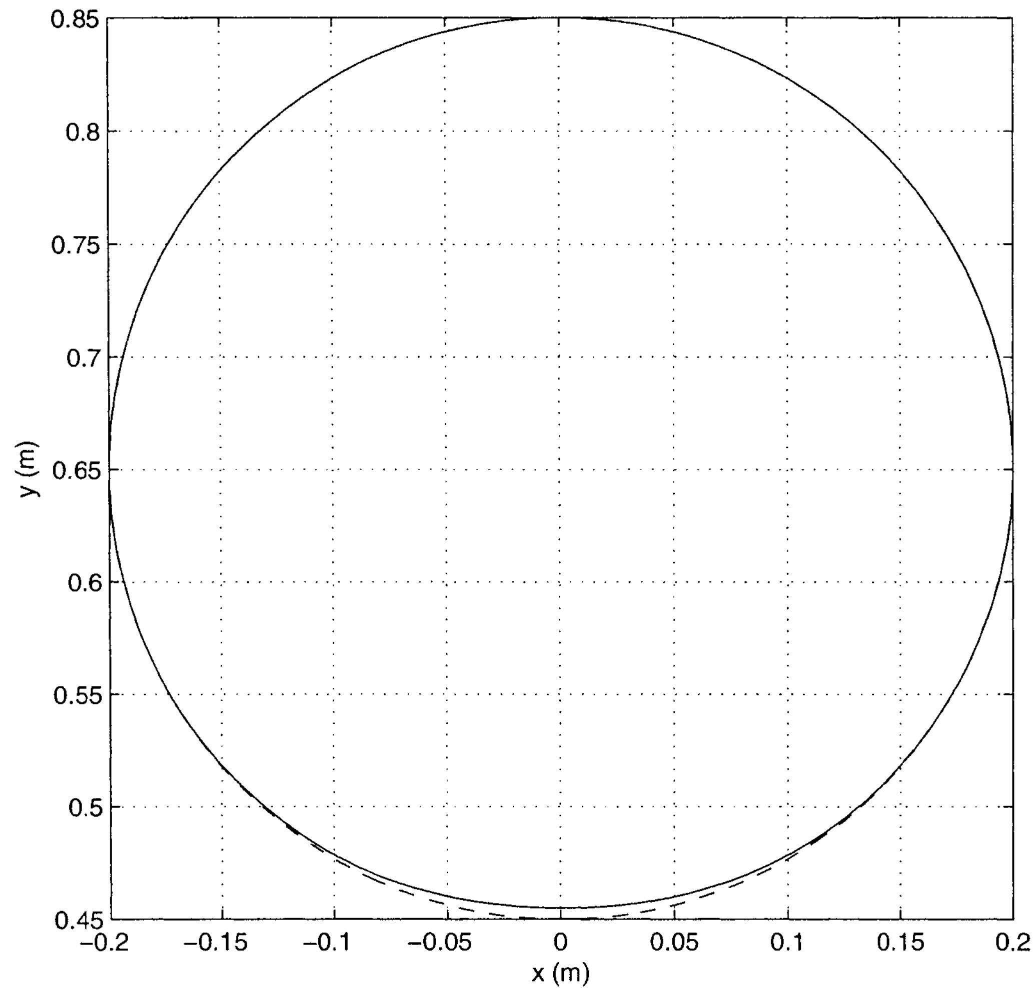

Figure 4-8: The end effector trajectory of tracking a circular trajectory in Case 2 based on the APD in simulation. Dashed line — the desired, solid line — the actual.

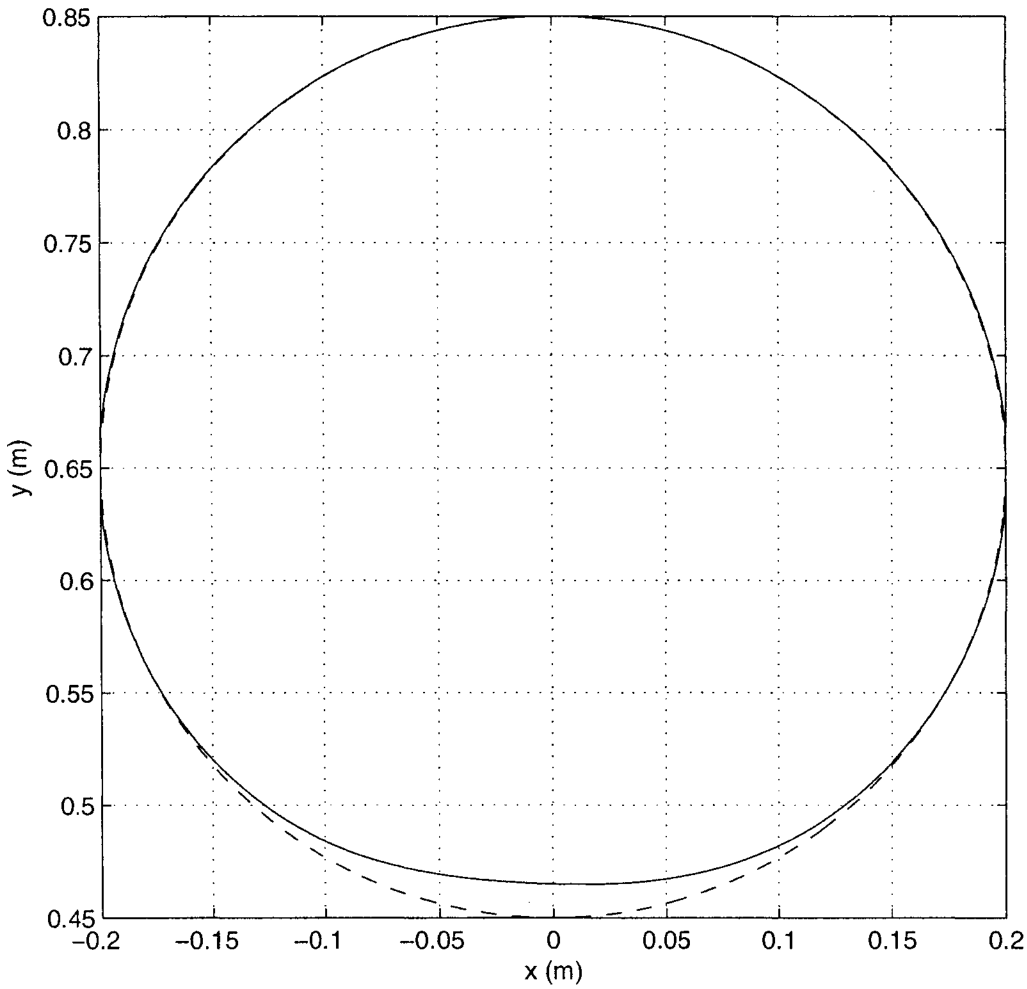

Figure 4-9: The end effector trajectory of tracking a circular trajectory in Case 3 based on the APD in simulation. Dashed line — the desired, solid line — the actual.

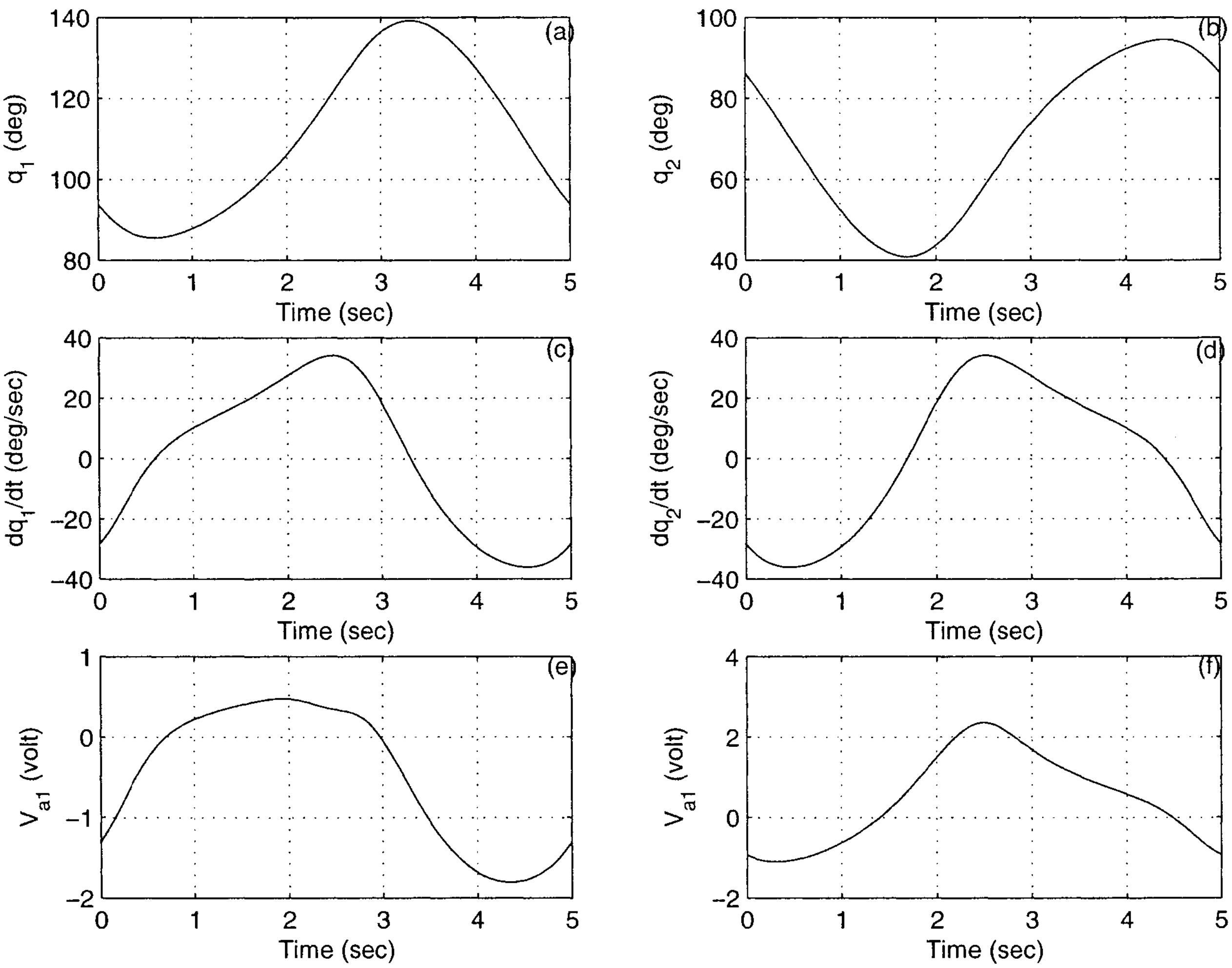

Figure 4-10: The simulation results for tracking a circle in Case 1 based on the APD. (a) q_1, (b) q_2, (c) dq_1/dt, (d) dq_2/dt, (e) Va_1, and (f) Va_2.

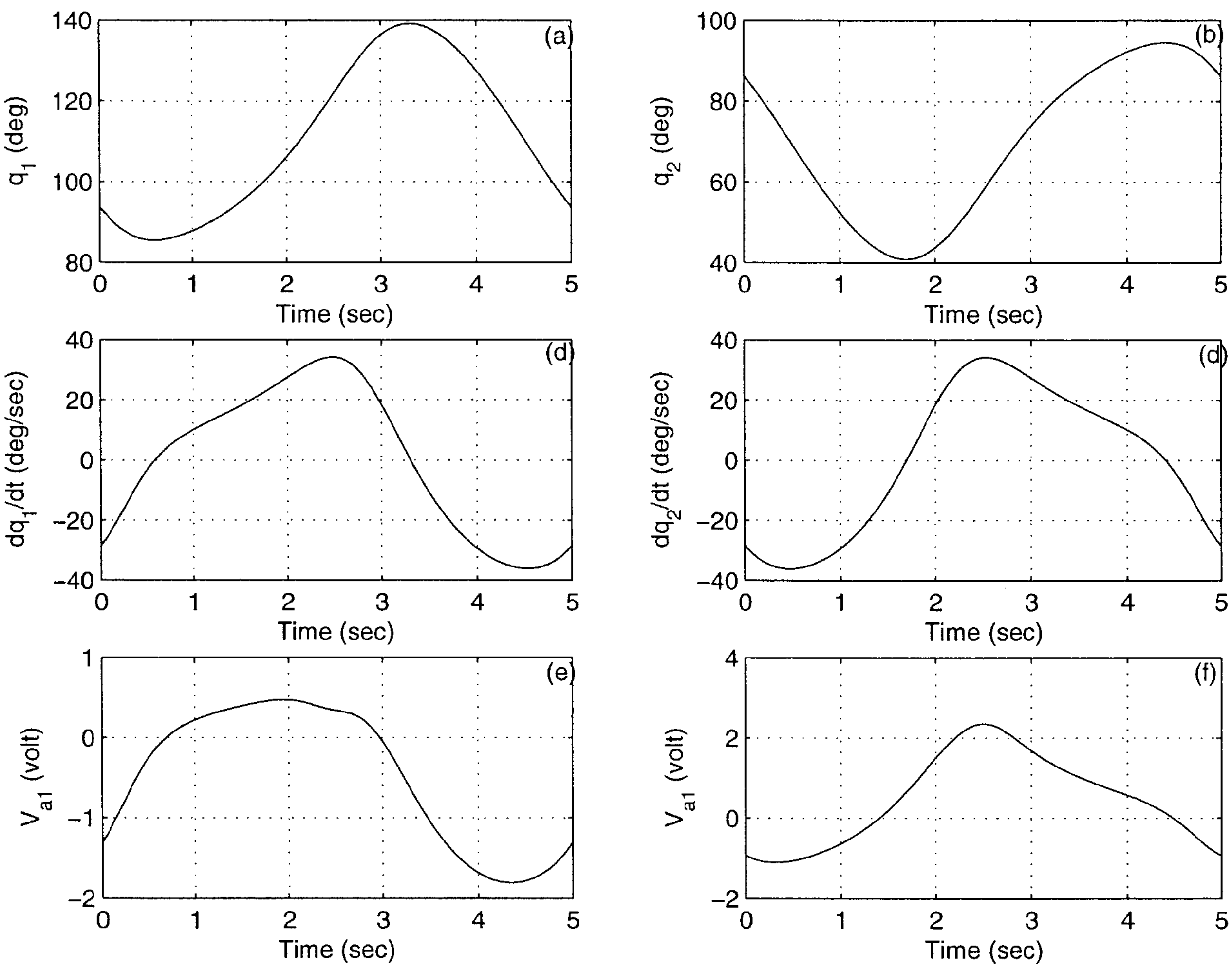

Figure 4-11: The simulation results for tracking a circle in Case 2 based on the APD. (a) q_1, (b) q_2, (c) dq_1/dt, (d) dq_2/dt, (e) Va_1, and (f) Va_2.

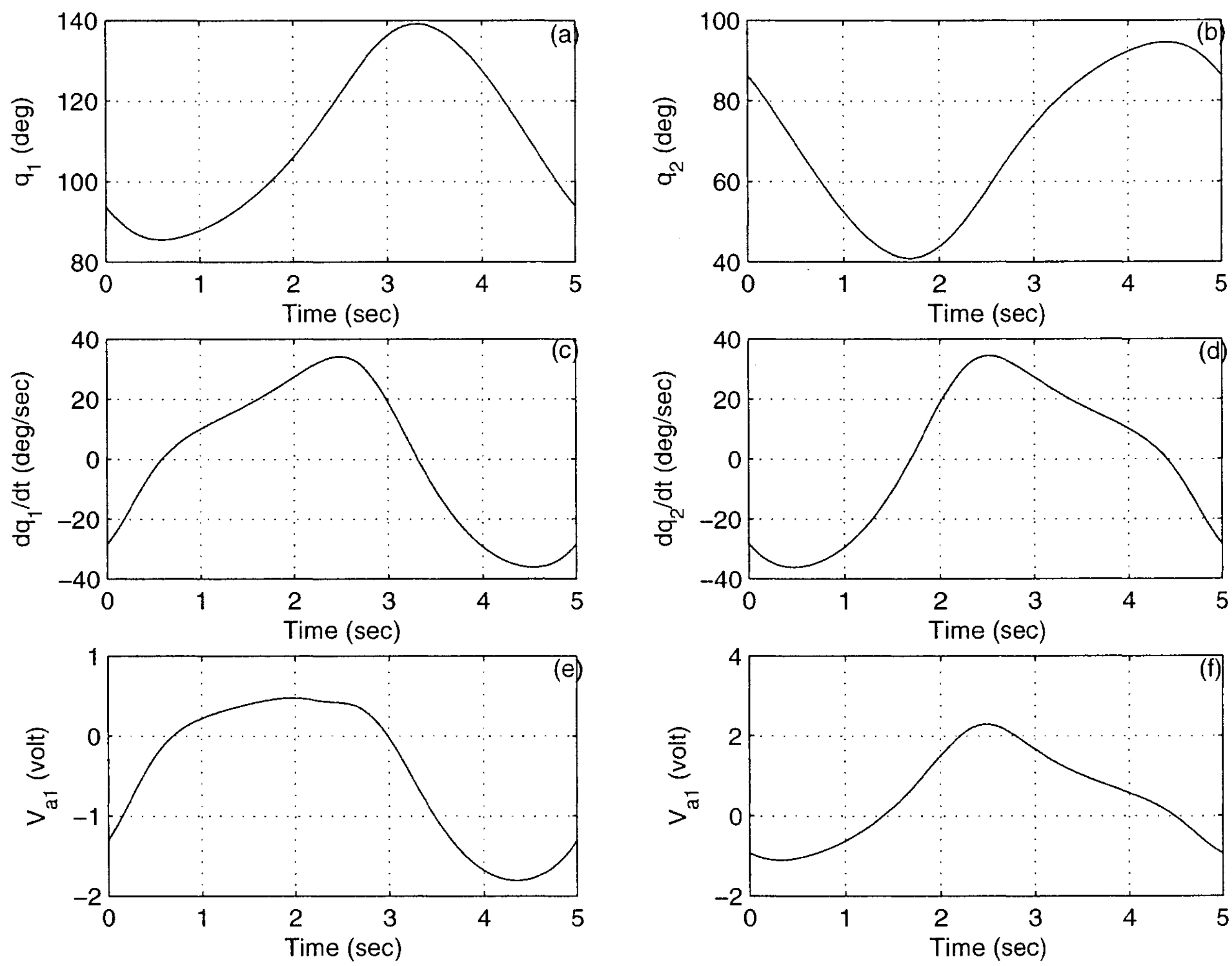

Figure 4-12: The simulation results for tracking a circle in Case 3 based on the APD. (a) q_1, (b) q_2, (c) dq_1/dt, (d) dq_2/dt, (e) Va_1, and (f) Va_2.

4.2.2 Line Tracking

For line tracking, the desired linear trajectory is from $(-0.312, 0.7)$ to $(0.288, 0.7)$ based on the coordinates defined in Fig. 2-2 and the desired tracking speed is 0.1 m/s. It can be checked that this line does not contain any singular points and is at least 35 centimeters away from the singular region. Fig. 4-13 shows line tracking by the adaptive backstepping controller while Fig. 4-14 is for the adaptive PD controller. The simulation results show that ABS performs as well as APD.

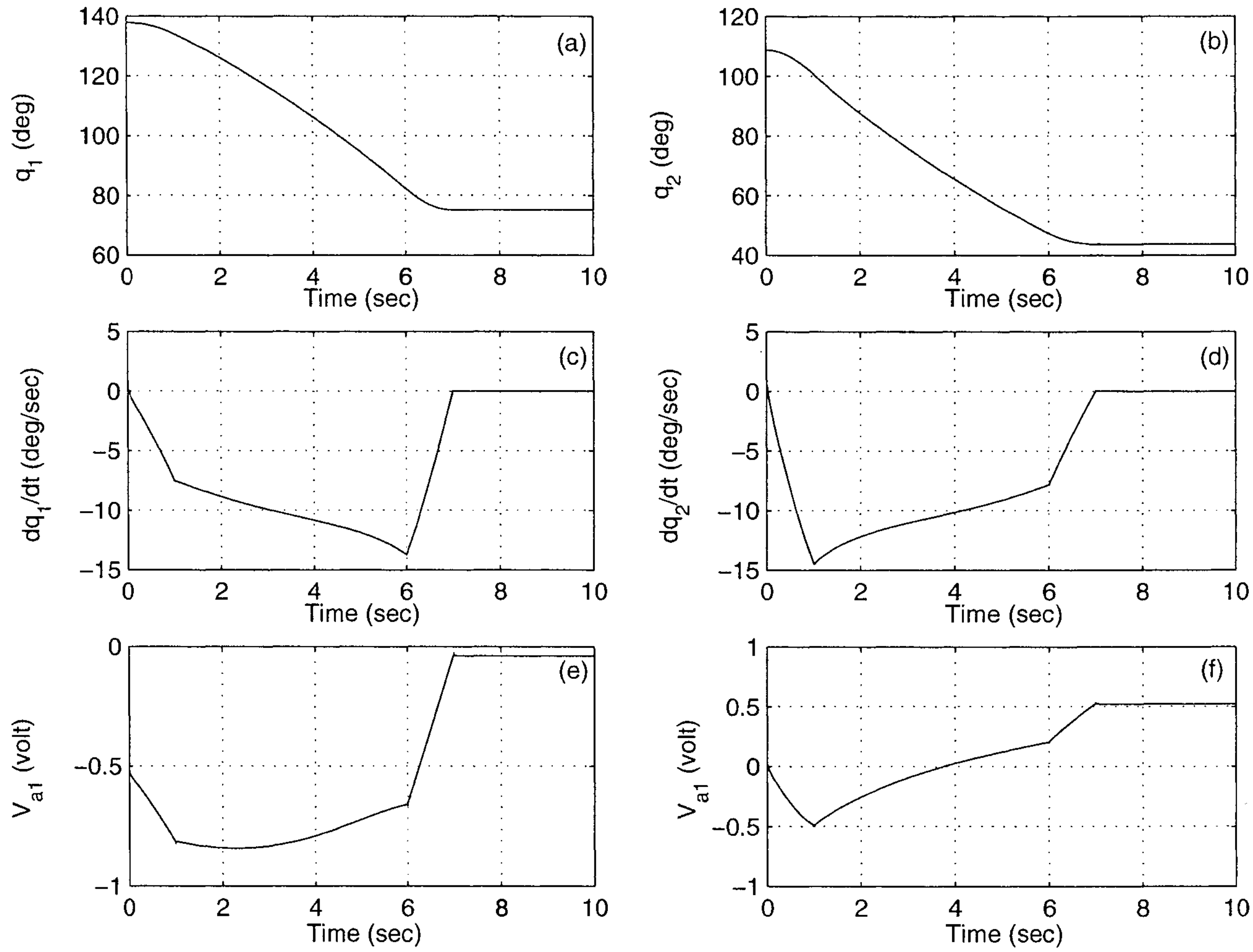

Figure 4-13: The simulation results for tracking a line based on the ABS. (a) q_1, (b) q_2, (c) dq_1/dt, (d) dq_2/dt, (e) Va_1, and (f) Va_2.

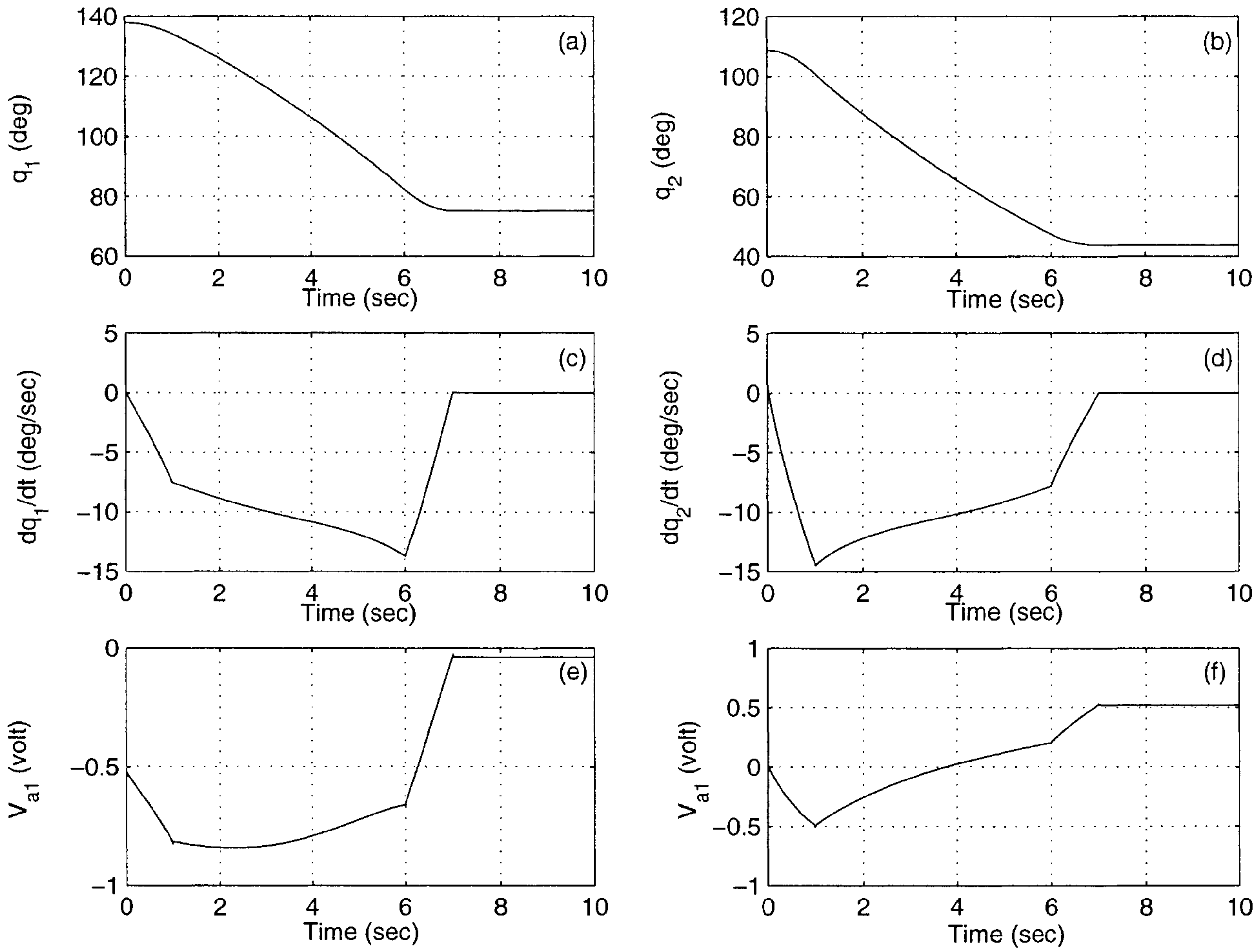

Figure 4-14: The simulation results for tracking a line based on the APD. (a) q_1, (b) q_2, (c) dq_1/dt, (d) dq_2/dt, (e) Va_1, and (f) Va_2.

4.2.3 Square Tracking

For square tracking, the four apexes are at $(-0.1, 0.6)$, $(0.1, 0.6)$, $(0.1, 0.8)$ and $(-0.1, 0.8)$ based on the coordinates defined in Fig. 2-2, and the desired tracking speed is 0.1 m/s. It can be checked that this square does not contain any singular points and the area encircled by this square is at least 25 centimeters away from the singular region. Fig. 4-15 to Fig. 4-16 show the results based on the ABS while Fig. 4-17 to Fig. 4-18 show the results based on the APD. The simulation results show that ABS performs as well as APD.

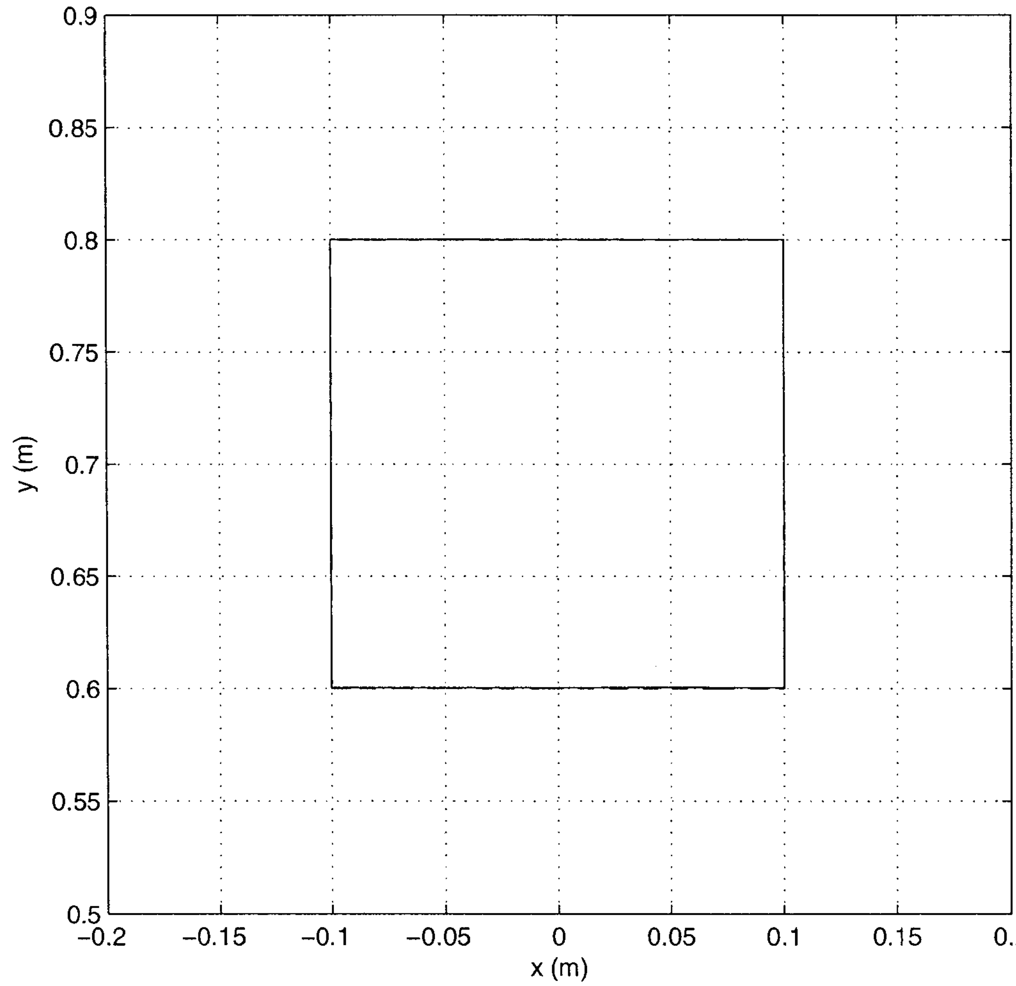

Figure 4-15: The end effector trajectory of tracking a square trajectory based on the ABS in simulation. Dashed line — the desired, solid line — the actual.

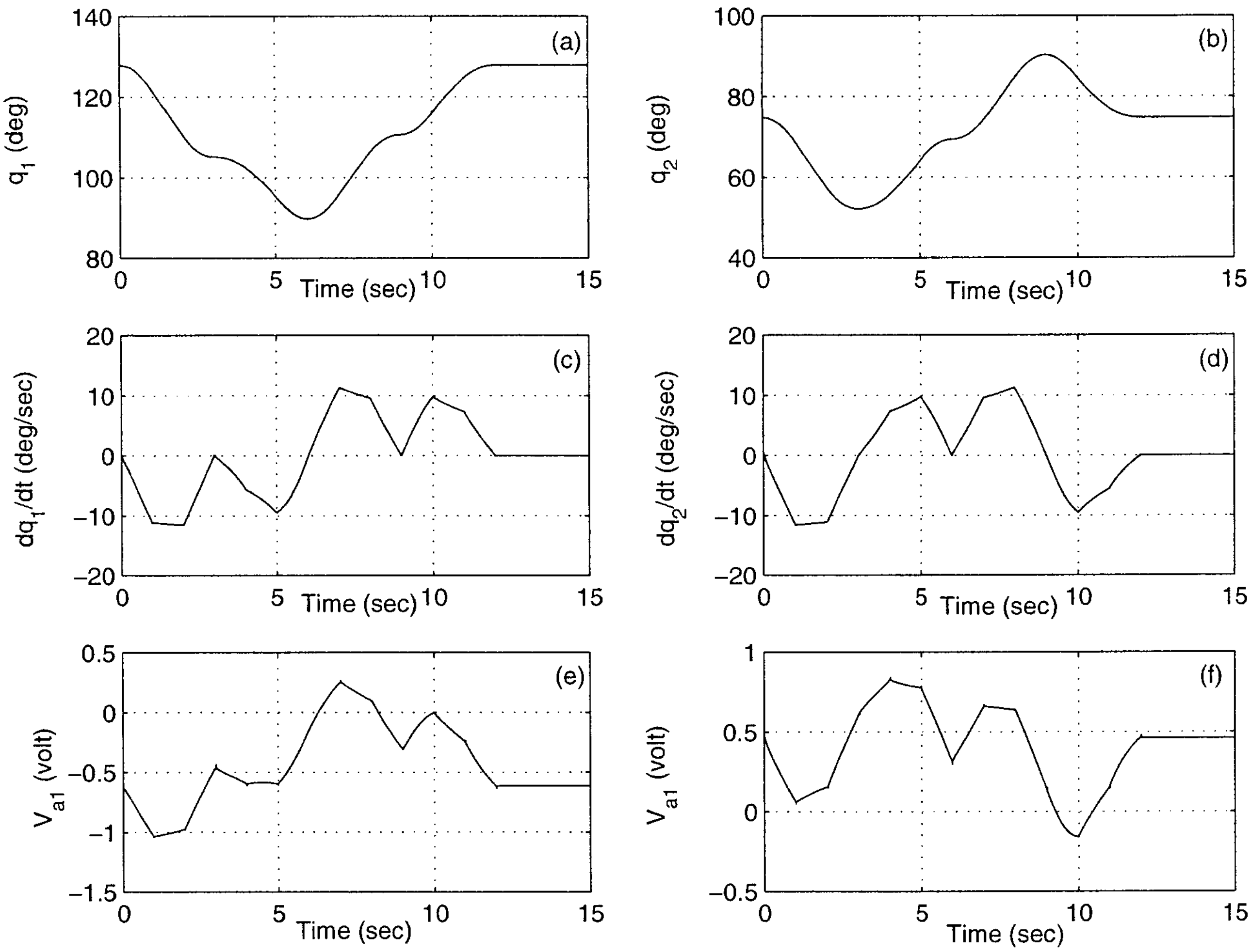

Figure 4-16: The simulation results for tracking a square based on the ABS. (a) q_1, (b) q_2, (c) dq_1/dt, (d) dq_2/dt, (e) Va_1, and (f) Va_2

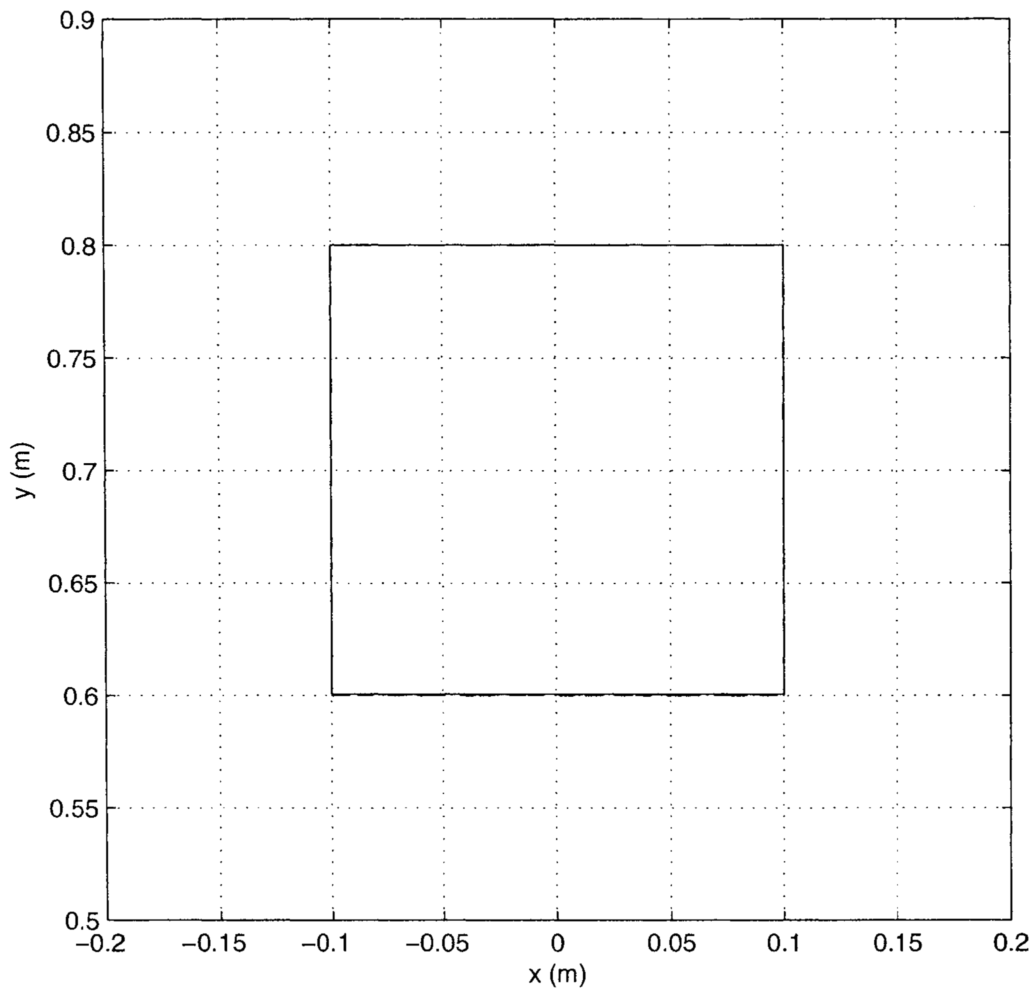

Figure 4-17: The end effector trajectory of tracking a square trajectory based on the APD in simulation. Dashed line — the desired, solid line — the actual.

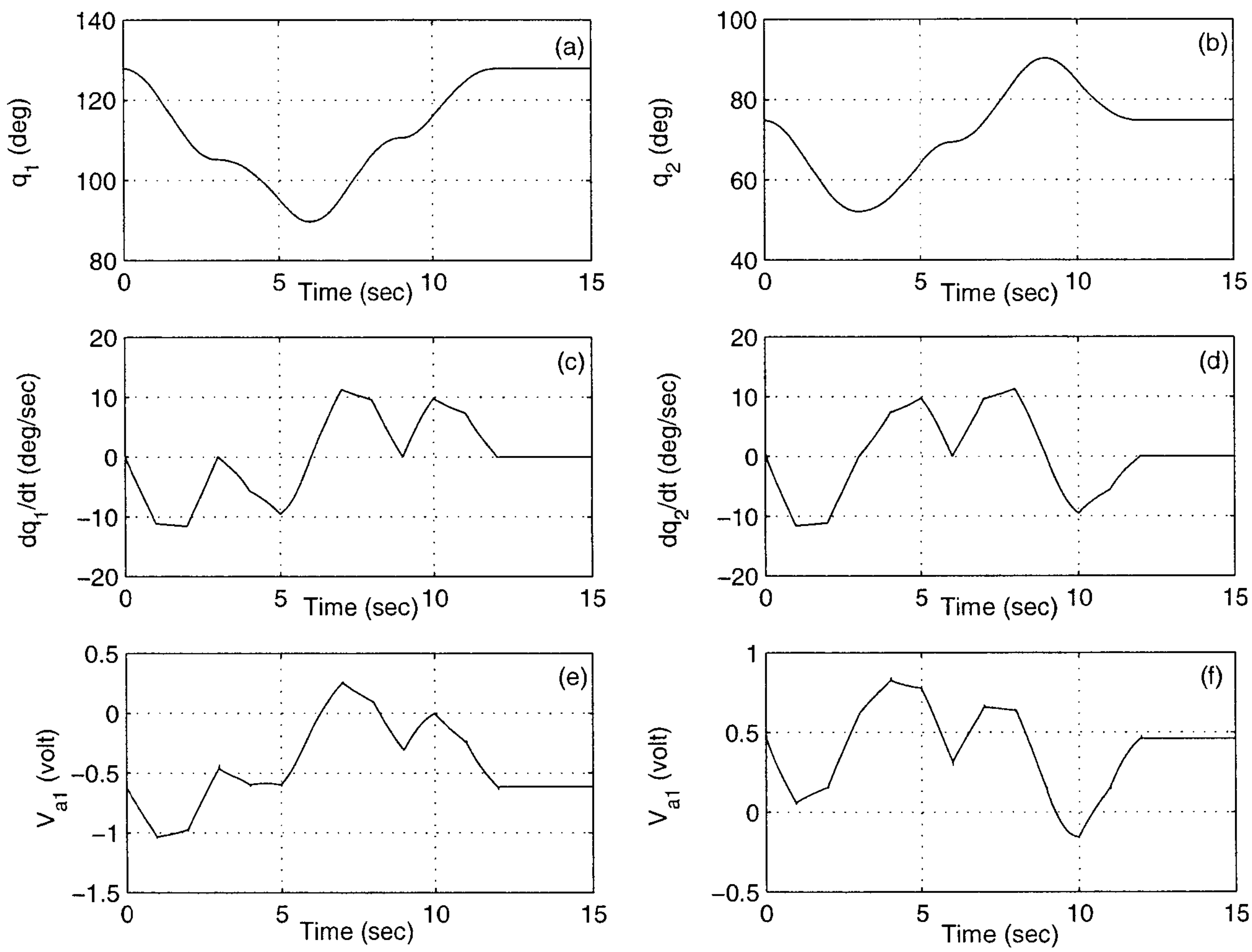

Figure 4-18: The simulation results for tracking a square based on the APD. (a) q_1, (b) q_2, (c) dq_1/dt, (d) dq_2/dt, (e) Va_1, and (f) Va_2.

Chapter 5

Controller Implementation and Experimental Results

5.1 Experimental Setup

Fig. 5-1 shows a photo of a planar 2-DOF parallel robot built for the purpose of this study. Links 1 and 2 are driven by two direct current (DC) gear head motors, respectively, and links 3 and 4 are not actuated. The parallel robot is controlled by a computer-based control system.

The computer control system is composed of four main parts: the computer, two data requisition (DAQ) boards, two motor drivers, and two DC motors. The Pentium III personal computer is used for reading the pulses from the encoder through two analog low pass filters and DAQ boards, computing control signals, and sending control signals through DAQ boards to motor drivers to control the two DC motors. The DAQ boards (PCI-6024E and PCI-MIO-16E, NI) act as interface between the computer and the motor drivers and encoders. The motor driver is built with the H-Bridge circuit for converting PWM signals from the DAQ boards to armature voltages. The two gear head DC motors are driven by two H-Bridge circuits on the motor drivers and the optical encoders built in DC motors provide angular position measurements of links 1 and 2. The motors are made by Kollmorgen Motion Technologies Group. The gear ratio is 99 : 1 and the peak torque is 17.1 N-m. The optical encoders of the motors has the resolution of 1000 pulses per revolution. The values of the link parameters are given in Table 2-1. The distance between the shafts of the motors is $c = 0.4240$ m.

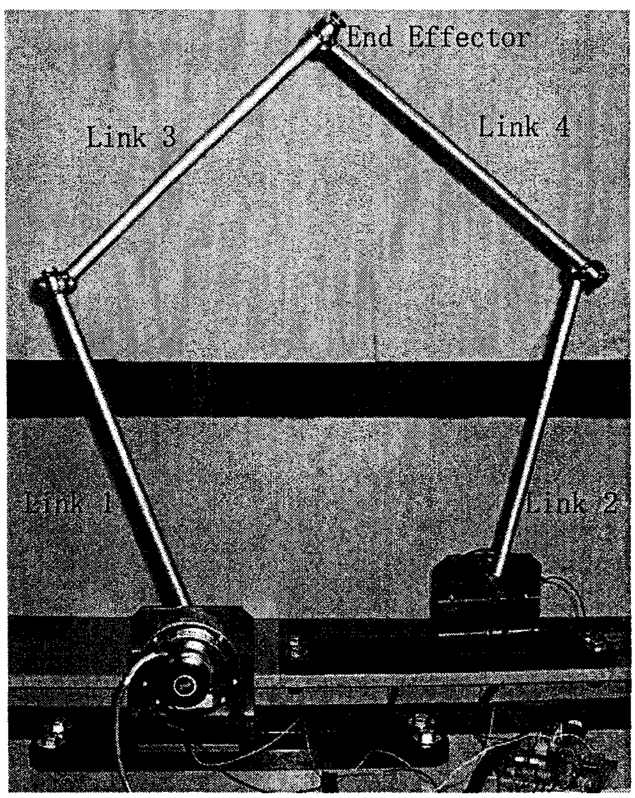

Figure 5-1: Photo of the 2-DOF robot.

Angular velocities of links 1 and 2 are calculated digitally based on the position measurements. A digital low pass filter is used for the velocity calculation, which is given by:

$$v_{k+1} = (p_{k+1} - p_k + \tau v_k)/(\tau + T) \tag{5.1}$$

where v_k and v_{k+1} are the angular velocities at the sampling instants k and $k+1$, p_k and p_{k+1} are the angle measurements of the links at the sampling instants k and $k+1$, respectively, T is the sampling period, and τ is the time constant set to 0.1.

As for experiments, the control inputs are not torque applied to the joints. The direct control inputs are the armature voltages of the DC motors. Therefore, in order to implement the designed controllers in terms of motor torque, the computed torque is converted into the armature voltages of the DC motors. The conversion formula is given as follows:

$$u_i = \frac{GK_t}{R}(V_{ai} - K_e G\omega_i), i = 1, 2 \tag{5.2}$$

where u_i is the torque applied by the motor, V_{ai} is the armature voltage, $G = 99$ is the gear ratio of the motor, $K_t = 0.02282\ N \cdot m/Amp$ is the torque constant, $K_e = 0.02282\ V/\,(rad/s)$ is the back electromotive force (EMF) constant, $R = 0.640\ Ohms$ is the armature resistance, and ω_i is the angular velocity of the gear shaft. The maximum voltage of the driver board is 15 volts.

In the experiment, a sampling period of 0.8 millisecond was used. In each sampling period, the computer obtains the current positions and velocities of links 1 and 2, calculates the armature voltages in terms of duty cycles of the PWM signals, and sends the PWM signals to the driver boards to control the DC motors.

To compensate the effect of backlash between gears in the two motors, a voltage compensation is applied in the experiments. When the computed armature voltage is larger than 0.01 volts, the armature voltage used in experiment is increased by 0.05 for motor 1 and 0.35 for motor 2; when the computed armature voltage is less than −0.01 volts, the armature voltage used in experiment is increased by −0.65 for both motors.

5.2 Experimental Results for Set Point Control

Recall Fig. 3-1 which shows two configurations of the robot. The robot moves from configuration one to configuration two (downward) and back to configuration one (upward).

In the set point control experiments, for the ABS controller, the initial values of the unknown parameters Θ are set to

$$\Theta(0) = \begin{bmatrix} 0.08 & 0.08 & 0.02 & 0.02 & 0.03 & 0.03 & 1.8 & 1.8 & 0.6 & 0.6 \end{bmatrix}$$

and for the APD control, the initial values of the unknown parameters Θ_{pd} are set to

$$\Theta_{pd}(0) = \begin{bmatrix} 0.02 & 0.02 & 0.03 & 0.03 & 1.8 & 1.8 & 0.6 & 0.6 \end{bmatrix}$$

To test the adaptability of both adaptive controllers, a 100 gram load was attached to the end effector of the parallel robot.

Fig. 5-2 to Fig. 5-5 show the experimental results of the ABS controller with $c_1 = 3$, $c_2 = 3$, $c_3 = 10$, $c_4 = 10$, $\gamma_i = 30$, $i = 1$ to 7, $\gamma_8 = 60$, $\gamma_9 = 150$, and $\gamma_{10} = 150$ and the APD controller with the controller parameters $k_{p1} = 35$, $k_{p2} = 35$, $k_{v1} = 11$, $k_{v2} = 11$, and $\gamma_{pdi} = 10$, $i = 1$ to 8, respectively. The set point control is also implemented based on non-adaptive controller based on backstepping technique and PD plus gravity, and the Coriolis and centrifugal terms compensation. The same c_i $(i = 1$ to $4)$, k_{pj}, and k_{vj}, $(j = 1$ to $2)$ are used for non-adaptive controllers.

Fig. 5-2 to Fig. 5-3 and Fig. 5-4 to Fig. 5-5 are the results without and with load based on adaptive controllers, respectively. It can be seen that when there is a change in the system parameters caused by the load change, both adaptive controllers can achieve no more than $1.5°$ steady state errors. The steady state errors and the average steady state error for each movement and each controller, ABS BS APD and PD, are listed in Table 5.1 and Table 5.2 separately.. When there is an additional load attached to the end effector, adaptive controllers can achieve less steady state errors than those non-adaptive controllers.

Table 5-1 Steady State Error For Set Point Control

	q_1 (degree)				q_2 (degree)			
Movement / load (g)	ABS	BS	APD	PD	ABS	BS	APD	PD
Downward/ 0	**0.7924**	0.8360	**0.2215**	0.6767	0.9269	**0.8360**	**0.6860**	0.9014
Upward / 0	0.4111	**0.1598**	0.3771	**0.1420**	**0.1420**	0.1893	**0.1125**	0.2934
Downward/ 100	**0.1858**	1.0804	**1.4840**	1.9676	**0.0913**	0.8614	**0.0695**	0.0978
Upward/ 100	**0.6402**	3.2184	**0.7675**	0.9929	**0.1161**	0.1925	0.5416	**0.4725**

Table 5-2 Average Steady State Error For Set Point Control

	Average Errors (degree)			
Movement / load (g)	ABS	BS	APD	PD
Downward/ 0	**0.8597**	0.8360	**0.4538**	0.7891
Upward / 0	0.2766	**0.1746**	0.2398	**0.2182**
Downward/ 100	**0.1386**	0.9709	**0.7768**	1.0327
Upward/ 100	**0.3782**	1.7055	**0.6546**	0.7327

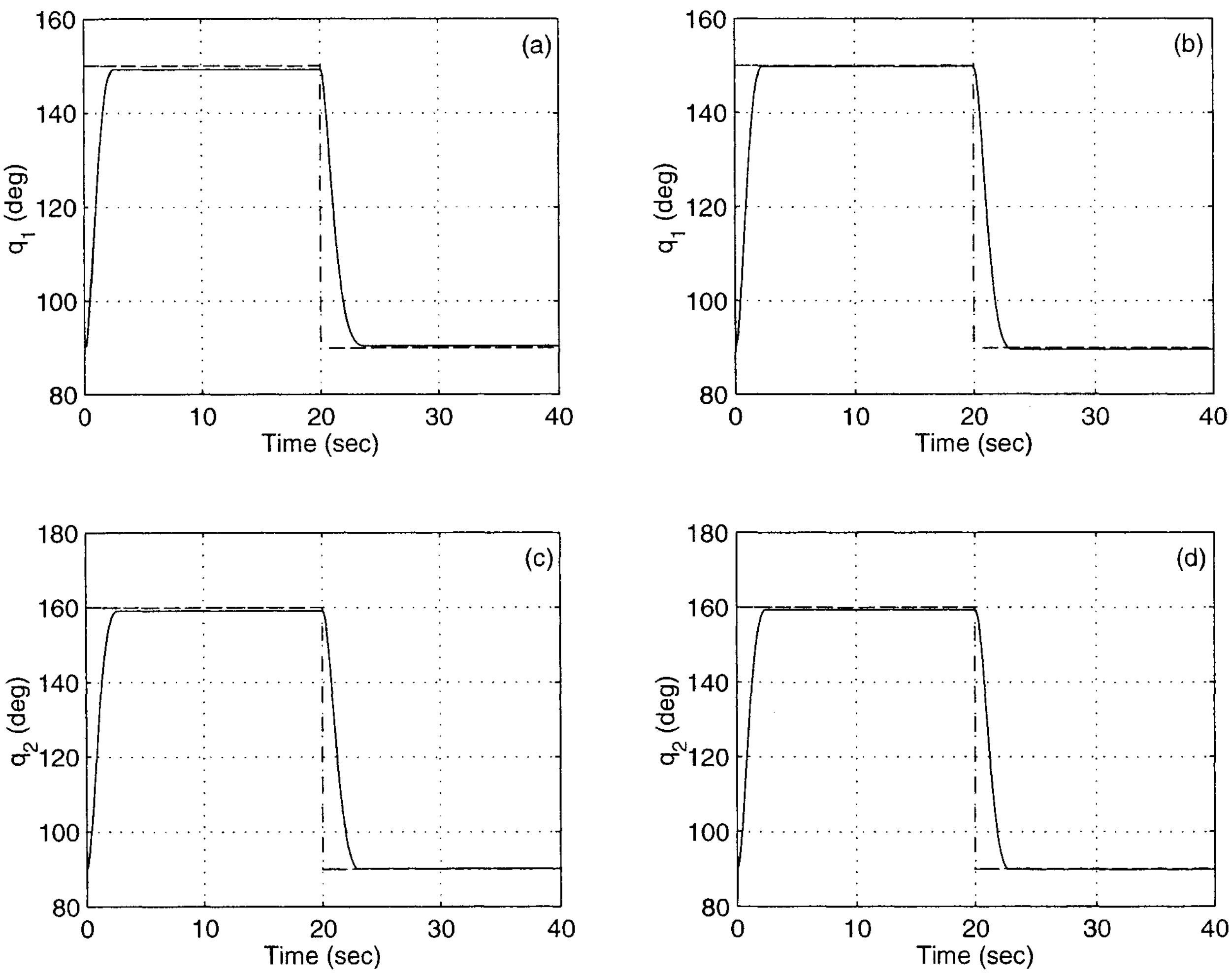

Figure 5-2: The results of set point control without load. (a) q_1 based on the ABS, (b) q_1 based on the APD, (c) q_2 based on the ABS, and (d) q_2 based on the APD. Dashed line — the desired, solid line — the actual.

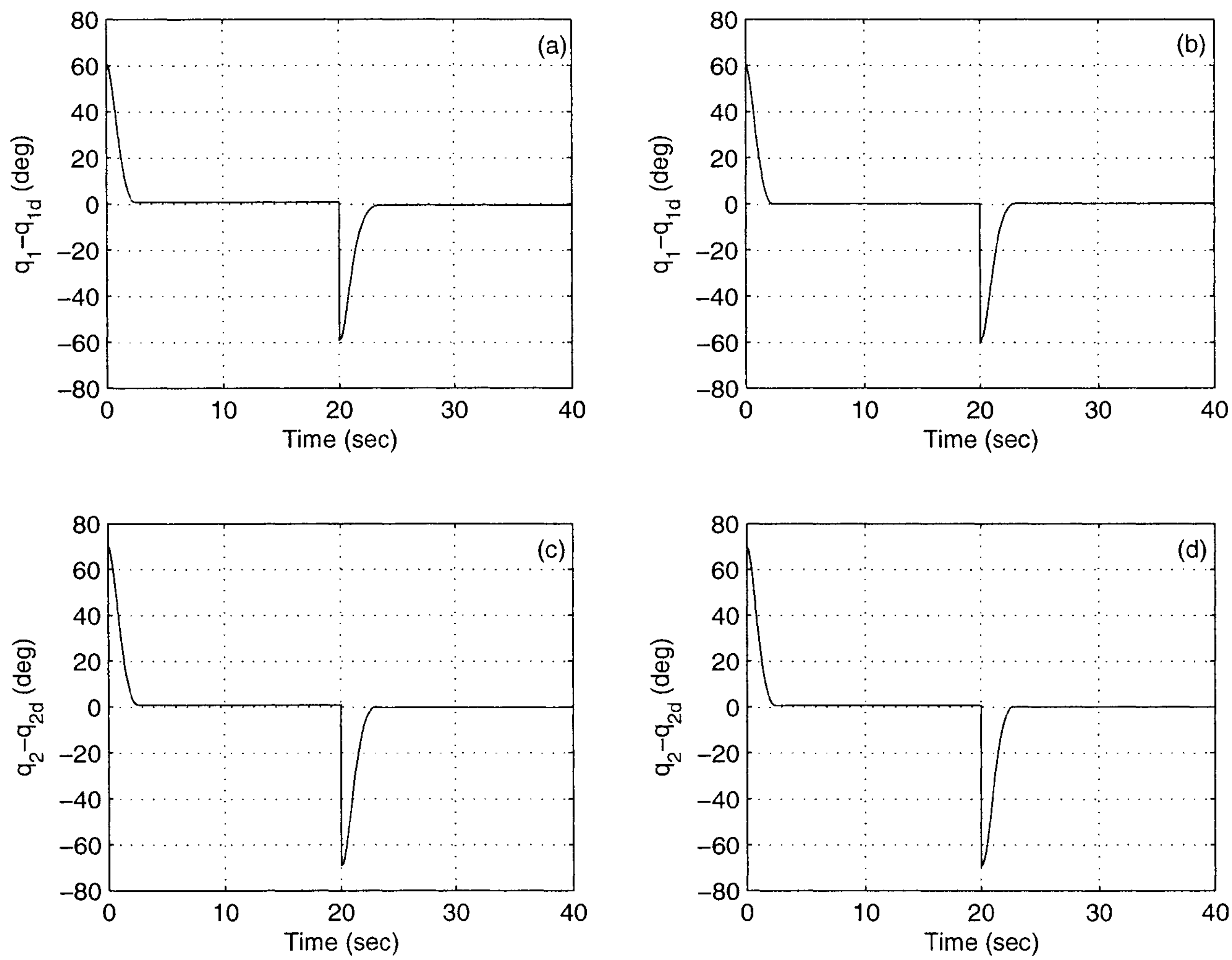

Figure 5-3: The error of q_1 and q_2 without load. (a) $q_{1d} - q_1$ based on the ABS, (b) $q_{1d} - q_1$ based on the APD, (c) $q_{2d} - q_2$ based on the ABS, and (d) $q_{2d} - q_2$ based on the APD.

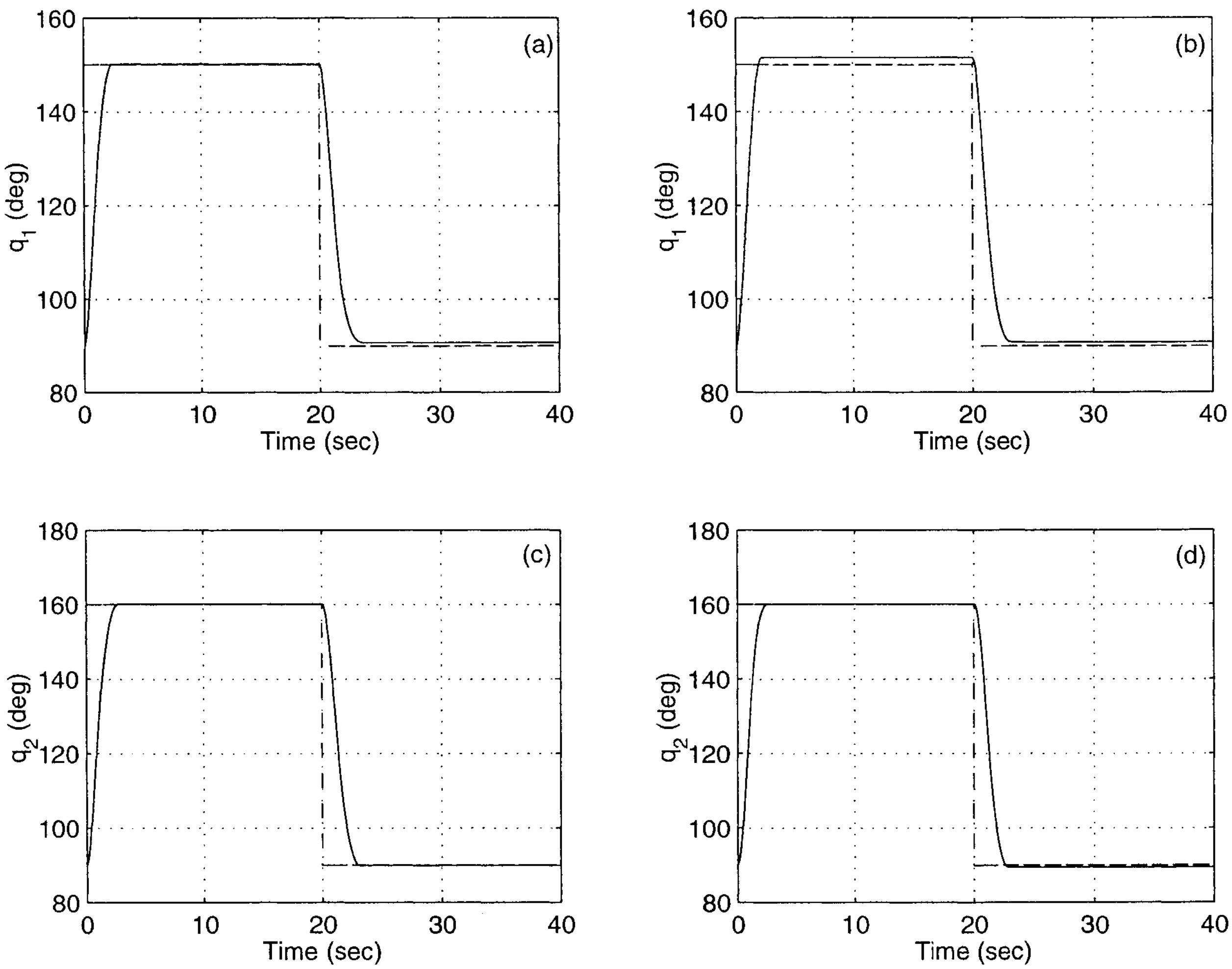

Figure 5-4: The results of set point control with load. (a) q_1 based on the ABS, (b) q_1 based on the APD, (c) q_2 based on the ABS, and (d) q_2 based on the APD. Dashed line — the desired, solid line — the actual.

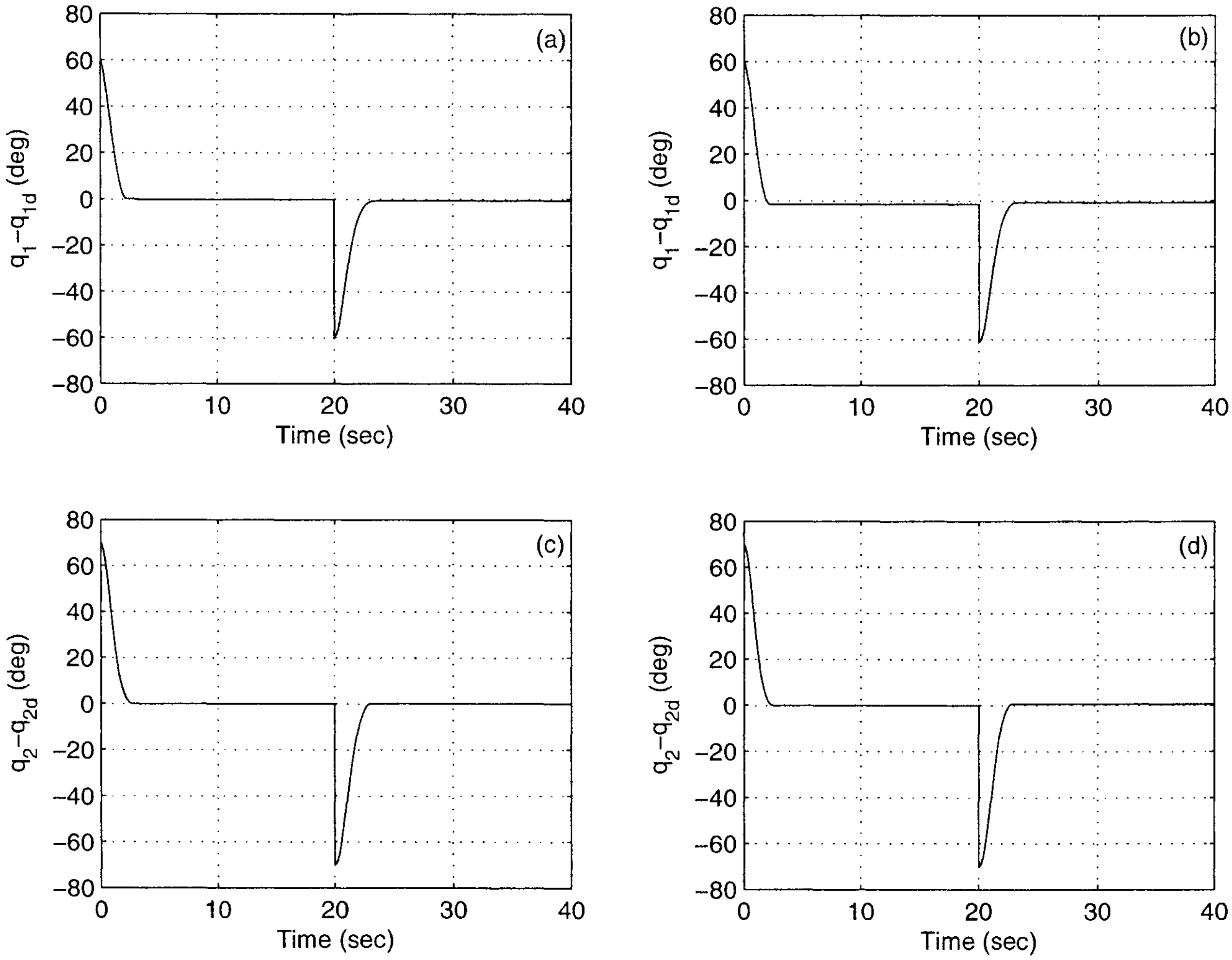

Figure 5-5: The error of q_1 and q_2 with load. (a) $q_{1d} - q_1$ based on the ABS, (b) $q_{1d} - q_1$ based on the APD, (c) $q_{2d} - q_2$ based on the ABS, and (d) $q_{2d} - q_2$ based on the APD.

5.3 Experimental Results for Tracking Control

The four controllers were implemented for tracking control, the ABS, the BS, the APD, and the PD. The desired trajectories to be tracked are circle, line, and square. The controller parameters are chosen as follows. For the ABS and the BS, $c_1 = 20$, $c_2 = 20$, $c_3 = 80$, and $c_4 = 80$. For the APD and the PD, $k_{p1} = 1600$, $k_{p2} = 1600$, $k_{v1} = 80$, and $k_{v2} = 80$. For the adaptive controllers (ABS and APD), $\gamma_i = 30$, $i = 1$ to 7, $\gamma_8 = 60$, $\gamma_9 = 150$, and $\gamma_{10} = 150$. In the tracking control experiments, the initial values of the unknown parameters Θ are set to

$$\Theta(0) = \begin{bmatrix} 0.08 & 0.08 & 0.02 & 0.02 & 0.03 & 0.03 & 1.8 & 1.8 & 0.6 & 0.6 \end{bmatrix}$$

To test the adaptability of the adaptive controllers, some loads were attached to the end effector.

5.3.1 Circle Tracking

For circle tracking, the desired circle placement and desired tracking speed used here are the same as in Section 4.2. Four radii were used: $r = 0.05$, 0.1, 0.15, and 0.2 m, and three tracking frequencies were tested: $f = 0.05$, 0.1, and 0.2 Hz. It can be checked that these circles do not contain any singular points and the areas encompassed by the circles are at least 5 centimeters away from the singular region. The following four sets of experimental results are shown in figures, in which the load attached to the end effector is 100 g.

Case 1: Fig. 5-6 to Fig. 5-9 show the tracking results for the circle with $r = 0.05$ and $f = 0.05$.

Case 2: Fig. 5-10 to Fig. 5-13 give the results for tracking a circle with $r = 0.2$ and $f = 0.05$.

Case 3, Fig. 5-14 to Fig. 5-17 demonstrate circle tracking with $r = 0.05$ and $f = 0.2$.

Case 4: Fig. 5-18 to Fig. 5-21 exhibit the tracking performance with the circle of $r = 0.2$ and $f = 0.2$.

From these figures, it is not difficult to see that the tracking errors increase with larger radius or higher tracking frequency.

The norms of the tracking circle errors and the average of the tracking errors' norms with various radii, frequencies and loads are given in Table 5-3 to Table 5-8. For each radius and frequency the errors are given in the following order, no load, 100 g load, 161 g load and 261 g load. From Tables 5-3 to 5-8, it is hard to see which controller gives better performance and there is not significant difference between no load test and with load test when tracking circles with small radii or at low tracking frequency However the advantages of adaptive controllers are obvious in tracking a large circle and at high tracking speed, especially when there is a load attached to the end effector. Comparing the results of the adaptive controllers with those of non-adaptive controllers, the smaller tracking errors are shown in bold format.

Adaptive controllers need much more time to calculate the control effort, which will result in negative influence in the experimental results, especially for small circles and low tracking speeds in no load test. When the radii of the desired circle and the tracking speed increase, the advantages of adaptive controllers are obvious in the load test. The smaller tracking errors can be achieved by adaptive controllers when there is a heavier additional load attached to the end effector, especially when the parallel robot intends to track a circle with large radius and high frequency. Comparing the results from load test with the results from no load test, the norms of tracking errors of adaptive controllers increase less than those of non-adaptive controllers.

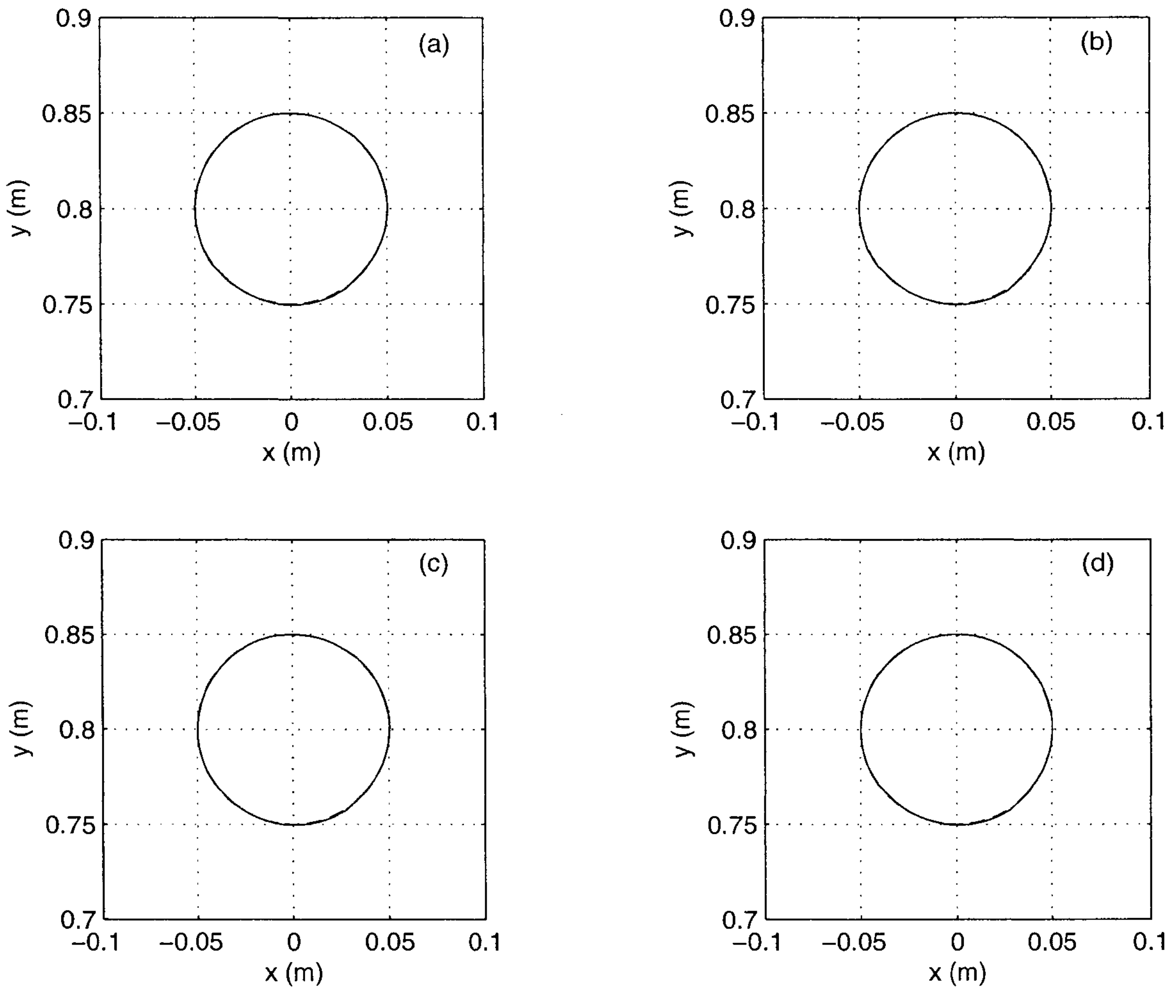

Figure 5-6: The results of tracking a circular trajectory in Case 1 without load. (a) the ABS, (b) the BS, (c) the APD, and (d) the PD. Dashed line — the desired, solid line — the actual.

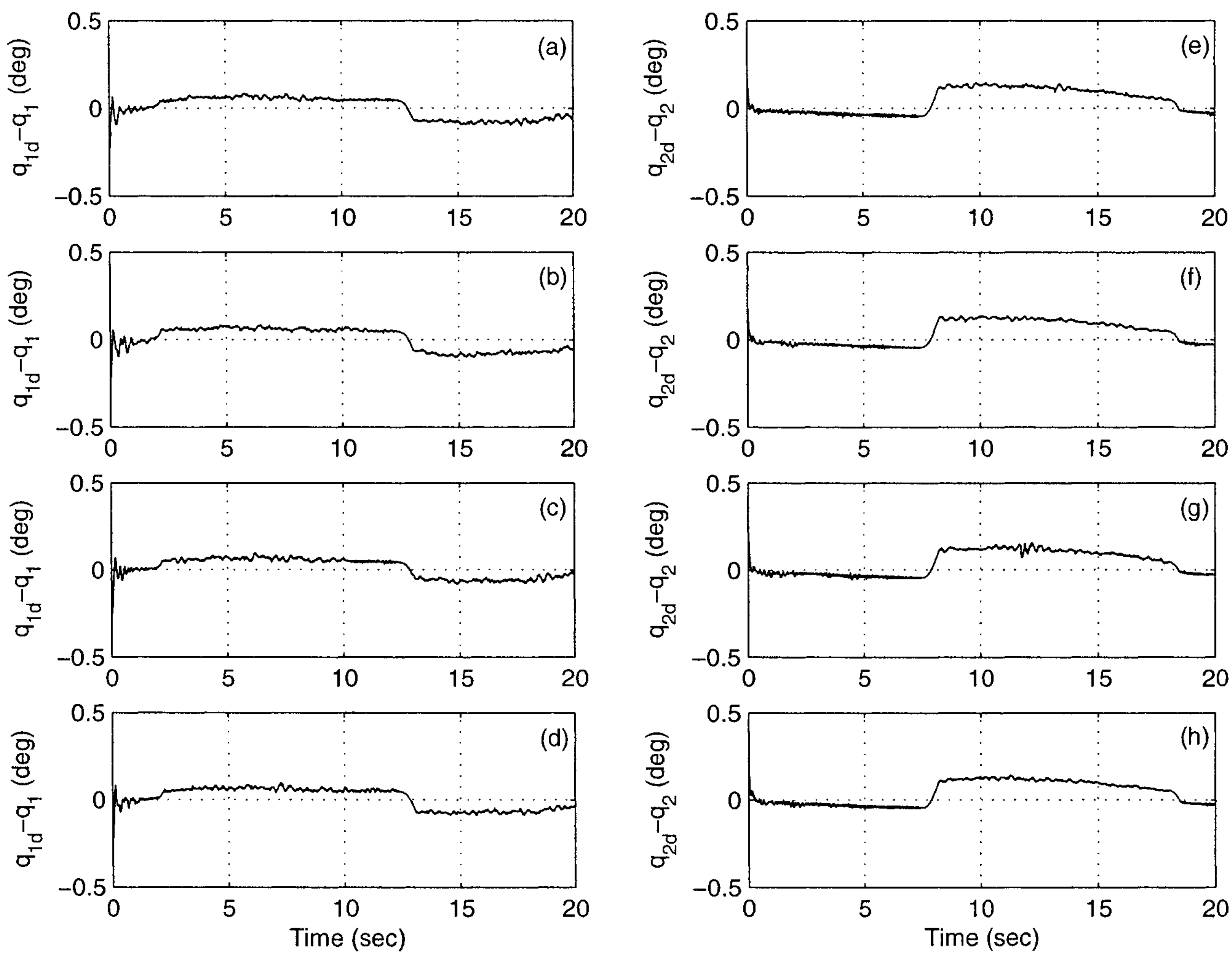

Figure 5-7: The tracking error of q_1 and q_2 for the circular trajectory in Case 1 without load: (a) $q_{1d} - q_1$ based on the ABS, (b) $q_{1d} - q_1$ based on the BS, (c) $q_{1d} - q_1$ based on the APD, (d) $q_{1d} - q_1$ based on the PD, (e) $q_{2d} - q_2$ based on the ABS, (f) $q_{2d} - q_2$ based on the BS, (g) $q_{2d} - q_2$ based on the APD, and (h) $q_{2d} - q_2$ based on the PD.

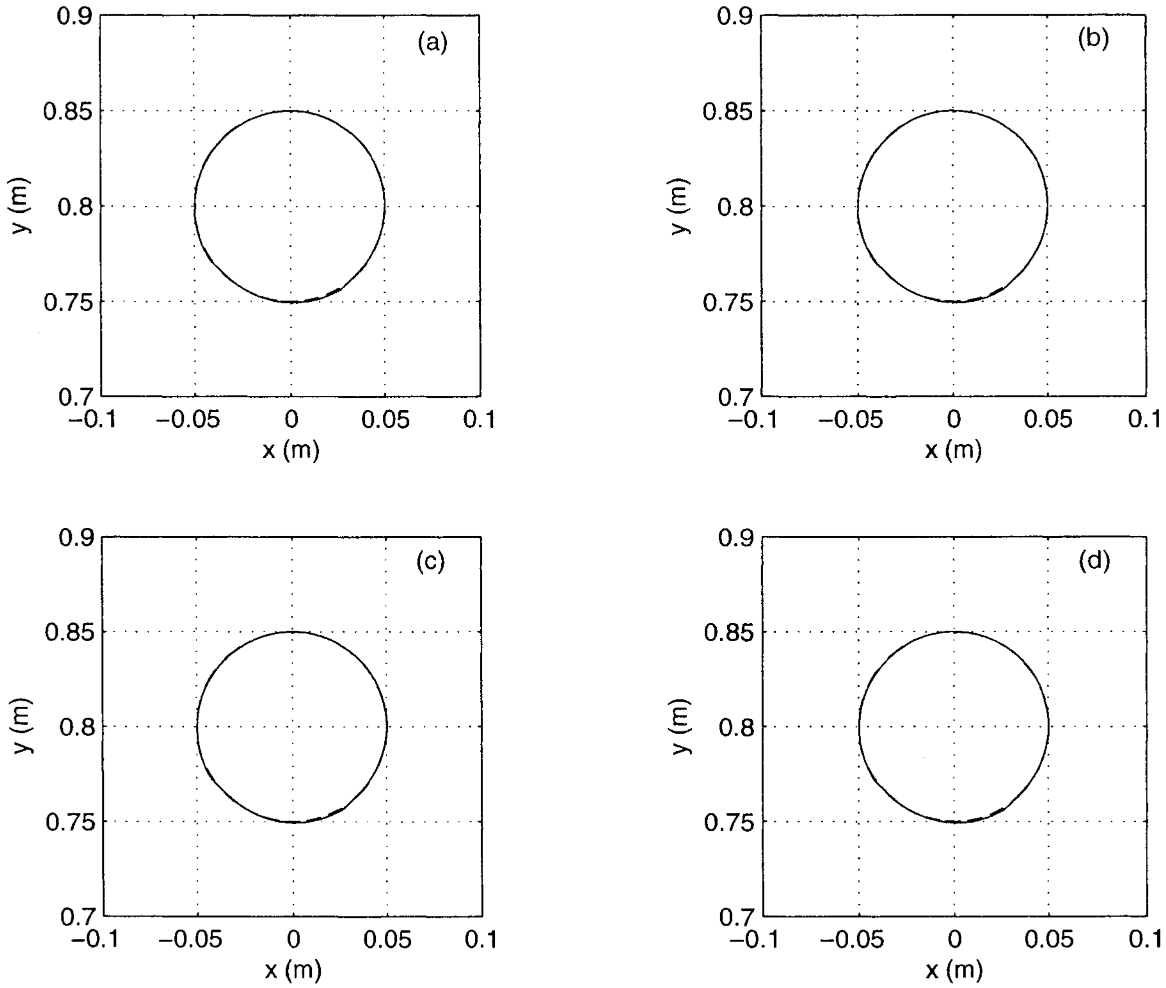

Figure 5-8: The results of tracking a circular trajectory in Case 1 with load. (a) the ABS, (b) the BS, (c) the APD, and (d) the PD. Dashed line — the desired, solid line — the actual.

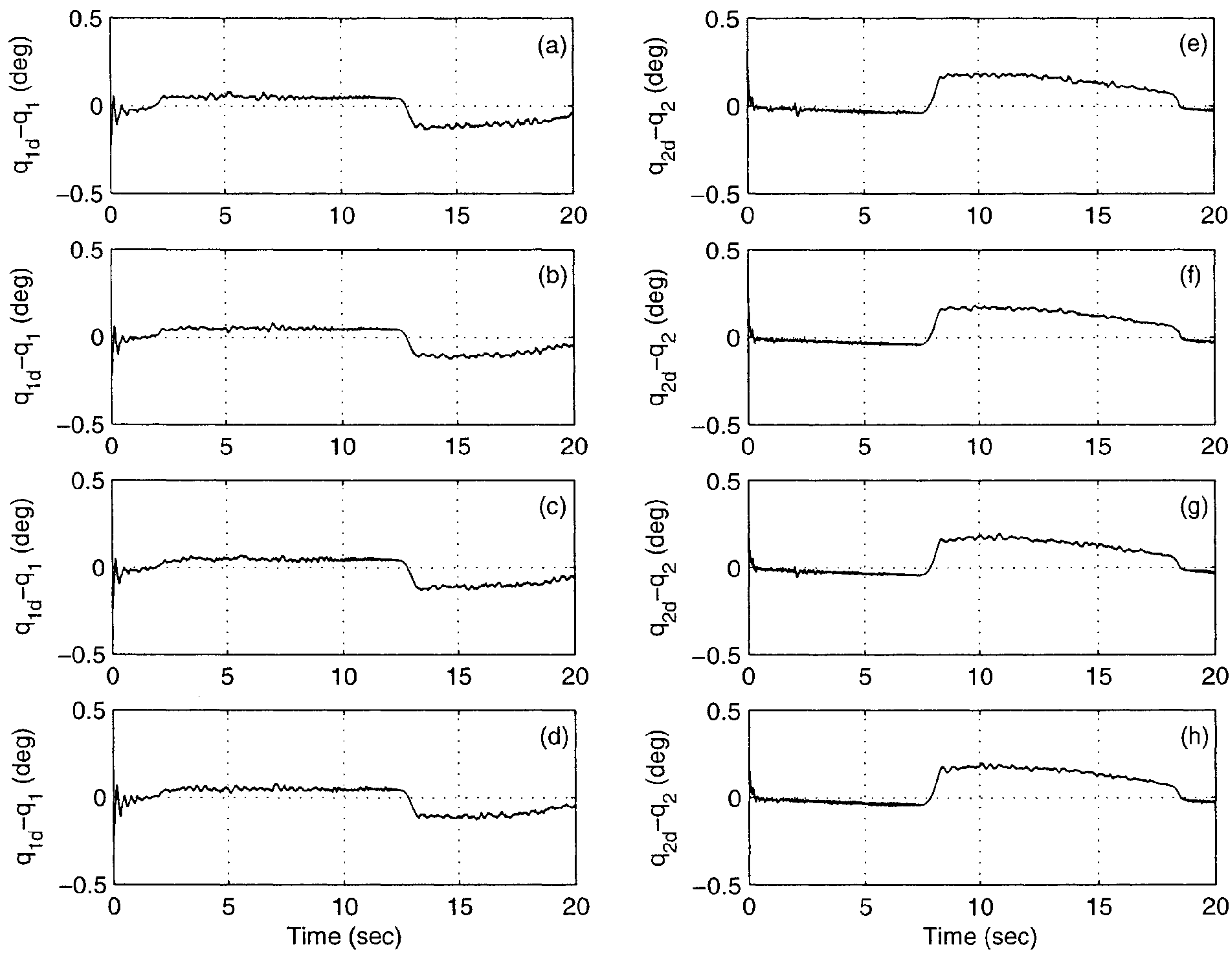

Figure 5-9: The tracking error of q_1 and q_2 for the circular trajectory in Case 1 with load: (a) $q_{1d} - q_1$ based on the ABS, (b) $q_{1d} - q_1$ based on the BS, (c) $q_{1d} - q_1$ based on the APD, (d) $q_{1d} - q_1$ based on the PD, (e) $q_{2d} - q_2$ based on the ABS, (f) $q_{2d} - q_2$ based on the BS, (g) $q_{2d} - q_2$ based on the APD, and (h) $q_{2d} - q_2$ based on the PD.

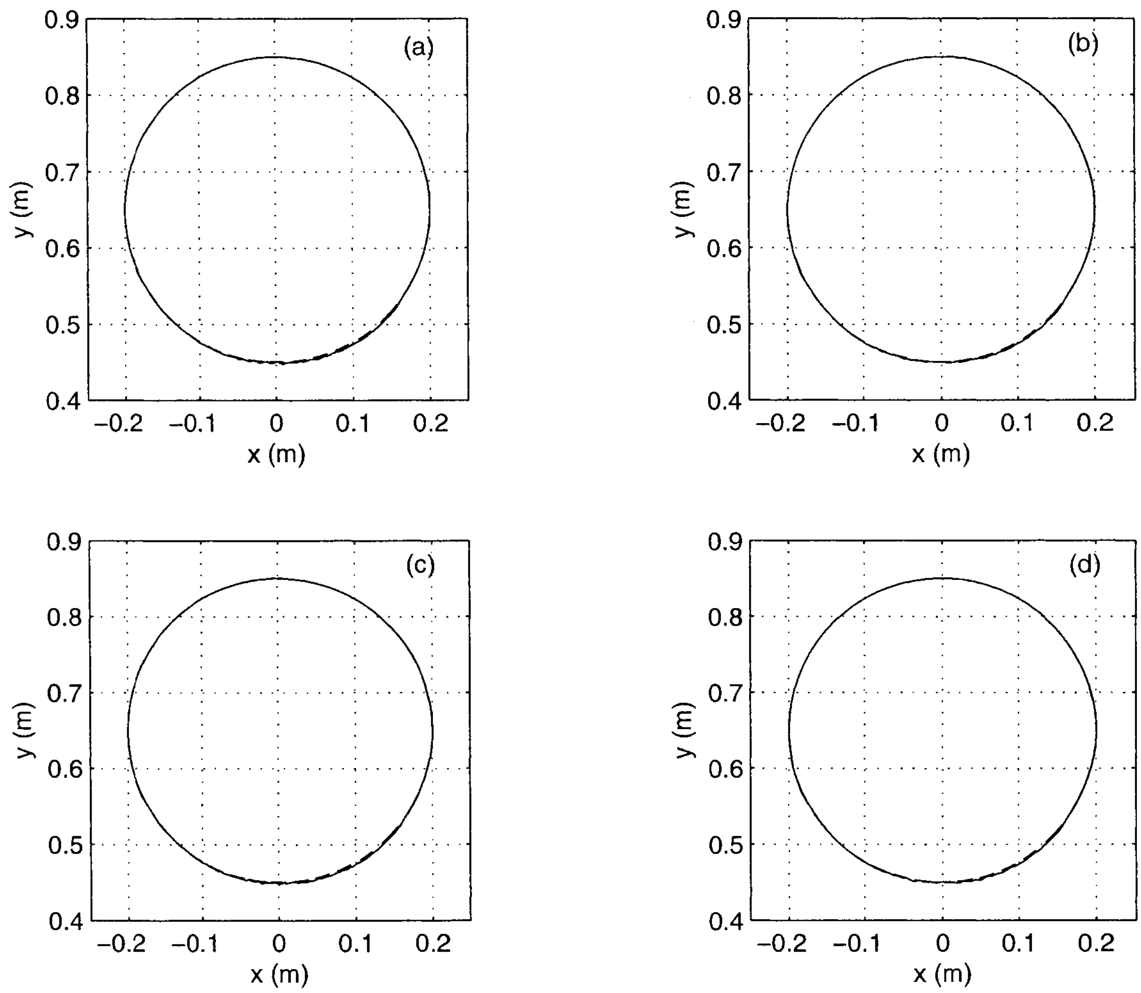

Figure 5-10: The results of tracking a circular trajectory in Case 2 without load. (a) the ABS, (b) the BS, (c) the APD, and (d) the PD. Dashed line — the desired, solid line — the actual.

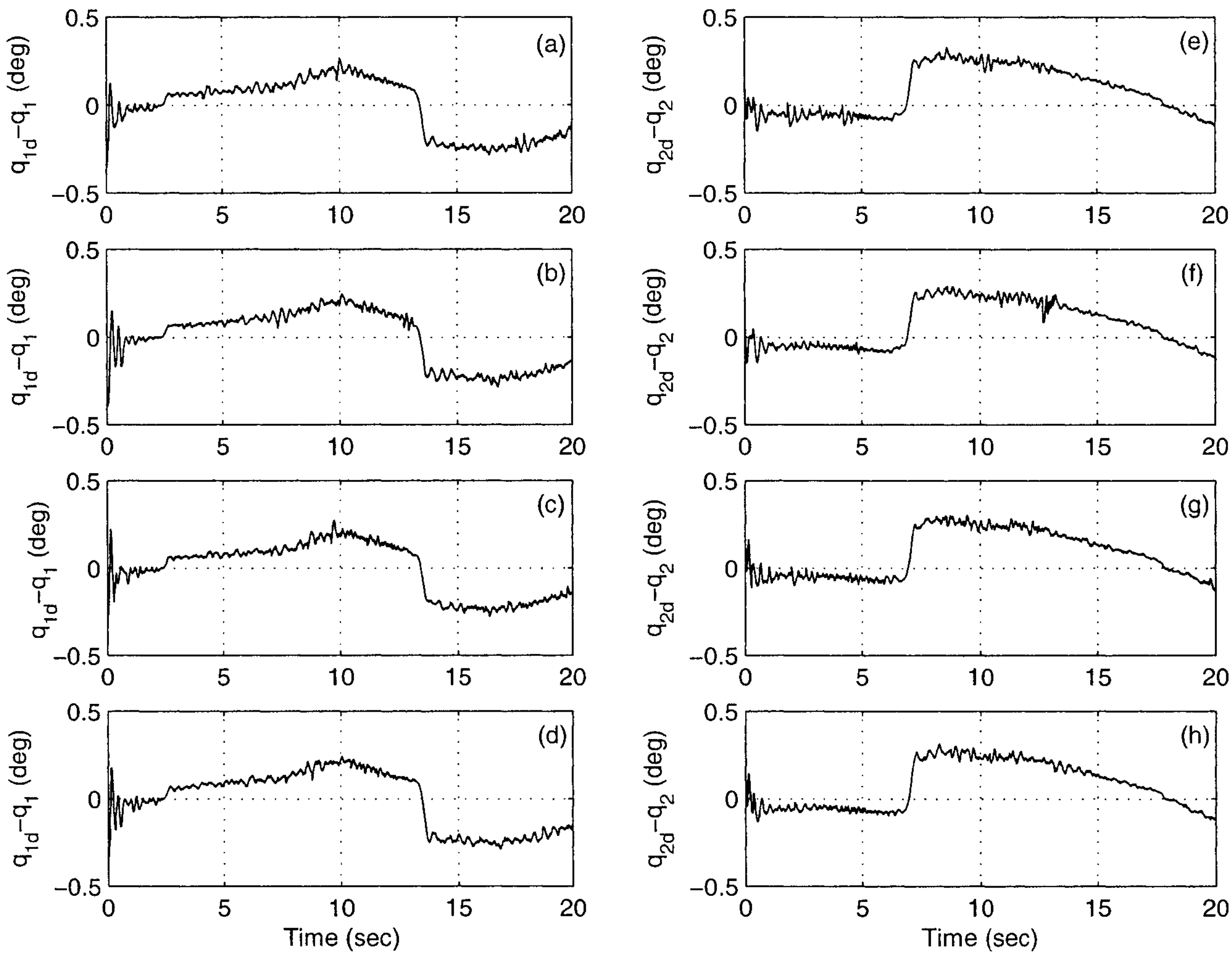

Figure 5-11: The tracking error of q_1 and q_2 for the circular trajectory in Case 2 without load: (a) $q_{1d} - q_1$ based on the ABS, (b) $q_{1d} - q_1$ based on the BS, (c) $q_{1d} - q_1$ based on the APD, (d) $q_{1d} - q_1$ based on the PD, (e) $q_{2d} - q_2$ based on the ABS, (f) $q_{2d} - q_2$ based on the BS, (g) $q_{2d} - q_2$ based on the APD, and (h) $q_{2d} - q_2$ based on the PD.

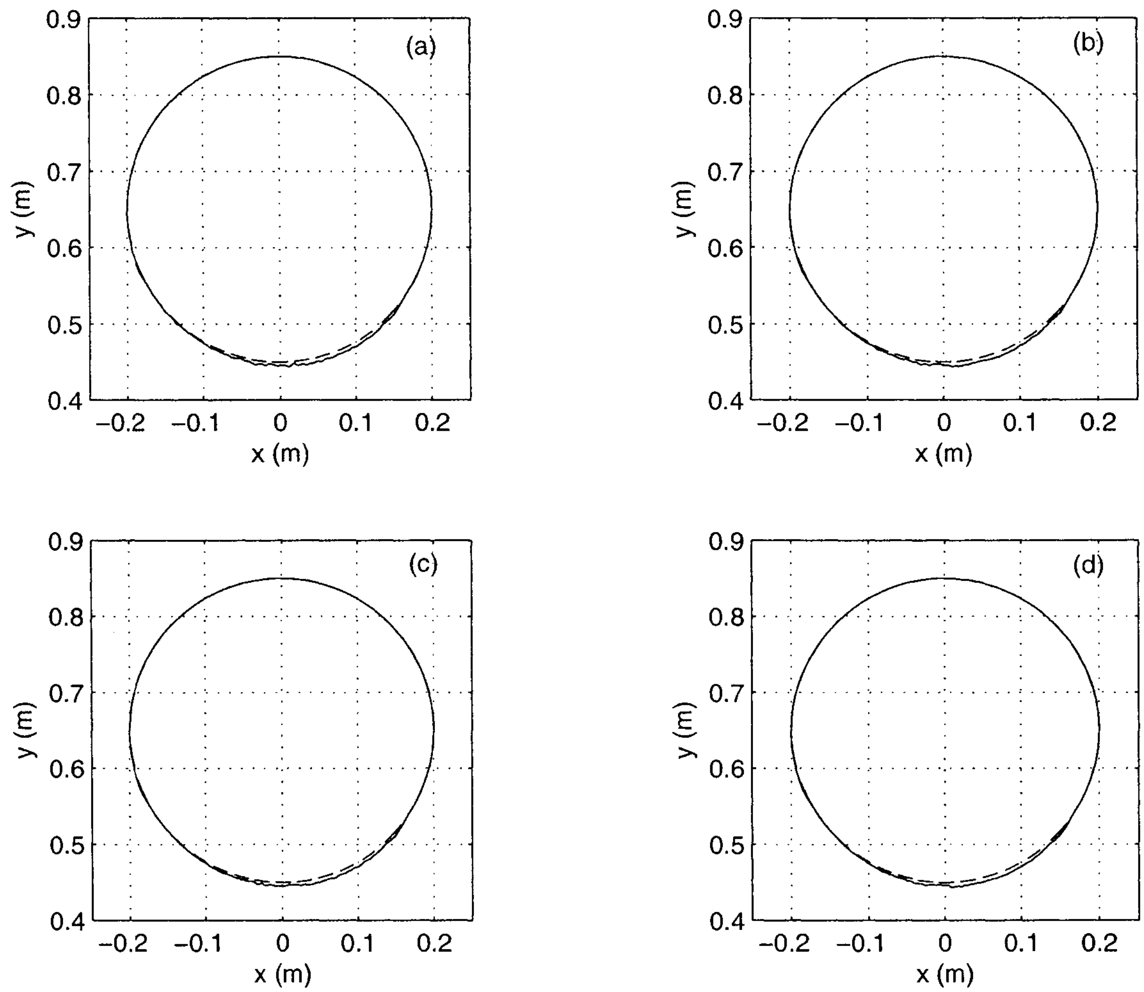

Figure 5-12: The results of tracking a circular trajectory in Case 2 with load. (a) the ABS, (b) the BS, (c) the APD, and (d) the PD. Dashed line — the desired, solid line — the actual.

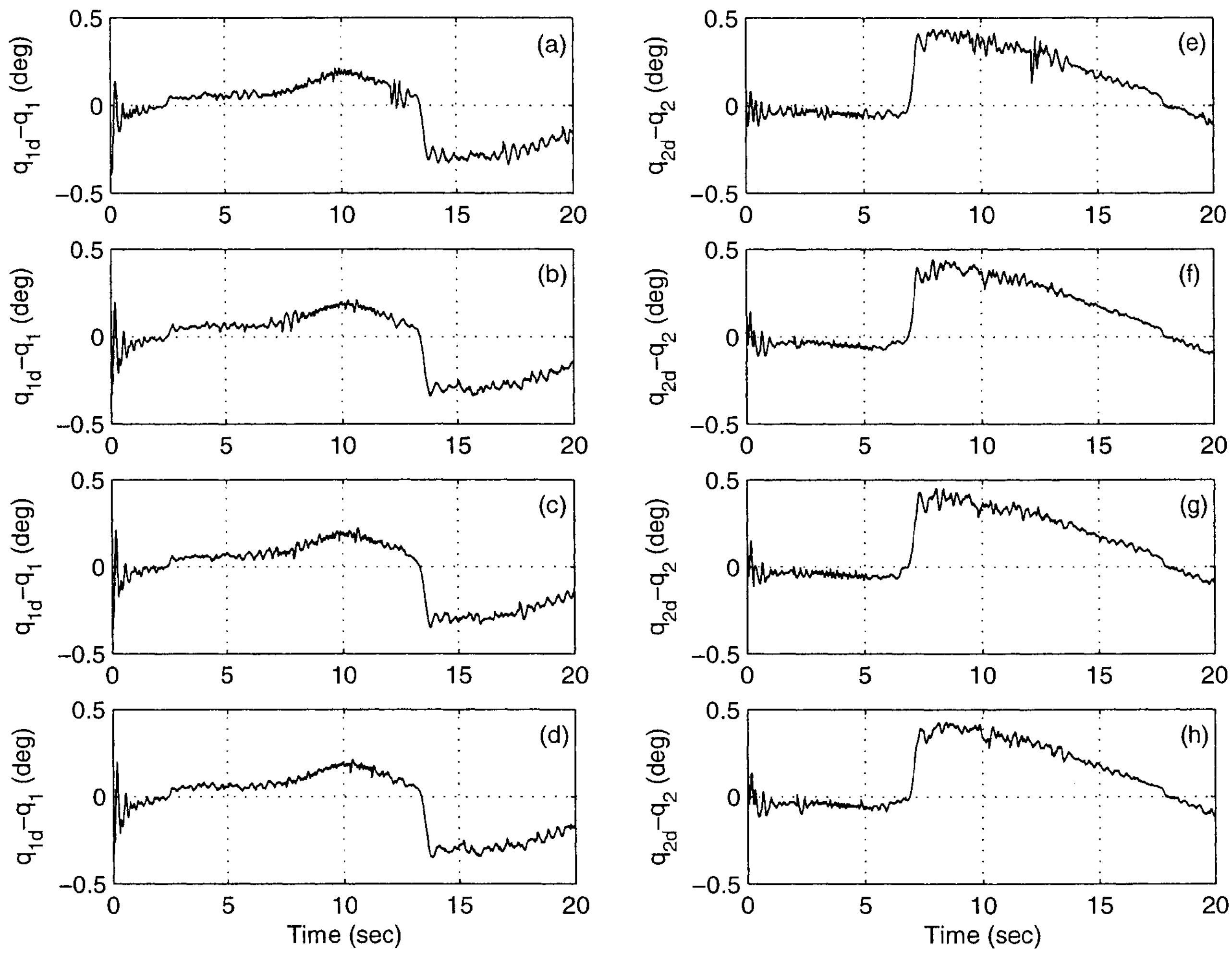

Figure 5-13: The tracking error of q_1 and q_2 for the circular trajectory in Case 2 with load: (a) $q_{1d} - q_1$ based on the ABS, (b) $q_{1d} - q_1$ based on the BS, (c) $q_{1d} - q_1$ based on the APD, (d) $q_{1d} - q_1$ based on the PD, (e) $q_{2d} - q_2$ based on the ABS, (f) $q_{2d} - q_2$ based on the BS, (g) $q_{2d} - q_2$ based on the APD, and (h) $q_{2d} - q_2$ based on the PD.

Table 5-3. The Norms of Tracking Circle Errors

at $f = 0.05\ Hz$ with Different Controllers and Circle Radii

f=0.05 Hz	q_1 (degree)				q_2 (degree)			
r(m) / load(g)	ABS	BS	APD	PD	ABS	BS	APD	PD
0.05 / 0	**9.6773**	10.1668	**8.9826**	9.5528	12.817	**12.3420**	12.5900	**12.4275**
0.05 / 100	11.4879	**10.6450**	11.1612	**10.7253**	16.9555	**16.0715**	**16.2636**	17.0593
0.05 / 161	12.5090	**11.9298**	**12.4440**	12.6267	17.6126	**16.8336**	18.8909	**17.7438**
0.05 / 261	**13.4038**	14.0760	14.5037	**14.1142**	20.9580	**19.7260**	22.4735	**19.6430**
0.1 / 0	**14.2549**	14.9761	**13.8097**	14.3092	17.4950	**17.3841**	17.7268	**17.3200**
0.1 / 100	16.7974	**16.4818**	**16.6078**	16.6197	23.7062	**22.5968**	**22.6431**	23.7274
0.1 / 161	17.9706	**17.3125**	17.9917	**17.8787**	24.3977	**24.3036**	26.3363	**25.3855**
0.1 / 261	20.3599	**19.9698**	20.7737	**20.7043**	29.8095	**28.4155**	31.7409	**28.2703**
0.15 / 0	19.3585	**19.1693**	**18.6362**	19.9475	21.5342	**21.3604**	21.9035	**21.7665**
0.15 / 100	21.7893	**21.4424**	21.2988	**21.1773**	29.9689	**28.4184**	**28.5961**	29.1667
0.15 / 161	23.4758	**22.8140**	23.3992	**23.2517**	31.8915	**31.0577**	34.3338	**32.7344**
0.15 / 261	26.0329	**25.5379**	**25.8343**	25.9281	39.5663	**37.4643**	42.4979	**37.5174**
0.2 / 0	25.3285	**25.2606**	**24.2149**	26.1350	24.7362	**23.2537**	24.4715	**24.2378**
0.2 / 100	**27.1548**	27.5782	**27.4446**	28.0907	33.6891	**33.3109**	**33.3480**	33.4573
0.2 / 161	29.5642	**29.0670**	29.1630	**29.0957**	39.9839	**36.2254**	**37.0543**	37.5631
0.2 / 261	**31.7791**	32.1678	**32.5090**	33.2724	44.6722	**41.8624**	45.2928	**43.7665**

Table 5-4. The Average Norms of Tracking Circle Errors at $f = 0.05\ Hz$ with Different Controllers and Circle Radii

f=0.05 Hz	Average Errors (degree)			
r(m) / load(g)	ABS	BS	APD	PD
0.05 / 0	**11.2472**	11.2544	**10.7863**	10.9902
0.05 / 100	14.2217	**13.3583**	**13.7124**	13.8923
0.05 / 161	15.0608	**14.3817**	15.6675	**15.1853**
0.05 / 261	17.1809	**16.9010**	18.4886	**16.8786**
0.1 / 0	**15.8750**	16.1801	**15.7683**	15.8146
0.1 / 100	20.2518	**19.5393**	**19.6255**	20.1736
0.1 / 161	21.1842	**20.8081**	22.1640	**21.6321**
0.1 / 261	25.0847	**24.1927**	26.2573	**24.4873**
0.15 / 0	20.4463	**20.2649**	**20.2699**	20.8570
0.15/100	25.8791	**24.9304**	**24.9475**	25.1720
0.15 / 161	27.6837	**26.9359**	28.8665	**27.9931**
0.15 / 261	32.7996	**31.5011**	34.1661	**31.7228**
0.2 / 0	25.0324	**24.2572**	**24.3432**	25.1864
0.2 / 100	**30.4220**	30.4446	**30.3963**	30.7740
0.2 / 161	34.7741	**32.6462**	**30.3963**	33.3294
0.2 / 261	38.2257	**37.0151**	38.9009	**38.5195**

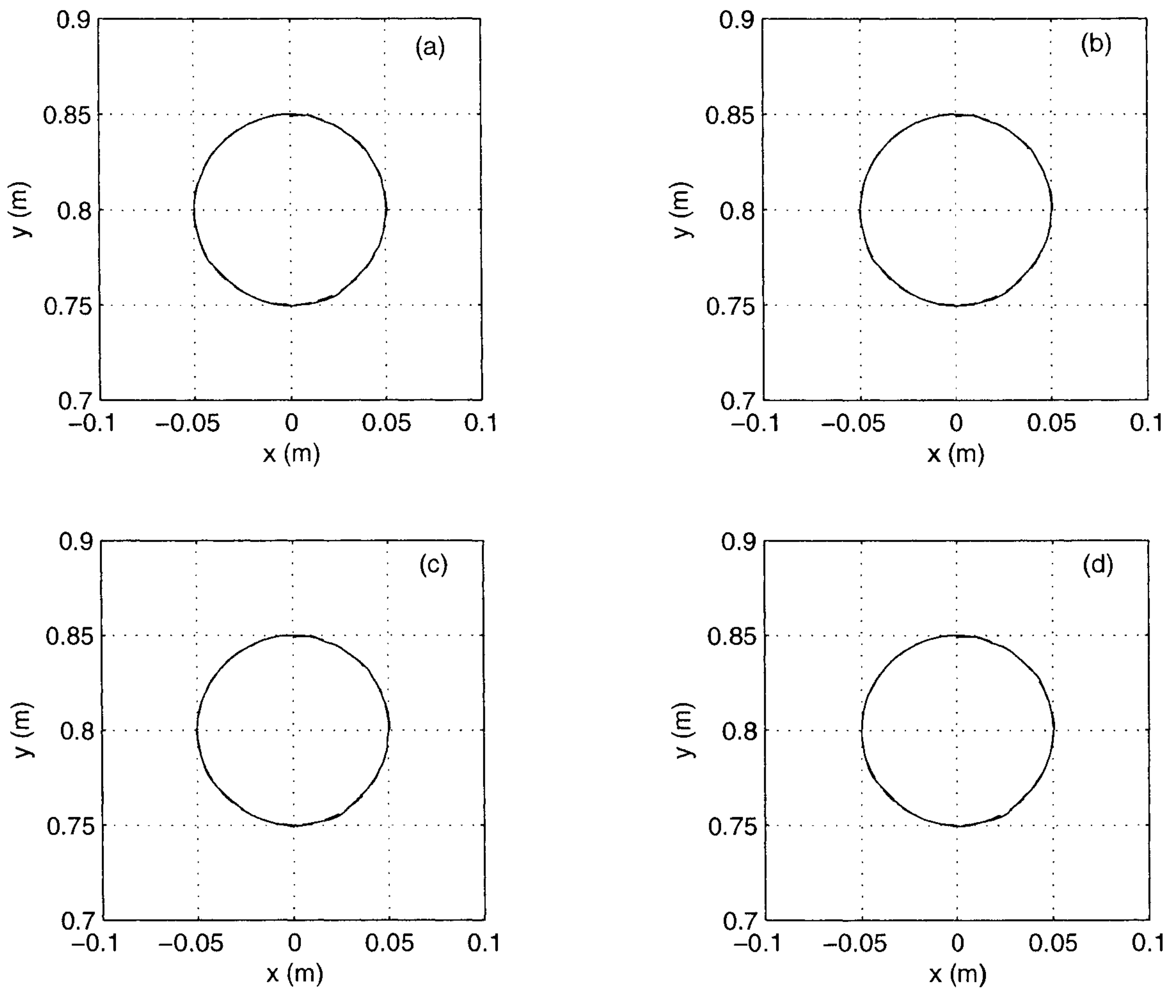

Figure 5-14: The results of tracking a circular trajectory in Case 3 without load. (a) the ABS, (b) the BS, (c) the APD, and (d) the PD. Dashed line — the desired, solid line — the actual.

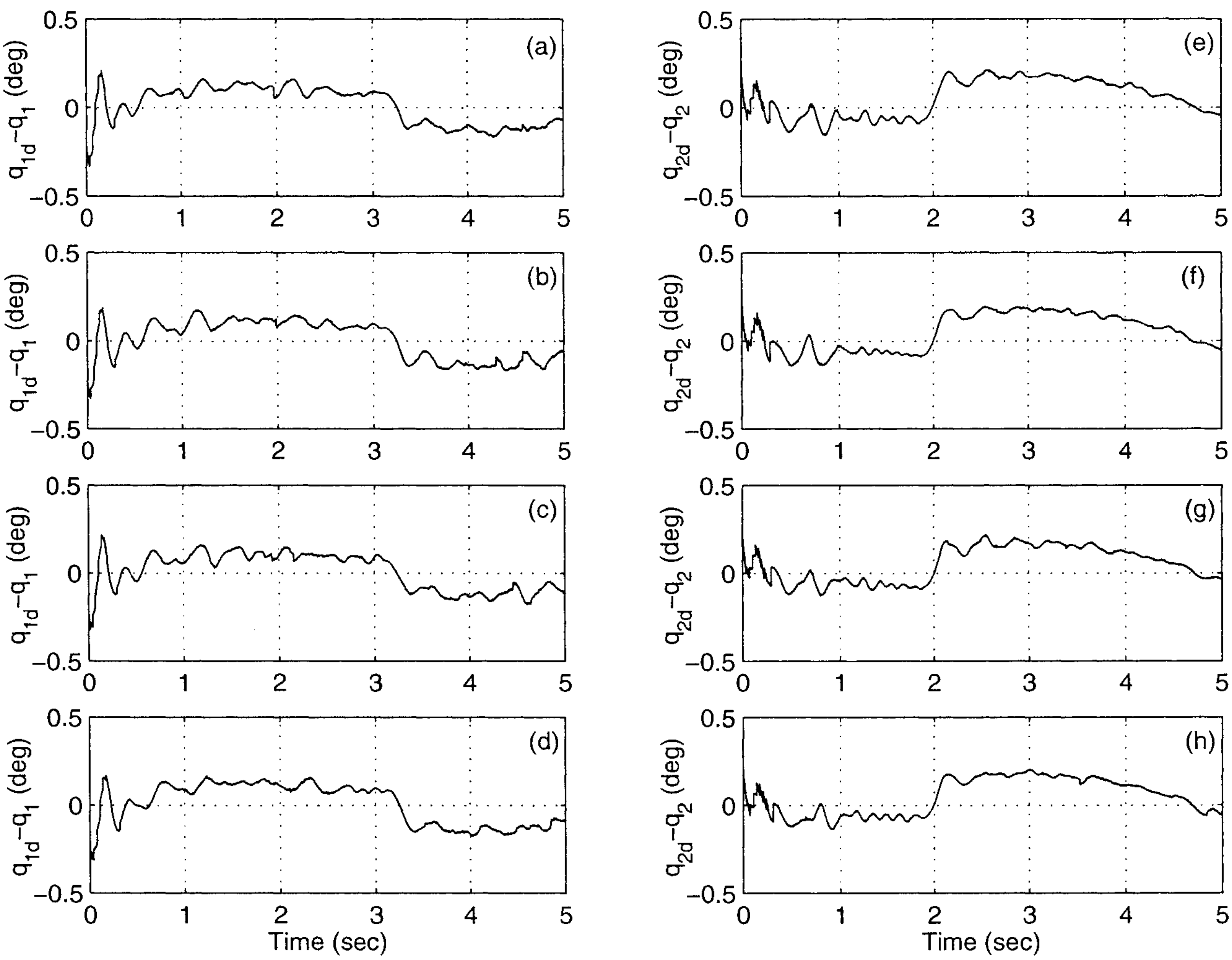

Figure 5-15: The tracking error of q_1 and q_2 for the circular trajectory in Case 3 without load: (a) $q_{1d} - q_1$ based on the ABS, (b) $q_{1d} - q_1$ based on the BS, (c) $q_{1d} - q_1$ based on the APD, (d) $q_{1d} - q_1$ based on the PD, (e) $q_{2d} - q_2$ based on the ABS, (f) $q_{2d} - q_2$ based on the BS, (g) $q_{2d} - q_2$ based on the APD, and (h) $q_{2d} - q_2$ based on the PD.

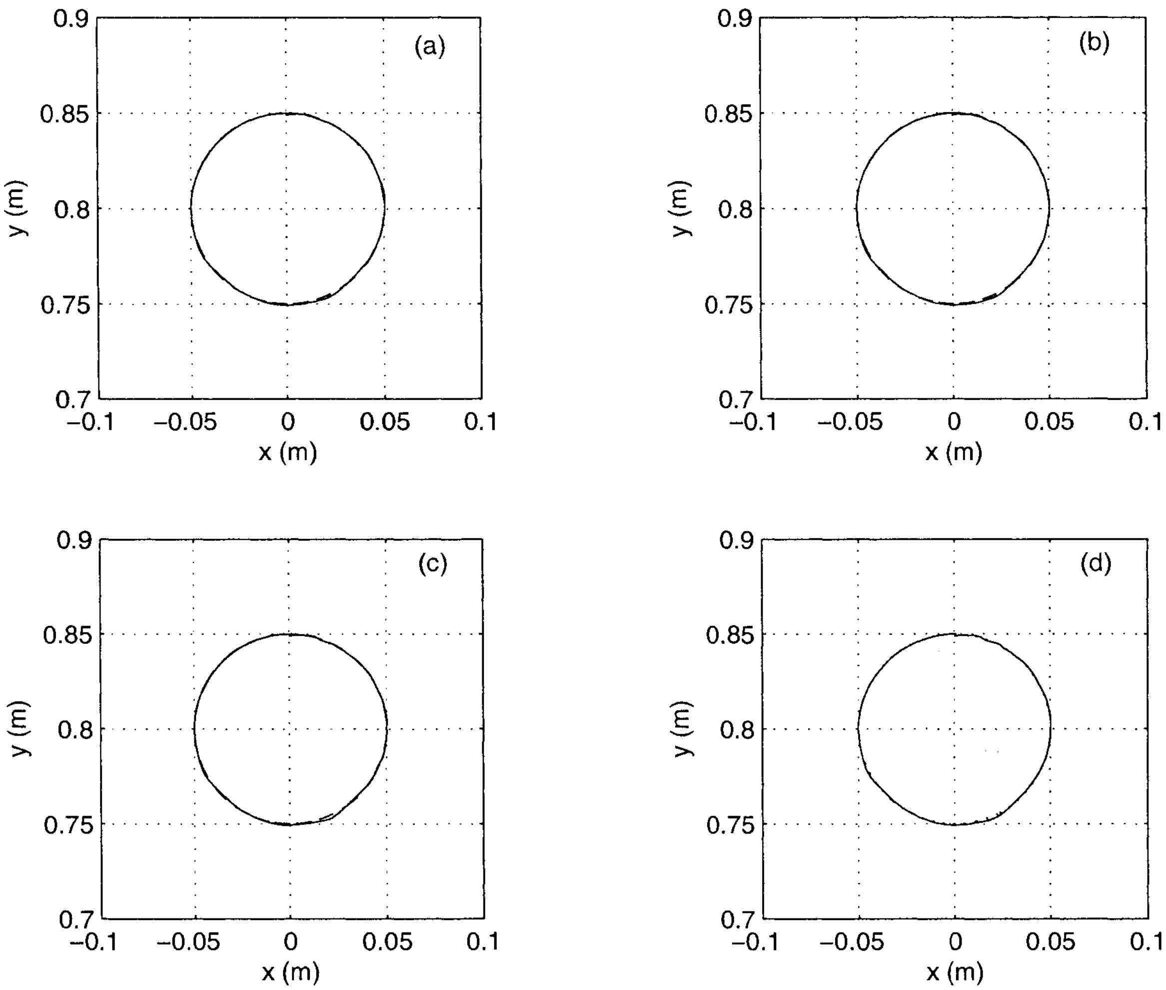

Figure 5-16: The results of tracking a circular trajectory in Case 3 with load. (a) the ABS, (b) the BS, (c) the APD, and (d) the PD. Dashed line — the desired, solid line — the actual.

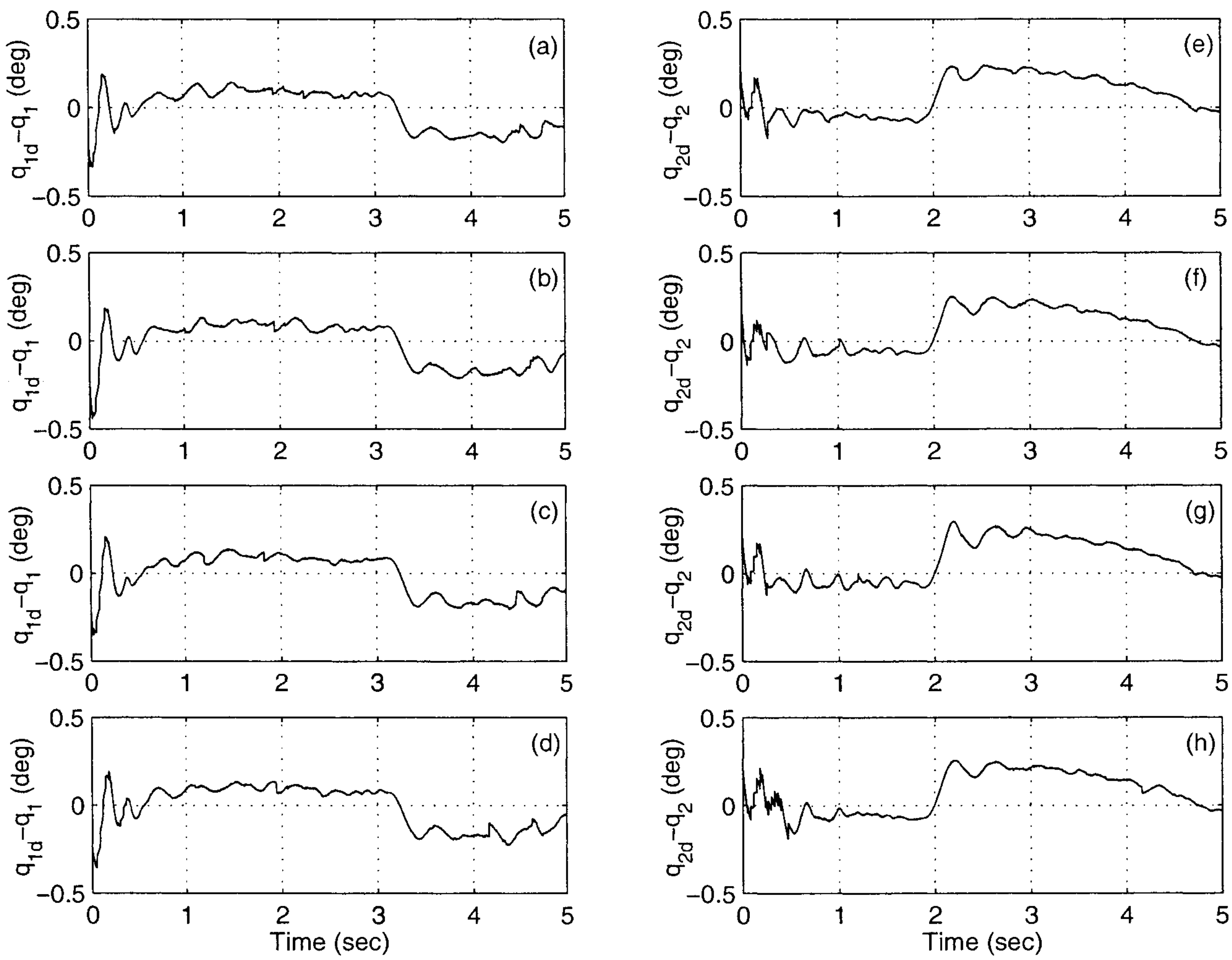

Figure 5-17: The tracking error of q_1 and q_2 for the circular trajectory in Case 3 with load: (a) $q_{1d} - q_1$ based on the ABS, (b) $q_{1d} - q_1$ based on the BS, (c) $q_{1d} - q_1$ based on the APD, (d) $q_{1d} - q_1$ based on the PD, (e) $q_{2d} - q_2$ based on the ABS, (f) $q_{2d} - q_2$ based on the BS, (g) $q_{2d} - q_2$ based on the APD, and (h) $q_{2d} - q_2$ based on the PD.

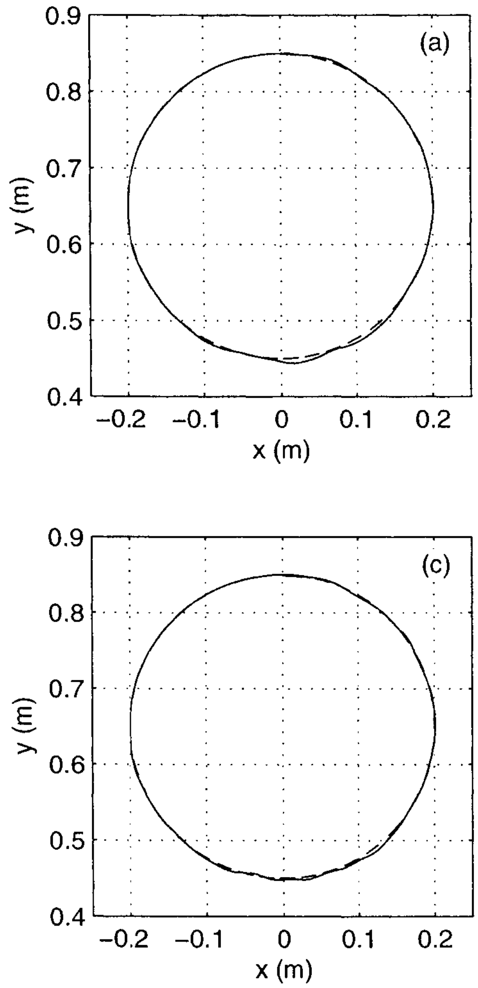

Figure 5-18: The results of tracking a circular trajectory in Case 4 without load. (a) the ABS, (b) the BS, (c) the APD, and (d) the PD. Dashed line — the desired, solid line — the actual.

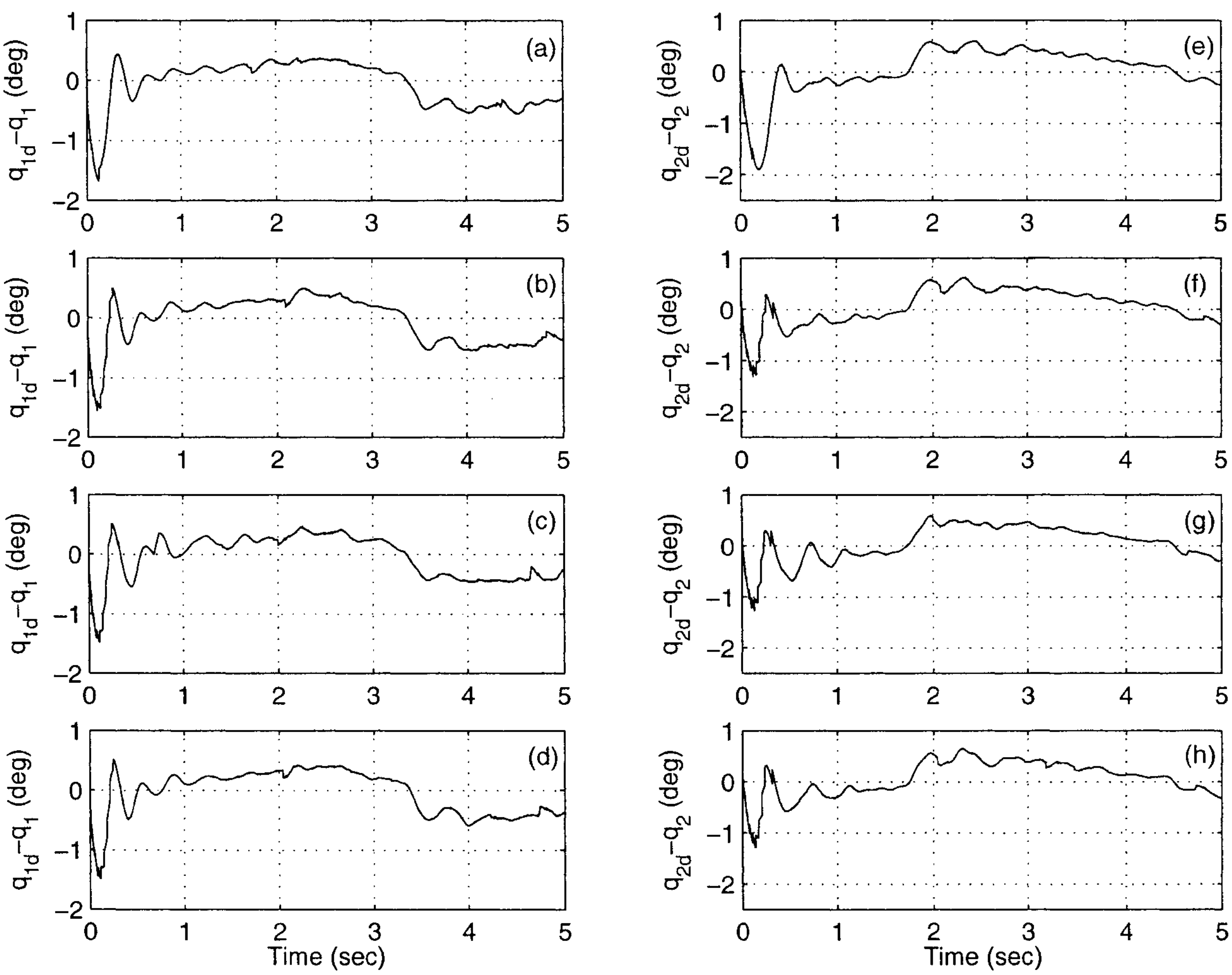

Figure 5-19: The tracking error of q_1 and q_2 for the circular trajectory in Case 4 without load: (a) $q_{1d} - q_1$ based on the ABS, (b) $q_{1d} - q_1$ based on the BS, (c) $q_{1d} - q_1$ based on the APD, (d) $q_{1d} - q_1$ based on the PD, (e) $q_{2d} - q_2$ based on the ABS, (f) $q_{2d} - q_2$ based on the BS, (g) $q_{2d} - q_2$ based on the APD, and (h) $q_{2d} - q_2$ based on the PD.

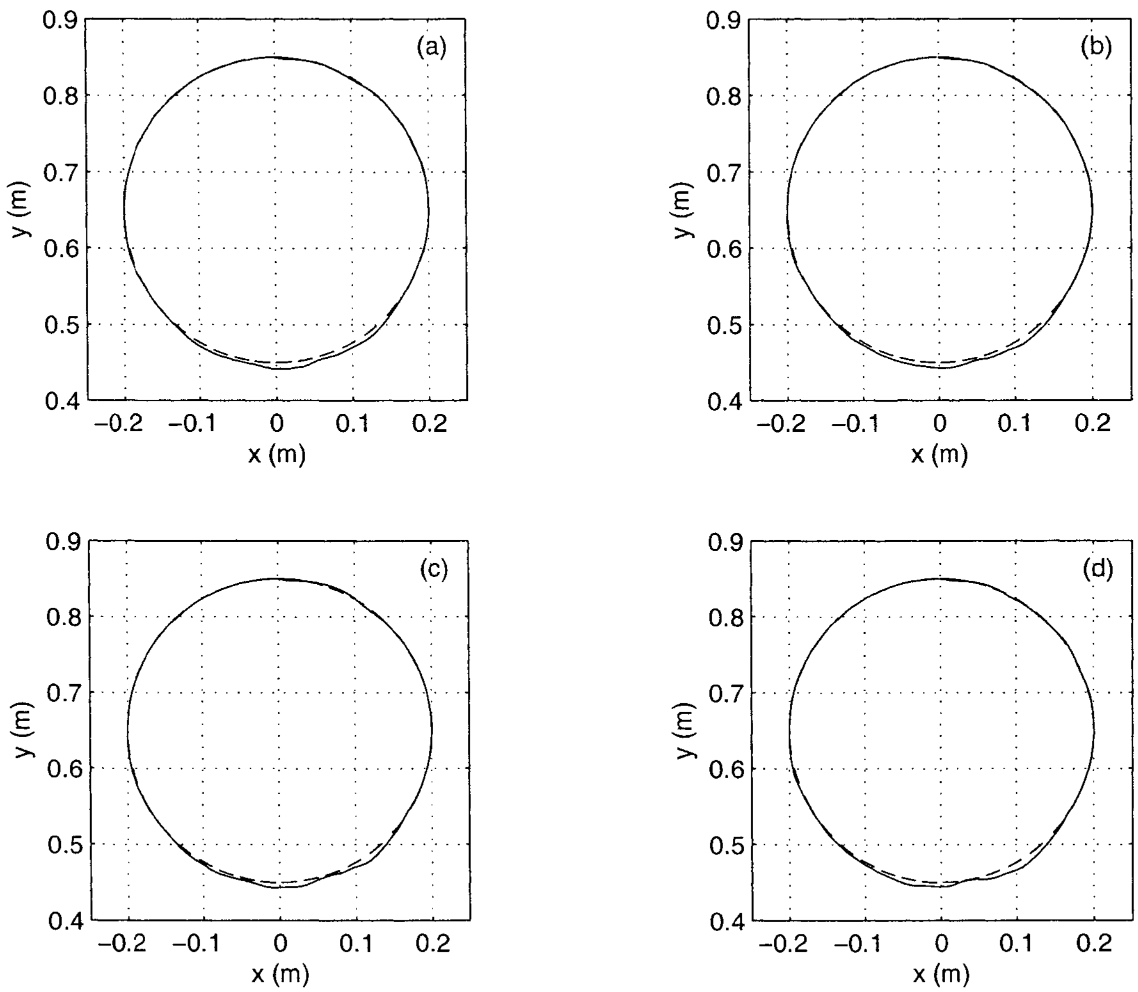

Figure 5-20: The results of tracking a circular trajectory in Case 4 with load. (a) the ABS, (b) the BS, (c) the APD, and (d) the PD. Dashed line — the desired, solid line — the actual.

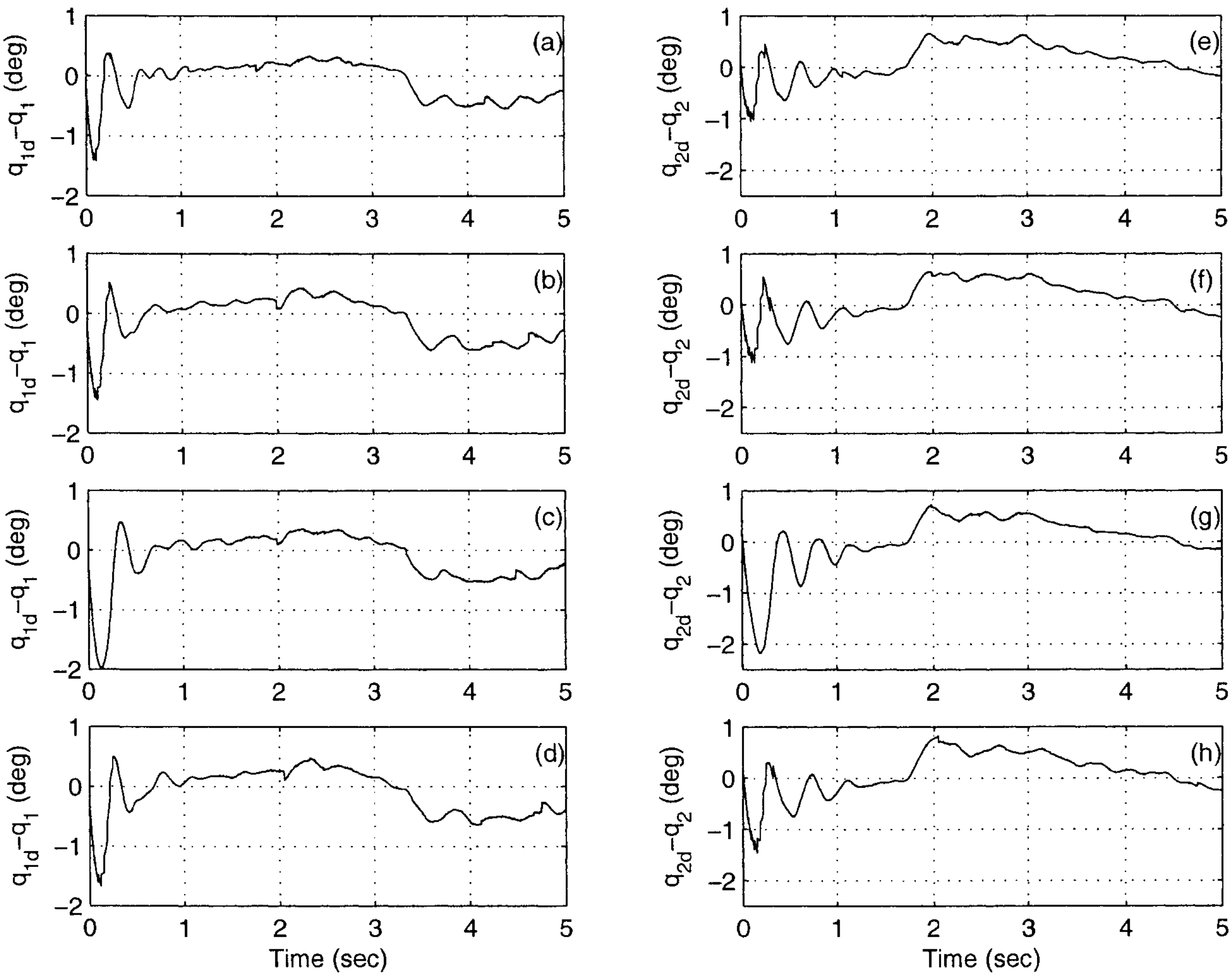

Figure 5-21: The tracking error of q_1 and q_2 for the circular trajectory in Case 4 with load: (a) $q_{1d} - q_1$ based on the ABS, (b) $q_{1d} - q_1$ based on the BS, (c) $q_{1d} - q_1$ based on the APD, (d) $q_{1d} - q_1$ based on the PD, (e) $q_{2d} - q_2$ based on the ABS, (f) $q_{2d} - q_2$ based on the BS, (g) $q_{2d} - q_2$ based on the APD, and (h) $q_{2d} - q_2$ based on the PD.

Table 5-5. The Norms of Tracking Circle Errors

at $f = 0.1\ Hz$ with Different Controllers and Circle Radii

f=0.1 Hz	q_1 (degree)				q_2 (degree)			
r(m) / load(g)	ABS	BS	APD	PD	ABS	BS	APD	PD
0.05 / 0	**13.3303**	13.9583	**13.5526**	13.8856	15.9025	**15.5717**	**15.8563**	15.6828
0.05 / 100	**14.1092**	14.2841	14.5868	**13.9304**	19.1460	**18.4733**	19.4476	**19.2779**
0.05 / 161	15.8536	**15.7814**	15.9229	**15.8975**	21.4469	**20.4738**	22.4738	**21.1455**
0.05 / 261	**17.0320**	17.0984	17.2991	**16.9053**	23.9651	**23.3258**	23.5461	**23.4933**
0.1 / 0	**21.0923**	21.7993	**21.1088**	21.6077	22.9516	**22.8734**	**23.8435**	23.9962
0.1 / 100	22.3061	**22.0770**	22.8010	**22.7638**	**27.5086**	27.5753	27.9461	**27.8490**
0.1 / 161	**24.4998**	24.3750	**24.3679**	24.4337	**30.4539**	31.5143	31.4998	**30.1806**
0.1 / 261	**26.0395**	26.6331	**25.0687**	26.7818	34.6253	**33.9757**	36.0918	**34.2551**
0.15 / 0	**28.5865**	29.0920	**28.5584**	29.1245	30.0482	**29.7383**	30.4563	**30.2596**
0.15 / 100	29.8701	**29.4884**	**29.7317**	30.2696	**37.4490**	37.4578	36.7600	**36.2170**
0.15 / 161	**31.5307**	33.2696	**30.9478**	32.6916	**40.1011**	40.4486	**39.7049**	41.2521
0.15 / 261	**34.0374**	35.0476	**34.8055**	36.2841	**47.5395**	47.5604	**48.2512**	48.6393
0.2 / 0	**37.4209**	38.0717	**36.8181**	39.9114	34.5624	**34.3471**	**36.7947**	37.0917
0.2 / 100	**37.0743**	38.1955	**37.2032**	38.7533	44.0338	**42.5040**	**43.2365**	43.8519
0.2 / 161	42.4050	**41.8295**	**40.4493**	41.0791	47.8825	**46.8907**	49.2206	**48.9343**
0.2 / 261	**42.6786**	43.6144	**44.0015**	44.6222	**52.0922**	53.9586	57.8091	**52.9764**

Table 5-6. The Average Norms of Tracking Circle Errors at $f = 0.1\ Hz$ with Different Controllers and Circle Radii

f=0.1 Hz	Average Errors (degree)			
r(m) / load(g)	ABS	BS	APD	PD
0.05 / 0	**14.6164**	14.7650	**14.7045**	14.7842
0.05 / 100	16.6276	**16.3787**	17.0172	**16.6042**
0.05 / 161	18.6503	**18.1276**	19.1984	**18.5215**
0.05 / 261	20.4986	**20.2121**	20.4226	**20.1993**
0.1 / 0	**22.0220**	22.3364	**22.4762**	22.8020
0.1 / 100	24.9074	**24.8262**	25.3736	**25.3064**
0.1 / 161	**27.4769**	27.9447	27.9339	**27.3072**
0.1 / 261	30.3324	**30.3044**	30.5803	**30.5185**
0.15 / 0	**29.3174**	29.4152	**29.5074**	29.6921
0.15 / 100	33.6596	**33.4731**	33.2459	**33.2433**
0.15 / 161	**35.8159**	36.8591	**35.3264**	36.9719
0.15 / 261	**40.7885**	41.3040	**41.5284**	42.4617
0.2 / 0	**35.9917**	36.2094	**36.8064**	38.5016
0.2 / 100	40.5541	**40.3498**	**40.2199**	41.3026
0.2 / 161	45.1438	**44.3601**	**44.8350**	45.0067
0.2 / 261	**47.3854**	48.7865	50.9053	**48.7993**

Table 5-7. The Norms of Tracking Circle Errors

at $f = 0.2\ Hz$ with Different Controllers and Circle Radii

f=0.2 Hz	q_1 (degree)				q_2 (degree)			
r(m) / load (g)	ABS	BS	APD	PD	ABS	BS	APD	PD
0.05 / 0	**20.5738**	21.0759	**20.1326**	21.9709	22.0201	**21.7119**	**21.0062**	21.6628
0.05 / 100	**21.5723**	22.6521	22.0990	22.3875	**23.9511**	24.0999	25.3657	**24.8289**
0.05 / 161	23.4274	**23.2146**	23.4818	23.6710	27.1643	**26.1233**	26.7804	**26.2534**
0.05 / 261	**23.3712**	24.8063	24.4320	26.3249	29.2008	**28.7704**	29.3043	**28.8645**
0.1 / 0	**34.8719**	35.6543	**33.7293**	36.6083	**35.3430**	35.3901	**34.3924**	36.3389
0.1 / 100	**35.3580**	36.7548	**34.8632**	36.2909	**39.0723**	39.9743	**38.3818**	38.6734
0.1 / 161	**38.4451**	39.4483	**36.3933**	38.6871	**43.3818**	43.6099	43.3520	**42.3060**
0.1 / 261	**40.0852**	41.2499	**39.3806**	40.3366	**46.2579**	46.8492	47.5575	**45.6447**
0.15 / 0	46.7107	**46.0188**	47.1770	48.7560	46.5369	**45.6803**	**47.2657**	47.8796
0.15 / 100	**51.0805**	52.4516	**49.5659**	54.0793	56.4757	**55.5808**	**53.7377**	57.0942
0.15 / 161	**52.5648**	54.0737	**50.9708**	51.6276	**58.6531**	60.6645	56.2147	**56.0200**
0.15 / 261	56.7268	**54.6750**	55.3109	59.1308	63.3346	**63.2048**	**64.7716**	65.0673
0.2 / 0	**65.1866**	67.6567	**63.9666**	67.1130	66.6977	**62.6557**	**60.7594**	62.5053
0.2 / 100	**61.2315**	66.6963	67.1193	68.6362	**63.3729**	68.2227	**70.6589**	70.7680

Table 5-8. The Average Norms of Tracking Circle Errors at $f = 0.2\ Hz$ with Different Controllers and Circle Radii

f=0.2 Hz	Average Error (degree)			
r(m) / load(g)	ABS	BS	APD	PD
0.05 / 0	**21.2970**	21.3939	**20.5694**	21.8169
0.05 / 100	**22.7617**	23.3760	23.7324	**23.6082**
0.05 / 161	25.2959	**24.6690**	25.1311	**24.9622**
0.05 / 261	**26.2860**	26.7884	**26.8682**	27.5947
0.1 / 0	**35.1075**	35.5222	**34.0609**	36.4736
0.1 / 100	**37.2152**	38.3646	**36.6225**	37.4822
0.1 / 161	**40.9135**	41.5291	**39.8727**	40.4966
0.1 / 261	**43.1716**	44.0496	43.4691	**42.9907**
0.15 / 0	46.6238	**45.8496**	**47.2214**	48.3178
0.15 / 100	**53.7781**	54.0162	**51.6518**	55.5868
0.15 / 161	**55.6090**	57.3691	**53.5928**	53.8238
0.15 / 261	60.0307	**58.9399**	**60.0413**	62.0991
0.2 / 0	65.9422	**65.1562**	**62.3630**	64.8092
0.2 / 100	**62.3022**	67.4595	**68.8891**	69.7021

5.3.2 Line Tracking

For line tracking, the desired line used here is the same as in Section 4.2. It can be checked that this line does not contain any singular points and is at least 35 centimeters away from the singular region. Fig. 5-22 to Fig. 5-23 are for the case without load while Fig. 5-24 to Fig. 5-25 are for the case with 100 gram load. Comparing the results from load test with the results from no load test, the norms of tracking errors of adaptive controllers increase less than those of non-adaptive controllers.

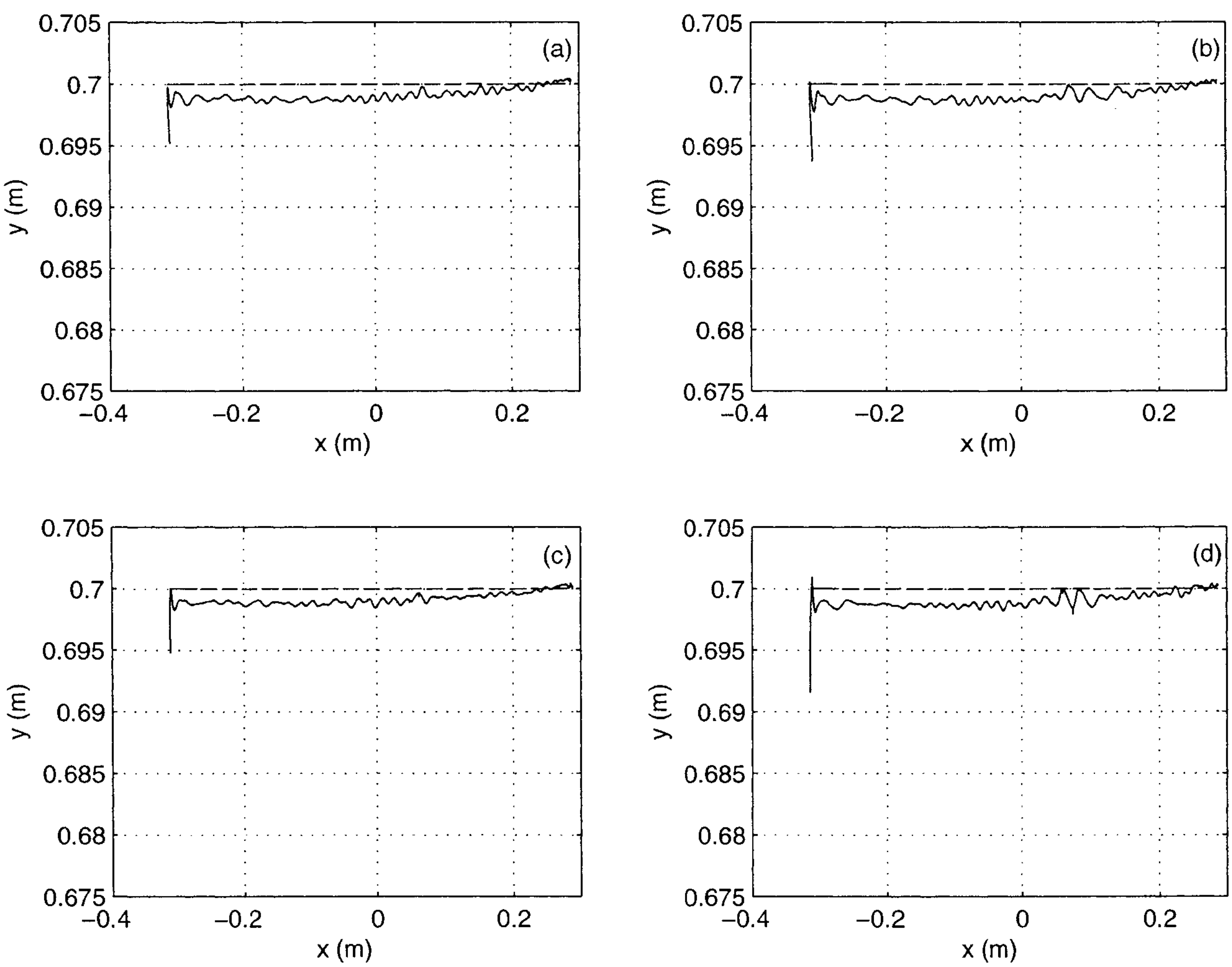

Figure 5-22: The results of tracking a linear trajectory without load. (a) the ABS, (b) the BS, (c) the APD, and (d) the PD. Dashed line — the desired, solid line — the actual.

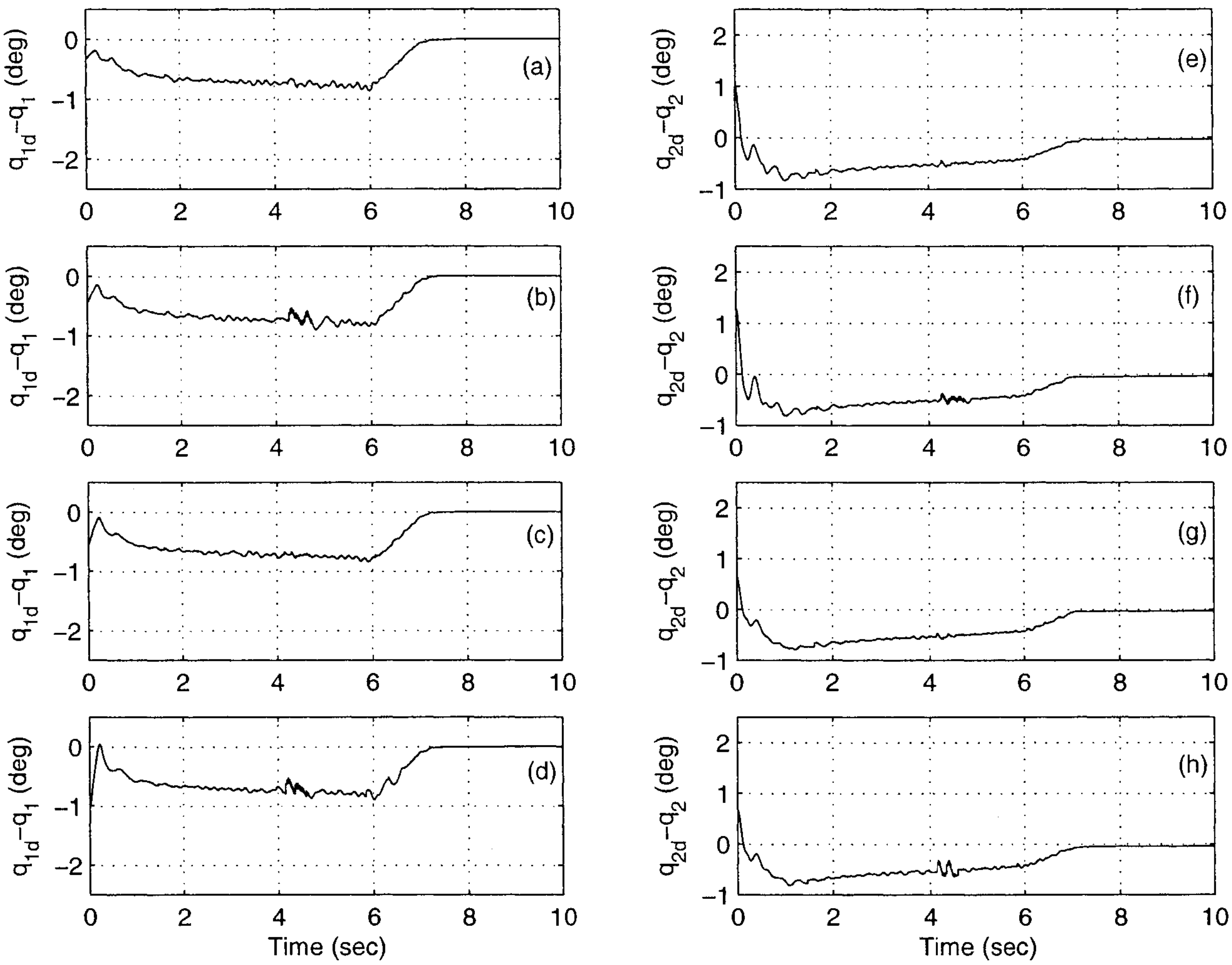

Figure 5-23: The tracking error of q_1 and q_2 for the linear trajectory without load: (a) $q_{1d} - q_1$ based on the ABS, (b) $q_{1d} - q_1$ based on the BS, (c) $q_{1d} - q_1$ based on the APD, (d) $q_{1d} - q_1$ based on the PD, (e) $q_{2d} - q_2$ based on the ABS, (f) $q_{2d} - q_2$ based on the BS, (g) $q_{2d} - q_2$ based on the APD, and (h) $q_{2d} - q_2$ based on the PD.

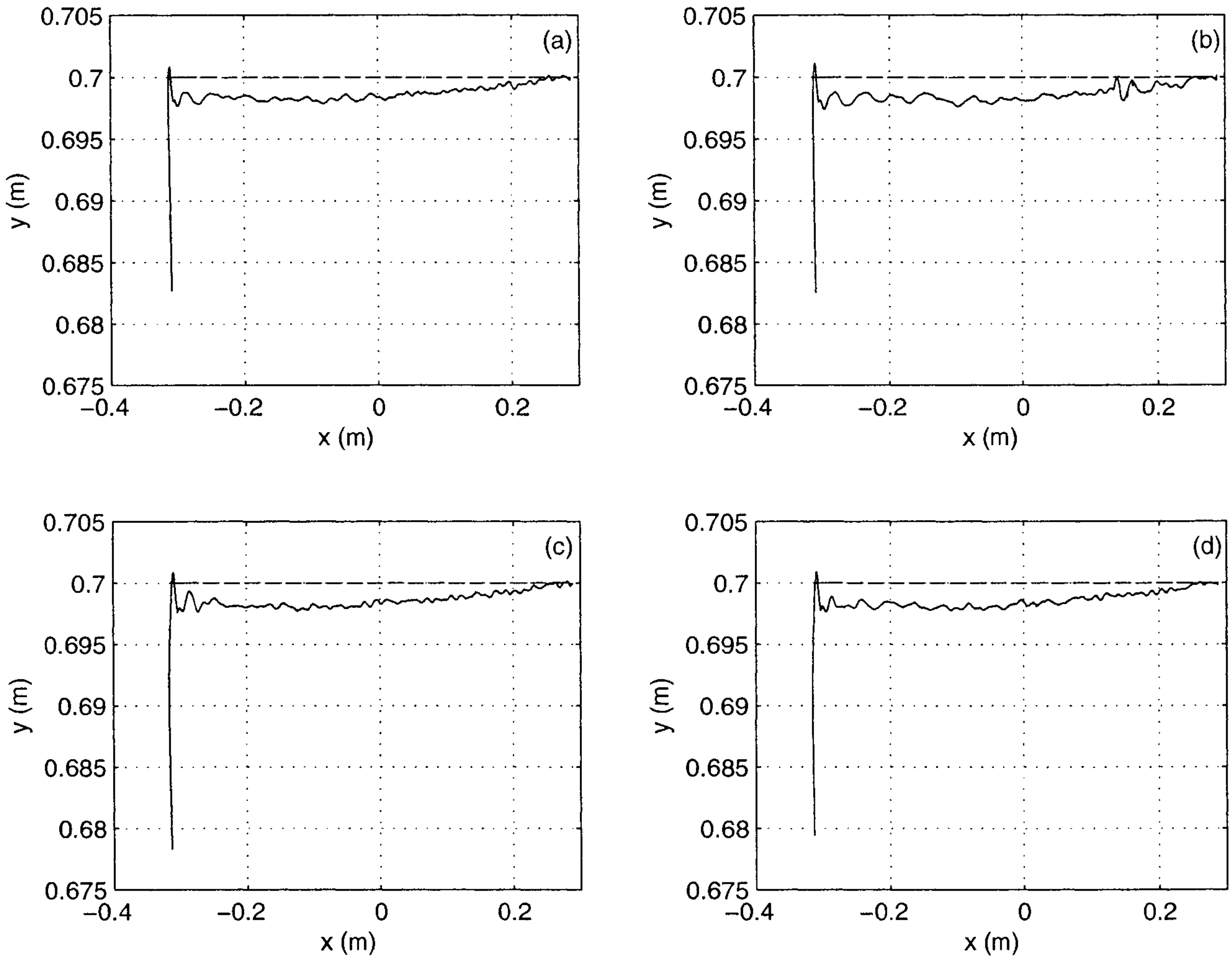

Figure 5-24: The results of tracking a linear trajectory with load. (a) the ABS, (b) the BS, (c) the APD, and (d) the PD. Dashed line — the desired, solid line — the actual.

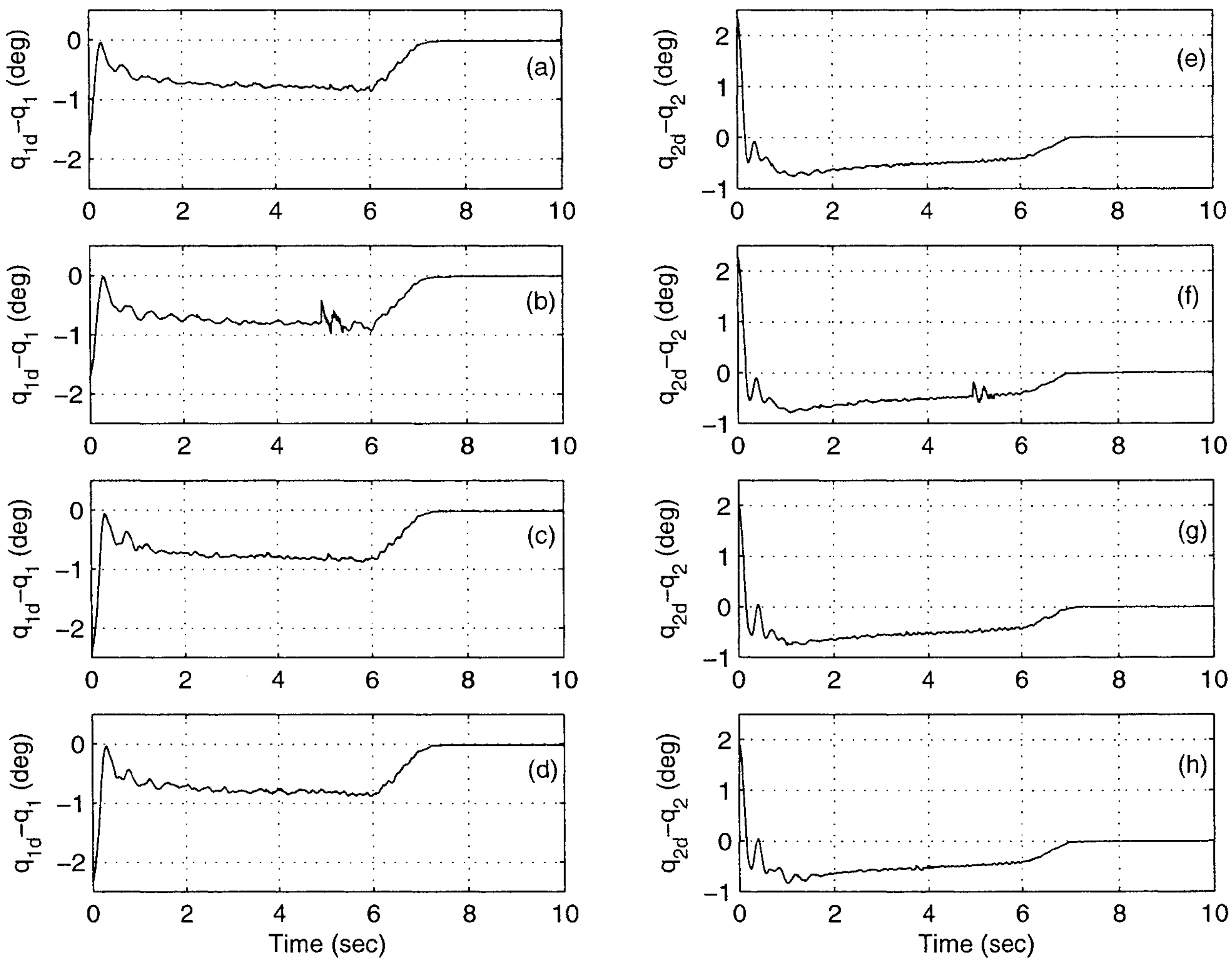

Figure 5-25: The tracking error of q_1 and q_2 for the linear trajectory with load: (a) $q_{1d} - q_1$ based on the ABS, (b) $q_{1d} - q_1$ based on the BS, (c) $q_{1d} - q_1$ based on the APD, (d) $q_{1d} - q_1$ based on the PD, (e) $q_{2d} - q_2$ based on the ABS, (f) $q_{2d} - q_2$ based on the BS, (g) $q_{2d} - q_2$ based on the APD, and (h) $q_{2d} - q_2$ based on the PD.

5.3.3 Square Tracking

For square tracking, the desired square used here is the same as in Section 4.2. It can be checked that this square does not contain any singular points and the area encircled by this square is at least 25 centimeters away from the singular region. Fig. 5-26 to Fig. 5-27 show the results without load while Fig. 5-28 to Fig. 5-29 show the results with 100 gram load. Comparing the results from load test with the results from no load test, the norms of tracking errors of adaptive controllers increase less than those of non-adaptive controllers.

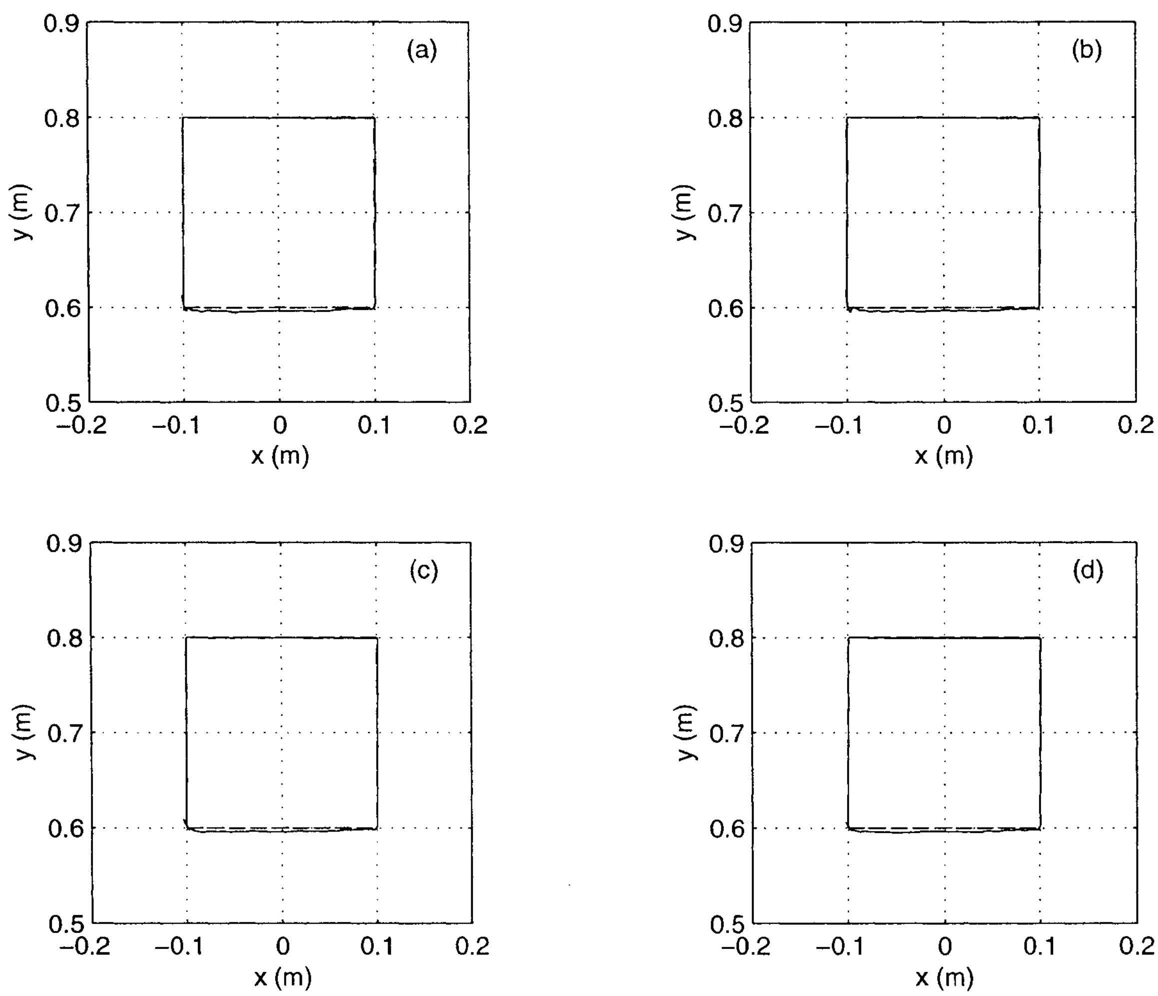

Figure 5-26: The results of tracking a square trajectory without load. (a) the ABS, (b) the BS, (c) the APD, and (d) the PD. Dashed line — the desired, solid line — the actual.

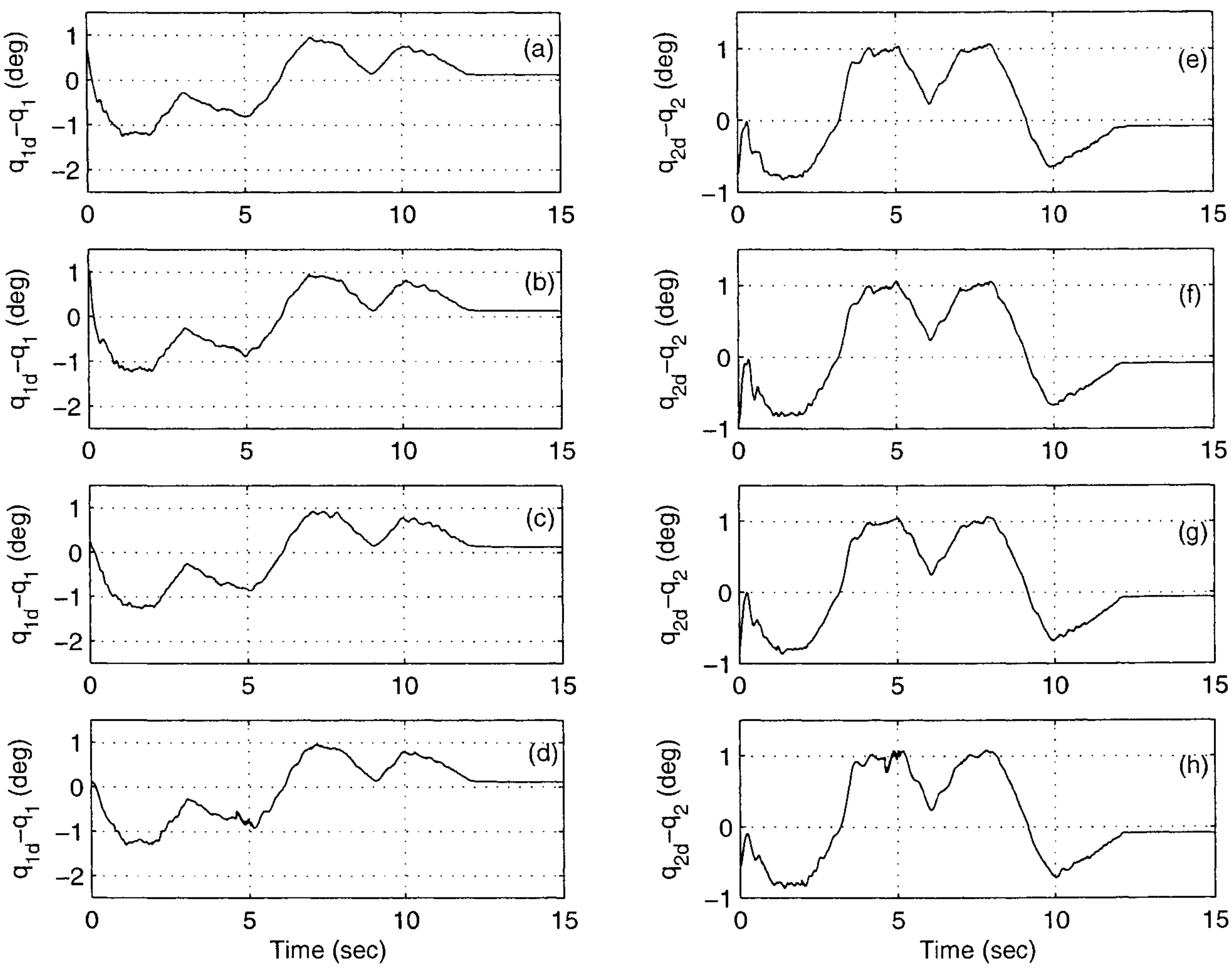

Figure 5-27: The tracking error of q_1 and q_2 for the square trajectory without load: (a) $q_{1d} - q_1$ based on the ABS, (b) $q_{1d} - q_1$ based on the BS, (c) $q_{1d} - q_1$ based on the APD, (d) $q_{1d} - q_1$ based on the PD, (e) $q_{2d} - q_2$ based on the ABS, (f) $q_{2d} - q_2$ based on the BS, (g) $q_{2d} - q_2$ based on the APD, and (h) $q_{2d} - q_2$ based on the PD.

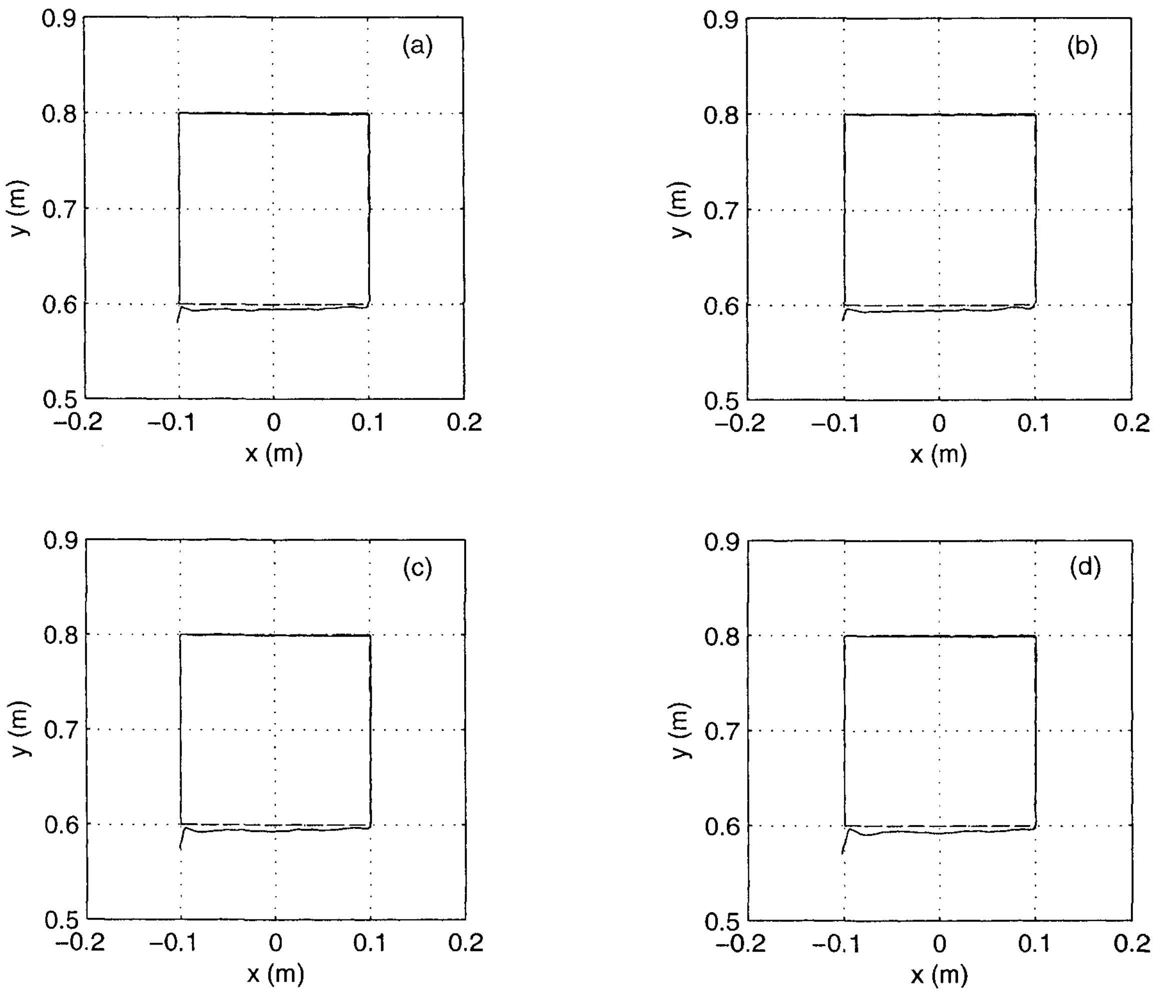

Figure 5-28: The results of tracking a square trajectory with load. (a) the ABS, (b) the BS, (c) the APD, and (d) the PD. Dashed line — the desired, solid line — the actual.

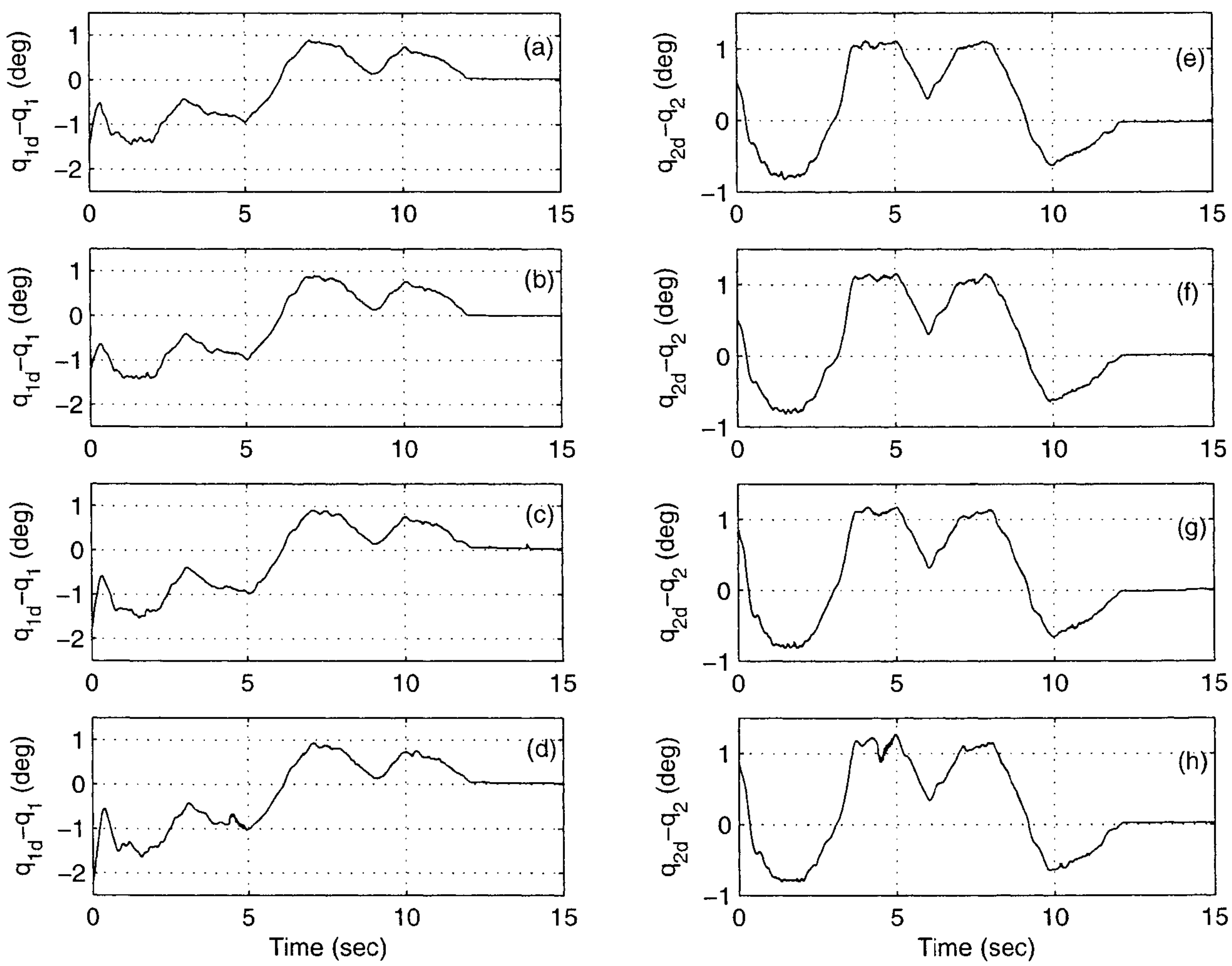

Figure 5-29: The tracking error of q_1 and q_2 for the square trajectory with load: (a) $q_{1d} - q_1$ based on the ABS, (b) $q_{1d} - q_1$ based on the BS, (c) $q_{1d} - q_1$ based on the APD, (d) $q_{1d} - q_1$ based on the PD, (e) $q_{2d} - q_2$ based on the ABS, (f) $q_{2d} - q_2$ based on the BS, (g) $q_{2d} - q_2$ based on the APD, and (h) $q_{2d} - q_2$ based on the PD.

The norms of the errors for the tracking line and square and the average of the tracking errors' norm without and with load are shown in Table 5-9 and 5-10 separately, where Traj. stands for Trajectory. It can be seen that when there is a change in the system parameters, the adaptive backstepping controller can achieve tracking errors with smaller norm values in most cases.

Table5-9. The Norms of Tracking Line and Square Error Based On Different Controllers

	q_1 (degree)				q_2 (degree)			
Traj./load (g)	ABS	BS	APD	PD	ABS	BS	APD	PD
Line / 0	60.4127	60.7254	**60.2202**	62.2550	50.7545	50.5922	**50.4511**	50.6989
Line / 100	**66.7663**	68.4194	72.2895	72.4075	53.1071	53.5801	52.1231	**52.1197**
Square / 0	**84.7476**	86.0015	86.9251	88.1923	81.5424	82.0528	**82.3448**	83.5541
Square / 100	**93.3803**	95.4894	98.9047	103.0862	86.0076	87.6588	**89.1881**	90.3474

Table 5-10. The Average Norms of Tracking Line and Square Error Based On Different Controllers

	Average Error (degree)			
Trajectory/load (g)	ABS	BS	APD	PD
Line / 0	55.5791	55.6588	**55.3357**	56.4770
Line / 100	**59.9367**	60.9998	62.2063	62.2636
Square / 0	**83.1450**	84.0272	84.6350	85.8732
Square / 100	**89.6940**	91.5741	94.0464	96.7168

Chapter 6

Conclusions and Future Work

6.1 Conclusions

An adaptive controller based on backstepping technique and an adaptive PD controller are applied to set point control of the planar 2-DOF parallel robot. The designed controllers guarantee the stability of the closed-loop system and are able to handle parameter uncertainties. The experiments have been conducted to compare four controllers: adaptive backstepping, non-adaptive backstepping, adaptive PD and PD plus compensation terms. The results have shown that all the controllers perform similarly in no load test, but adaptive controllers can achieve less average steady state error in with load test. The steady state errors are no more 1.5°, which is satisfactory since the backlash exists in the DC motors and the friction has not been taken into account in the controller design process.

Two backstepping based controllers: non-adaptive backstepping controller and adaptive backstepping controller, have been presented for tracking control of the same parallel robot. Both controllers guarantee the stability of the closed-loop system. The adaptive controller based on backstepping technique is able to handle parameter uncertainties even though the parameters' estimations don not converge to their real values. The PD controller and adaptive PD controller have been also applied to the parallel robot for comparison with the backstepping design method. The backstepping controller is a nonlinear controller while the PD controller is a linear controller with Coriolis and centrifugal terms, and gravity compensation. The ABS and APD demand more computation time than those non-adaptive controllers, which leads to the difficulty in real time control of a parallel robot with high degree of freedom in practice.

The experiments for tracking control have been conducted to compare four controllers: adaptive backstepping, non-adaptive backstepping, adaptive PD, and non-adaptive PD. Desired trajectories, such as circle, line and square, are tracked in the experiments. Different radii and tracking frequencies are used in circle tracking and the experimental results reveal that higher tracking speed results in larger tracking errors. Moreover the results have shown that all the controllers perform similarly when there was no additional payload. However, when an additional payload was added to the robot, the adaptive controller were able to achieve the smaller tracking errors than non-adaptive controllers especially in those cases with high tracking speed. ABS performs a little bit better than APD when the tracking frequency is high.

The experiments have also revealed a need to consider friction and backlash existing in the motors in order to further reduce the steady state errors for set point control and the tracking errors for tracking control.

6.2 Future Work

The experimental results are satisfactory based on the limitation of the mechanical system and the data acquisition system. However, more accurate results can be achieved with a better mechanical system. The experimental results shown by the figures in the thesis are the best readings after many trials. Repeating the experiments with the same parameters may not give the exactly same results. In order to further reduce the steady state errors for set point control and the tracking errors for tracking control, the following work should be done in future:

1. Update the mechanical system to reduce the flaws such as backlash.

2. Build more sophisticated model including backlash, friction and the dynamics of DC motors.

3. For tracking control, reduce the sampling period to improve the tracking performance by choosing DSP to accomplish data communication instead of DAQ.

Bibliography

[1] Y. Amiral, G. Francois, and M. Dafaoui. Design and control of a new six-dof parallel robot: Application to equestrian gait simulation. *Mechatronics*, 6:227–239, 1996.

[2] P. Begon, F. Pierrot, and P. Dauchez. Fuzzy sliding control of a fast parallel robot. In *Proc. IEEE Int. Conf. in Robotics and Automation*, pages 1178–1183, Nayoga, Japan, 1995.

[3] C. Boer, L. Molinari-Tosatti, and K. Smith. *Parallel Kinematic Machines.* Springer-Verlag, Berlin, 1999.

[4] A. Codourey. Dynamic modeling of parallel robots for computed-torque control implementation. *Int. J. Robot Research*, 17:1325–1336, 1998.

[5] J. Dabney, F. Ghorbel, and Z. Wang. Modeling closed kinematic chains via singular perturbations. In *Proc. of the American Control Conf.*, Anchorage, AK, USA, 2002.

[6] A. Fattah, J. Angeles, and A. Misra. Dynamics of a 3-dof spatial parallel manipulator with flexible links. In *Proc. IEEE Int. Conf. in Robotics and Automation*, pages 627–632, Nayoga, Japan, 1995.

[7] E. Fichter. A stewart platform-based manipulator: General theory and practical construction. *Int. J. Robotics Research*, 5:157–182, 1986.

[8] Z. Geng and L. haynes. Dynamic control of a parallel link manipulator using a cmac neural network. *Compt. Elect. Eng.*, 19:265–276, 1993.

[9] F. Ghorbel, O. Chetelat, R. Gunawardana, and R. Longchamp. Modeling and set point control of closed-chain mechanisms: Theory and experiment. *IEEE Transaction on Control Systems Technology*, 8:801–815, 2000.

[10] F. Ghorbel, R. Gunawardana, and J. Dabney. Experimental validation of a reduced model based tracking control of parallel robots. In *Proc. of the 2001 IEEE International Conf. on Control Applications*, pages 375–382, Mexico City, Mexico, 2001.

[11] C. Gosselin. *Kinematic Analysis,Optimization and Programming of Parallel Robotic Manipulators.* Ph.D. thesis, McGill University, 1988.

[12] C. Gosselin. Parallel computational algorithms for the kinematics and dynamics of parallel manipulators. In *Proc. IEEE Int. Conf. in Robotics and Automation*, pages 883–888, Atlanta, GA, USA, 1993.

[13] C. Gosselin. Parallel computational algorithms for the kinematics and dynamics of planar and spatial parallel manipulators. *ASME Journal of Dynamics System, Measurement, and Control*, 118:22–28, 1996.

[14] K. Hunt. *Kinematic Geometry of Mechanisms.* Clarendon Press, Oxford, 1978.

[15] I. Kanellakopoulos, P. Kokotovic, and A. S. Morse. Systematic design of adaptive controllers for feedback linearizable systems. *IEEE Transactions on Automatic Control*, 36:1241–1253, 1991.

[16] T. Kokkinis and R. Stoughton. Dynamics and control of closed-chain robot arms with application to a new direct-drive robot arm. *Int. Journal of Robotics and Automation*, 6:131–145, 1991.

[17] M. Krstic, I. Kanellakopoulos, and P. Kokotovic. *Nonlinear and adaptive control design.* Wiley, New York, 1995.

[18] Q. Li and F. Wu. Control performance improvement of a parallel robot via the design for control approach. *Mechatronics*, 14:947–964, 2004.

[19] F. Lin and C. Lee. Adaptive backstepping control for linear induction motor drive to track periodic references. *IEE Proc. Electric Power Applications*, 147:449–458, 2000.

[20] S. Lin. Dynamics of the manipulator with closed chains. *IEEE Trans. Robot. Automat.*, 6:496–501, 1990.

[21] A. Lotfazar, M. Eghtesad, and M. Mohseni. Integrator backstepping control of a 5 dof robot manipulator incorporating actuator dynamics. In *Control Applications, 2003. CCA 2003. Proceedings of 2003 IEEE Conference on*, pages 1007–1012, Istanbul, Turkey, 2003.

[22] J. Luh and Y. Zeng. Computation of input generalized forces for robots with closed kinematic chain mechanisms. *IEEE J. Robot. Automat.*, 1:95–103, 1985.

[23] S. Ma, T. Chung, Y. Kim, and M. Oh. Tracking control of a welding mobile robot based on adaptive backstepping method. In *International Symposium on Electrical& Electronics Engineering*, pages 43–52, HCM City, Vietnam, 2005.

[24] F. Mnif. Recursive backstepping stabilization of a wheeled mobile robot. *International Journal of Advanced Robotic Systems*, 1:287–294, 2004.

[25] Y. Nakamura and M. Ghodoussi. Dynamics computation of closed-link robot mechanisms with nonredundant and redundant actuators. *IEEE Trans. Robot. Automat.*, 5:294–302, 1989.

[26] D. Stewart. A platform with six degree of freedom. *Proc. of the Institution of Mechanical Engineers*, 180:371–386, 1965.

[27] C. Su and Y. Stepanenko. Backstepping-based hybrid adaptive control of robot manipulators incorporating actuator dynamics. *International Journal of Adaptive Control and Signal Processing*, 11:141–153, 1997.

[28] J. Uicker. Dynamic behavior of spacial linkages-part 1: Exact equations of motion. *J. Eng. Ind.*, 91:251–258, 1969.

[29] A. Vivas and P. Poignet. Predictive functional control of a parallel robot. *Control Engineering Practice*, 13:863–874, 2005.

[30] D. Zhang. *Kinetostatic Analysis and Optimization of Parallel and Hybrid Architectures for Machine Tools.* Ph.D. thesis, Laval University, Quebec, Canada, 2000.

[31] J. Zhou, Y. Wang, and R. Zhou. Adaptive backstepping control of separately excited dc motors with uncertainties. *Proc. of the IEEE Conf. on Power System Technology*, 1:91–96, 2000.